Switching and memory effects in electron-vibron systems: from single-site junctions to chains and networks

D I S S E R T A T I O N

zur Erlangung des
DOKTORGRADES DER NATURWISSENSCHAFTEN (DR. RER. NAT.)
der Naturwissenschaftlichen Fakultät II - Physik
der Universität Regensburg

vorgelegt von
PINO D'AMICO
aus ***Quadri*** *(Italien)*
im Mai 2010

Switching and memory effects in electron-vibron systems: from single-site junctions to chains and networks

DISSERTATION

Die Arbeit wurde angeleitet von:
Prof. Dr. Klaus Richter

Promotionsgesuch eingereicht am:
13. 01. 2010

Prüfungsausschuß:

Vorsitz:	Prof. Dr. Franz J. Gießibl
Erstgutachten:	Prof. Dr. Klaus Richter
Zweitgutachten:	Prof. Dr. Milena Grifoni
Weiterer Prüfer:	Prof. Dr. Andreas Schäfer

Contents

1 Introduction **5**

1.1 Molecular Electronics 5

1.1.1 Experiments on single molecule junctions 7

1.1.2 Theoretical approaches for transport 8

1.2 Switching and bistability in nature 9

1.3 Thesis overview 12

2 Model and Methods **13**

2.1 Model Hamiltonian 13

2.2 Green functions 15

2.2.1 Equation of Motion method 18

2.3 Density Matrix approach 20

2.3.1 Generalized Master Equation 21

2.3.2 Master Equation for the populations 22

3 Single-site junctions: charge memory effects **27**

3.1 Introduction 27

3.2 Intermediate coupling to the leads 29

3.2.1 Spectral function, average charge and current 30

3.2.2 Equation of Motion method for the single-level electron-vibron Hamiltonian 31

3.2.3 Self-consistent Hartree approximation 32

3.2.4 Second approximation 33

3.2.5 Results and discussion for the intermediate case 34

3.3 Weak system-to-leads coupling 38

3.3.1 Eigenstates and Master Equation 38

3.3.2 Charge, current and life-times 41

3.3.3 Conclusion for weak coupling case 44

4 Single-site junctions: spin memory effects **47**
4.1 Model Hamiltonian 48
4.2 Weak lead-to-molecule coupling 49
4.2.1 Model, states and energies 50
4.2.2 Rates and Master Equation 52
4.2.3 Charge, spin polarization and lifetimes 52
4.3 Intermediate lead-to-molecule coupling 56

5 Chains of electron-vibron systems **65**
5.1 Two-level-systems: intermediate coupling 67
5.1.1 Bias-independent and bias-dependent energy levels . . 69
5.1.2 Extended analysis for the bias-dependent case 72
5.1.3 Memory effects 75
5.2 Two-level-system: analytical considerations for weak coupling 77
5.3 Three-level system in the intermediate lead-to-molecule coupling 82
5.4 Conclusions 84

6 Networks of electron-vibron elements **89**
6.1 Introduction 89
6.2 Model Hamiltonian 90
6.3 2 by 2 square lattice 91
6.4 3 by 3 square lattice 94

7 Conclusions and perspectives **101**

Bibliography **104**

Chapter 1

Introduction

1.1 Molecular Electronics

The general framework in which this thesis is embedded is called Molecular Electronics [1]. In this field the dream is to be able to produce stable junctions in which a given molecule is in contact with a certain number of electrodes. Those allow to apply voltages and to perform specific tasks, exploiting the functionality of the molecule itself.

Different kinds of molecules have specific electronic, structural and vibrational properties, but there is something that can be thought as a general property: the typical dimension of a molecule is in general very small (of the order of nanometers or smaller). Molecules can undergo structural changes when additional charges are inserted through electron-tunneling in transport setups. Because of that, the electronic and the vibrational degrees of freedom are strongly related in molecules and their mutual interaction plays a fundamental role in the investigation of a molecular junction and in view of possible applications.

In general we can consider a molecule as a very tiny object that is flexible and has localized vibrations. This property is peculiar of molecules and is absent in semiconductor devices like quantum-dots, two dimensional electron gases and bulk materials. In those systems the vibrational properties are associated to the phonon structure, i.e. to the lattice structure of the material one considers. The flexibility of the molecules make them interesting and different from semiconductors devices, opening new perspectives and bringing new effects into the game.

The idea of using single molecule junctions in order to obtain functional devices like switches, rectifiers and memory elements, dates back to 1974. In [2] Aviram and Ratner proposed to use a single organic molecule as a rectifier.

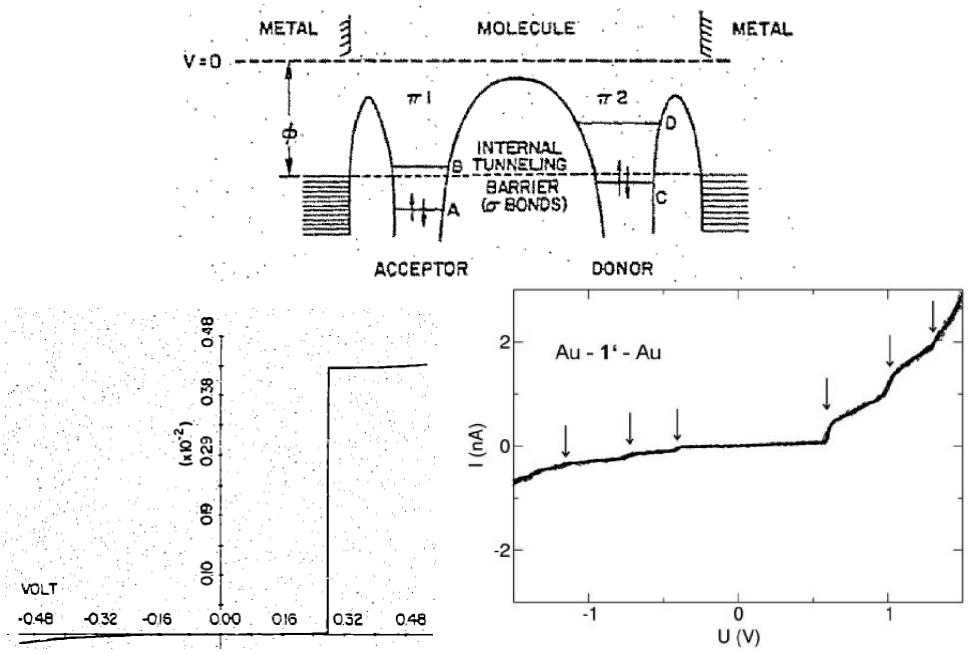

Figure 1.1: (Top) Original schematic representation of a molecular junction from [2]. The scheme represents the energetics of a molecular junction made of two metallic leads and a molecule placed between them. (Bottom) Current rectification calculated with the original proposed model [2] (left) and the measured current from [3] (right).

Only recently the corresponding experimental realization has been achieved by employing two weakly coupled π-systems with mutually shifted energy levels [3]. A scheme of the molecular rectifier from the original proposal is shown in Fig. 1.1, together with the calculated current and the experimental measurement from [3]. The Aviram-Ratner rectifier is based on a acceptor-donor sites system . If the acceptor and the donor are well isolated among each other, a current can flow only in one direction resulting in a rectification effect.

Though the Aviram-Ratner theoretical proposal has been experimentally observed, it has to be mentioned that the first measurement on a single molecule junction has been achieved by Reed et al. [4]. The molecule was a benzene-1,4-dithiol.

In the following we will review the experimental and theoretical methods used to investigate molecular junctions.

1.1.1 Experiments on single molecule junctions

The most challenging part of the experiments with single molecule junctions is to have a controllable method to contact the molecule and the reservoirs. Making a stable junction with a single molecule as a bridge and active part of the system is a very delicate task to accomplish for experimentalists. In general it is possible to realize single molecule junctions in two different ways:

- attaching a single molecule to the external leads through a single atomic contact using the molecule as a bridge;
- using a Scanning Tunneling Microscopy (STM) technique where the molecule is deposited on a given substrate and investigated through the tip of the apparatus.

The first setup (we call it *bridge setup*) can be realized with the Mechanically Controllable Break-Junction (MCBJ) technique (see for example chapter 9 in [1] and references therein) and also with the electromigration technique [5]. In both methods the final task is to obtain a gap into a metallic wire. The two metallic segments are then used as electrodes. The desired molecule is placed between the two electrodes and probed through a bias voltage (and possibly a gate voltage).

The STM setup is realized placing an ultrathin insulating layer on a metallic surface. The molecule (or the atom) of interest is deposited on top of the insulating layer. The tip of the STM is placed on top of the molecule in order to probe it with a voltage between the tip and the metallic surface [6, 7, 8].

In Fig. 1.2 we show the breaking resulting from the electromigration technique and an image taken with the STM setup.

In the bridge setup one has to be very careful in order to attribute the measurement to a very single molecule, because more than one molecule could be attached between the electrodes. In order to avoid this difficulty statistical approaches can be used to analyze the data, as for example in [9]. The STM setup gives instead the possibility to manipulate single molecules in a very precise way and to image molecular orbitals with high resolution producing beautiful images: it is really possible to look at the molecular orbitals. Thinking about possible realistic electronic applications, the bridge setup is more suitable because a single molecule clamped between electrodes can be a very small system and a chip-integration can be envisaged. On the other hand, an STM setup is usually a big experimental apparatus, more oriented to fundamental aspects.

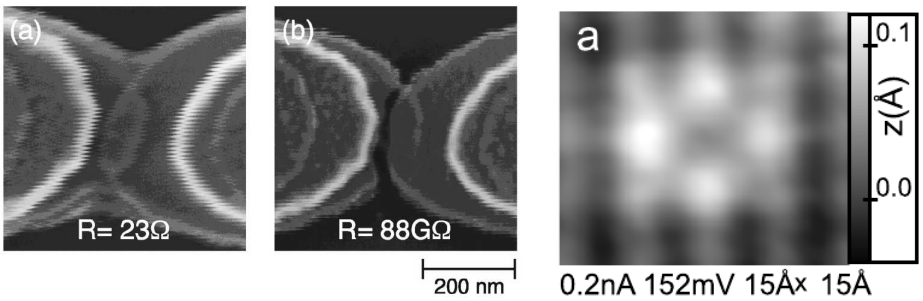

Figure 1.2: (Left) Field-emission scanning electron micrographs of a representative gold nanowire (a) before and (b) after the breaking procedure by electromigration. The nanowire consists of thin 10 nm and thick 90 nm gold regions. In the images, diffuse white lines separate these two regions[5]. (Right) STM image of an individual Cl vacancy in the top layer of a bilayer of NaCl on Cu(111) [6].

1.1.2 Theoretical approaches for transport

From a theoretical point of view, the transport across a system made of a single molecule in contact with external electronic reservoirs, is a very complex problem to treat. Fig. 1.3 shows a sketch of a molecule in contact with two reservoirs. The contact of the molecule with external reservoirs introduces the task of treating the tunneling of electrons through the molecule. The change of the electronic charge in the molecule due to tunneling processes deform the structure of the molecule itself. This is taken into account introducing interactions between electronic and vibrational degrees of freedom of the molecule. The combination of strong interactions and tunneling processes make the problem very interesting and also very challenging from a theoretical point of view. Interesting transport regimes can be investigated and different tools are suitable in different situations.

The theoretical methods used to deal with this problem can be grouped in general in two categories: *ab initio* and *model-based* approaches.

With *Ab initio* methods it is possible to numerically simulate the structure of the molecule in contact with the electronic reservoirs at atomic level. The physical quantities obtained in this way are then used in combination with other theoretical schemes in order to calculate the transport properties of the molecular bridge. An example of this method is the combination of DFT calculations with Green functions techniques [10, 11, 12, 13, 14, 15]: with DFT one calculates the properties of the junction and then Green function techniques are used to calculate the transport across the bridge. With

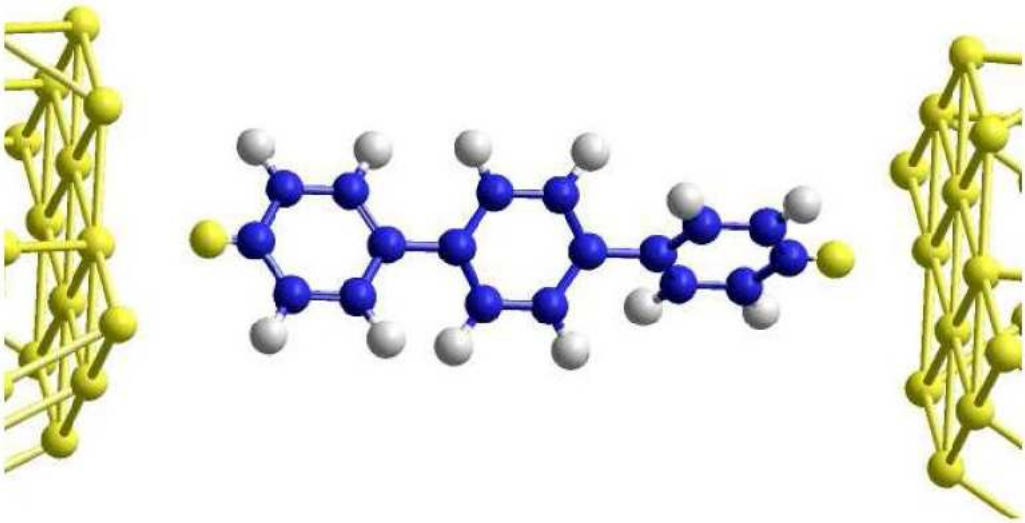

Figure 1.3: Image of a molecule in contact with two electronic reservoirs.

this method it is possible to treat the case of relatively strong molecule-to-electrodes coupling while the case of weak coupling and strongly localized interactions is not accessible. Additionally DFT calculations does not give the correct HOMO-LUMO gap and thereby transport calculations give wrong results.

In the *model-based* methods a simplified model is introduced in order to describe the considered physical system. Starting from a given model, different approaches are then used to calculate the transport properties of the junction. For example Density Matrix (DM) [16, 17, 18] and Green Function (GF) [19, 20, 21] techniques can be used to investigate the transport through the junction.

The choice of the technique depends on the molecule-to-lead coupling and on the interactions present in the system. With *model-based* methods the molecule-to-lead coupling and the interaction strengths are treated as parameters. The power of this approach is that if the models are well describing the physical systems, then it is possible to get a good physical insight into the problem with a reasonable amount of computational time.

1.2 Switching and bistability in nature

This work deals with a particular effect that can be achieved in molecular junctions: the switching between different states of the molecule and the

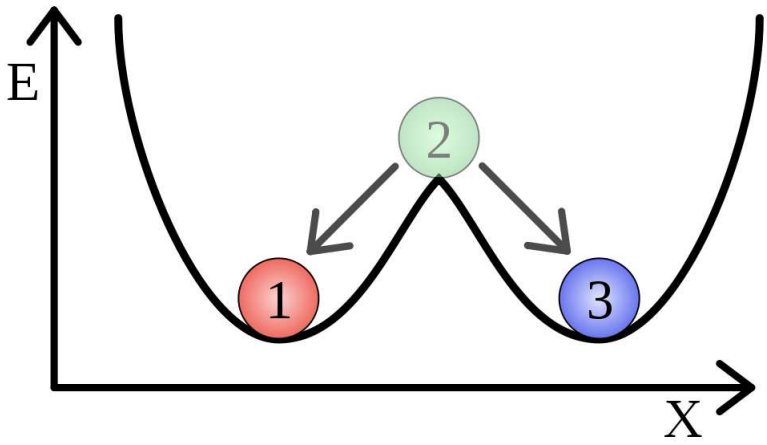

Figure 1.4: Energy profile of a bistable system. The X indicate a generic coordinate that can jumps from one value to another corresponding to two degenerate minima of the energy E.

associated bistability and hysteretic phenomena. Such effects are quite general in nature and they are also very important for applications. They are present in different areas like biology (decision-making in cell cycles [22], cellular differentiation [23] and apoptosis [24]), chemistry (relaxation kinetics [25]) and physics (ferromagnetism, ferroelectricity). They all have a common aspect: the energy profile of a bistable system has two meta-stable minima separated by an energy barrier between them, as shown in Fig. 1.4. The way the system can switch between those two minima depends on the specific case. Usually there is an energy source that allows the system to jump from one state to the other one. This energy can be available from a thermal environment, electronic sources and chemical reactions but there is a common process: absorb energy to overcome a given barrier. In some cases a bistable system is associated with a phase-transition, as for example in the case of ferroelectricity and ferromagnetism.

A good example is given by the phase diagram of the water: the line that separates the liquid from the gas phase describes a first order phase transition, and it can be seen as an energy barrier between states with the same symmetry. The other transitions (solid-liquid and solid-gas) are also associated with a spatial symmetry breaking and they are second order transitions.

In Molecular Electronics switching processes are related to various physical mechanisms, for example conformational changes of the molecule, charge rearrangement and molecular deformations. There are both experimental

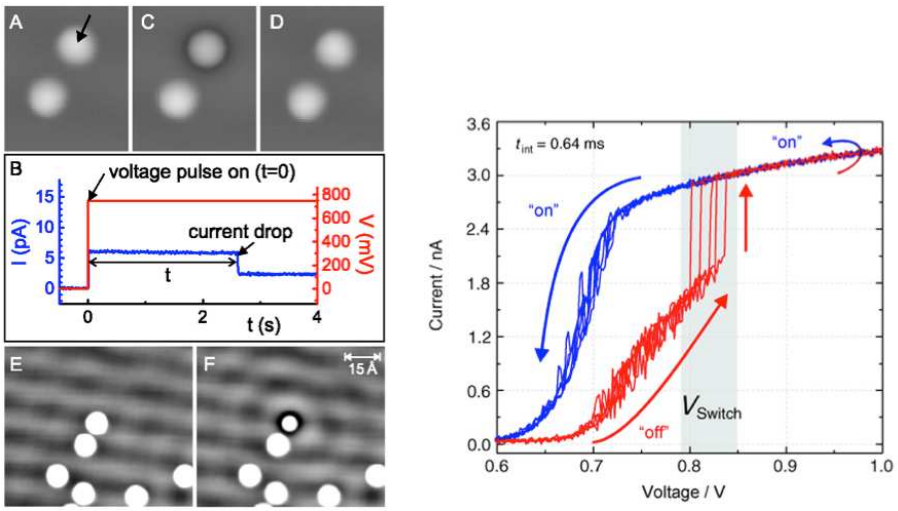

Figure 1.5: (Left) Images from [7]. The Au atom addressed with the tip of the STM is visualized before the application of a voltage pulse (A, neutral ad-atom), after the application of a voltage pulse (C, charged ad-atom) and when it returns to neutral state (D). The current profile shows steps corresponding to the transition from neutral-to-charged state and viceversa (B). The scattering of surface states from neutral and charged state are reported in E and F respectively. (Right) Current-voltage characteristic from [28]. Applying a time-dependent voltage with a chosen sweeping-velocity, a hysteretic region is clearly observed. It is possible to identify on and off states for logic operations and a switching-voltage region.

and theoretical works in which such interesting effects have been addressed. Experiments showing switching effects have been made both with STM [7, 8] and *b*ridge [26, 27, 28, 29] setups. In Fig. 1.5 we show results from those experiment. In the STM experiment it was demonstrated that charged and neutral states of Au ad-adatoms on ultrathin NaCl films are both long-living. The multistability has been explained in terms of polaronic coupling, due to the rearrangement of the charges in the insulating film. In the other experiment (right panel) a BPDN-DT molecule between gold leads shows hysteresis depending on the sweeping velocity of the applied voltage. In this case the effect is attributed to conformational reorientation of the molecule [30] . Theoretical investigations have been performed on switching and charge-memory effects using different methods and techniques to treat electron-vibron models [31, 32, 33, 34, 35, 36]. In the present work we investigate memory effects in electron-vibron systems, going from single site molecular

junctions to arrays.

1.3 Thesis overview

The thesis is organized in the following way: in chapter 2 we introduce the theoretical methods we have used for our research.

The third chapter is dedicated to the investigation of charge-memory effects in single-site molecular junctions [37, 38].

In the fourth chapter we extend the charge-memory to the spin-memory effect introducing ferromagnetic electronic reservoirs, still for the single electron-vibron molecular junction case [39].

We extend the investigation of memory-effects to chains of electron-vibron elements in the fifth chapter, having in mind *bridge setups*.

The sixth chapter is devoted to a further extension, namely an array of electron-vibron elements. In this case the array is thought to be deposited on an STM substrate and it is investigated through the tip of the apparatus.

In the last chapter we draw the conclusions of the present work and we suggest further research directions in order to extend the obtained results.

Chapter 2

Model and Methods

In this chapter we introduce our model Hamiltonian and the theoretical methods we use to calculate observables. The Hamiltonian we introduce here is expressed in the second quantization language and describes a *system* contacted to external *reservoirs*. The Hamiltonian of the system is general at this level, and it will be then reduced and adapted case by case in the next chapters for different physical situations. The Green Function (GF) and the Density Matrix (DM) approaches are also formulated in a general way and we will then apply them to particular cases and models in the next chapters.

The GF and the DM approaches are commonly used to describe transport phenomena in nanosystems. The two approaches approximate the system in a reasonable way for different physical situations. We are dealing with nanosystems in contact with external reservoirs and the coupling between the system and the reservoirs is a key parameter for the description of the system itself. In the case of intermediate-to-strong coupling between the system and the external reservoirs the Green function method is appropriate. In another limiting case, namely the case of weak system-to-reservoirs coupling, the density matrix is more suitable. The meaning of strong and weak coupling depends on the system and will be clarified when we treat specific models for our systems. The message is that in the strong-coupling case the system has to be seen more as a whole together with the reservoirs, while in the weak coupling case the system can be seen as a almost isolated part perturbed by tunneling to the reservoirs.

2.1 Model Hamiltonian

We construct the Hamiltonian step by step. The first part of the full Hamiltonian describes the *system* we want to investigate; we call this part H_S.

Our work focuses on molecular junctions and then the physical systems we are addressing are molecules. A simple model of a molecule encorporates its electronic and vibrational degrees of freedom in the following way [21]:

$$\begin{aligned} H_S &= \sum_{i,j} \epsilon_{ij} d_i^\dagger d_j + \sum_{i \neq j} U_{ij} \hat{n}_i \hat{n}_j \\ &+ \sum_q \omega_q a_q^\dagger a_q + \sum_{q;ij} \lambda_{ij}^q (a_q^\dagger + a_q) d_i^\dagger d_j. \end{aligned} \tag{2.1}$$

The d operators refers to the electronic degrees of freedom (labeled with indices i and j) and the a operators to the vibrational ones (labeled with the indice q). The first row of the Hamiltonian (2.1) contains the electronic free part and the electron-electron interaction respectively. The second row describes the free vibrons and the electron-vibration interaction.

The system is then connected to external electronic reservoirs. We introduce here the Hamiltonian for two reservoirs, the left and the right one. Those reservoirs are assumed to be Fermi gas and they are described in the following:

$$H_{Res} = \sum_{i=L,R;k} \epsilon_{ik} c_{ik}^\dagger c_{ik} = H_{Res,L} + H_{Res,R}, \tag{2.2}$$

where the c_i operators refer to electronic states in the two reservoirs (labeled with the indice k). The connection between the system and the reservoirs is given in terms of a tunneling Hamiltonian:

$$H_T = \sum_{k,i=L,R;j} V_{ik,j} c_{ik}^\dagger d_j + h.c. = H_{T,L} + H_{T,R}, \tag{2.3}$$

where V gives the strength of the coupling between the electronic states on the system and the states on the reservoirs. The full Hamiltonian is then given by the sum of the three parts (2.1, 2.2, 2.3):

$$H = H_S + H_{Res} + H_T. \tag{2.4}$$

In Fig. 2.1 we show a schematic representation of the Hamiltonian (2.4).

Starting from the Hamiltonian (2.4), we are interested in extracting physical informations from it. For example we want to know the density of states, how the electrons are energetically distributed and what are the effects of the reservoirs on the system. In the next two sections we introduce the theoretical methods we use to handle the Hamiltonian (2.4).

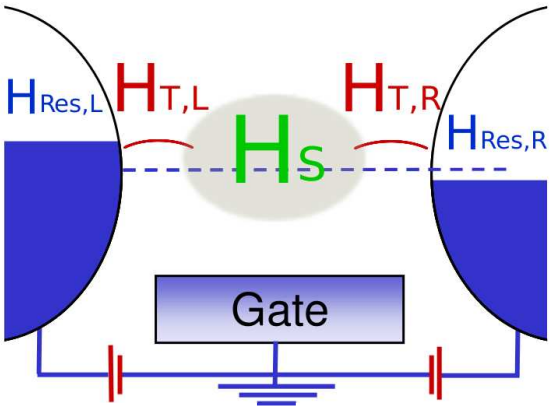

Figure 2.1: Schematic representation of the model Hamiltonian (2.4). A system coupled via tunneling Hamiltonians to two reservoirs. A possible gate is also sketched. The gate can act changing the energy of the electronic levels of the system.

2.2 Green functions

The Green function method is a general method for solving various kind of differential equations. In quantum mechanics it is a very useful tool to solve the Schrödinger equation in time-dependent and time-independent cases. The solution of the Schrödinger equation for a generic Hamiltonian, in both time-dependent and independent cases can be found for example in the book [40]. Before introducing explicitly the Green functions for the Hamiltonian (2.4), we briefly resume the Heisenberg representation of the operators. Given an operator O, the Heisenberg time-dependent expression is:

$$O(t) = e^{iHt} O e^{-iHt}. \tag{2.5}$$

We want to calculate density operators (both for the fermionic and for the bosonic sector of the system), distribution functions and currents. Their dependence on the interactions present in the system and on the reservoirs is essential. As we will see, those quantities are usually expressed in terms of products of operators and we are then interested in such products. Suppose for example that A and B are two generic operators of the problem. With the time-dependent operators defined in (2.5) we can treat combinations of operators containing two different times like $A(t)B(t')$.

We concentrate now on the fermionic terms of the system Hamiltonian, $d_i^\dagger$

and d_i. The index i represents the fermionic level that we are looking to, and the quantities that we will calculate (density of states, currents) are expressed as products of operators like $d_i^\dagger d_j$. After this intuitive discussion we can formally introduce the Green functions. First we should mention that there are different kinds of Green functions, namely the *retarded*, the *advanced*, the *lesser* and the *greater*. There are formal relations that connect those different functions and the meaning of those names will be clear after on. We start with the *retarded* Green function. The definition is the following:

$$G^r_{i,j}(t,t') = -i\Theta(t-t')\left\langle\left\{d_i(t), d_j^\dagger(t')\right\}\right\rangle, \tag{2.6}$$

where r stands for *retarded* and Θ is the step function. The brackets $\{\}$ represent the anticommutator and the brackets $\langle\rangle$ denote thermal averaging. As we can see from the definition (2.6), the Green function is in fact a matrix of functions, and its dimension depends on the number of states present in the system. The definition given in Eq. (2.6) refers to two electronic states, but the same expression can be applied to any couple of operators of the problem. One has to take care of the different commutation relations for bosons and fermions. The *advanced* Green function has the following similar structure to the *retarded* one:

$$G^a_{i,j}(t,t') = i\Theta(t'-t)\left\langle\left\{d_i(t), d_j^\dagger(t')\right\}\right\rangle, \tag{2.7}$$

where we can see that the difference is in the order of the time argument of the step function. This is also the motivation for the names *retarded* and *advanced*: the first describes the physical process of creating an electron in the state i at time t having destroyed an electron at time $t' < t$ in the state j, while the second describes the same process but the time order is inverted, $t < t'$. The other two Green functions (lesser and greater) have the following expressions:

$$\begin{aligned} G^<_{i,j}(t,t') &= -i\left\langle d_i^\dagger(t') d_j(t)\right\rangle \\ G^>_{i,j}(t,t') &= -i\left\langle d_i(t) d_j^\dagger(t')\right\rangle. \end{aligned} \tag{2.8}$$

The Green functions are usually expressed in the frequency (or energy) domain performing a Fourier transform. This operation is usually done after the assumption of stationary limit, i.e. assuming that the time appears as the time difference and not the two times separately (the Fourier transform is introduced explicitly in the next section 2.2.1). We introduce now important relations that connect the Fourier transform of the Green functions (2.6, 2.7,

2.8) with physical quantities like the spectral function and density of states. The details can be found in reference [40]. The spectral function is defined as

$$A_{i,j}(\omega) = -2iG^r_{i,j}(\omega), \tag{2.9}$$

and the density as

$$n_{i,j} = -i\int_{-\infty}^{\infty}\frac{d\omega}{2\pi}G^<(\omega). \tag{2.10}$$

In the study of nanosystems the electric current flowing across the system is one of the most used quantities in order to characterize the junction under investigation. The differential conductance can then be calculated taking a derivative of the electric current with respect to the applied voltage. Within the Green function formalism the current through the system can be expressed in an elegant way in terms of the Green functions. The analytical formulation of the current has been introduced by Meir and Wingreen in their original work [19]:

$$J = \frac{ie}{2\hbar}\int\frac{d\epsilon}{2\pi}Tr\left\{\left[\mathbf{\Gamma}^L - \mathbf{\Gamma}^R\right]\mathbf{G}^< + \left[f_L\mathbf{\Gamma}^L - f_R\mathbf{\Gamma}^R\right]\left[\mathbf{G^r} - \mathbf{G^a}\right]\right\}, \tag{2.11}$$

where L and R stands for right and left external reservoirs described by the Fermi functions f_L and f_R. The Green functions refer to the central system of the structure (the H_S of the full Hamiltonian in Eq. (2.4)) considered. The gamma matrices describe the coupling between the system and the reservoirs (leads) in terms of the tunneling Hamiltonian H_T. They are given by the following expression:

$$\Gamma^i_{n,m} = 2\pi\sum_k V_{ik,n}V^*_{ik,m}\delta(\epsilon - \epsilon_k), \tag{2.12}$$

where i labels the reservoirs, k the electronic states of the reservoirs and n, m the electronic states of the system. We have formally introduced the Green functions and the relationships that they have with the physical measurable quantities. We need now a method to explicitly calculate the Green functions. There are different calculation schemes used in order to obtain an expression for the different Green functions. For example Dyson equation, Path Integral, Diagrammatic, Equation of Motion. Every method has of course advantages and disadvantages and one has to make a choice. Our derivations are mainly based on the equation of motion (EOM) method. In the following section we introduce the basics of this tool that we will then use in the next chapters.

2.2.1 Equation of Motion method

As the name says this method relies on the time evolution of the Green function we want to calculate. The dynamics of the Green function is related to the time-evolution of the operators in the Heisenberg picture. The starting point of the method is to take a time derivative of the Green function under investigation. The first step is to write the time evolution of operators expressed in the Heisenberg picture. Starting from the Eq. (2.5) and taking a time derivative we obtain the following expression:

$$i\frac{\partial O(t)}{\partial t} = [O, H]\,, \tag{2.13}$$

where $O(t)$ is a generic operator in the Hamiltonian H. As we can see from (2.13), the time derivative correspond to commutators. We take now the time derivative of the retarded Green function (2.6), assuming the stationary limit and setting $t^{'} = 0$ (the Green function is then a function of t only). Using the above Eq. (2.13) the equation of motion then reads

$$i\frac{\partial G^r_{i,j}(t)}{\partial t} = \delta(t)\left\langle\left\{d_i(t), d_j^\dagger\right\}\right\rangle - i\Theta(t)\left\langle\left\{[d_i, H](t), d_j^\dagger\right\}\right\rangle, \tag{2.14}$$

where we use $d_j^\dagger \equiv d_j^\dagger(0)$. The next step is to rewrite Eq. (2.14) in the frequency (or energy) domain. We want an equation for the Fourier transform of the Green function (2.6). To this end we briefly rewrite here the principal properties of the Fourier transform (FT). First of all the definition: the FT of $G^r(t)$ is:

$$G^r(\omega) = \int_{-\infty}^{+\infty} e^{i\omega t} G^r(t) dt \equiv F\left[G^r(t)\right]. \tag{2.15}$$

The FT has its inverse, F^{-1} and also the following useful properties:

$$F\left[i\frac{\partial G^r(t)}{\partial t}\right] = (\omega + i\eta)G^r(\omega), \tag{2.16}$$

$$F\left[\delta(t)G(t)\right] = G(0). \tag{2.17}$$

A small imaginary parameter $i\eta$ is introduced to ensure the proper convergence of the FT. Before writing the EOM in the frequency domain we introduce the usual way to express the FT of a Green function:

$$F\left[G^r_{i,j}(t)\right] = \left\langle\left\langle d_i, d_j^\dagger\right\rangle\right\rangle. \tag{2.18}$$

With this instruments we can rewrite Eq. (2.14) in the frequency domain:

$$(\omega + i\eta)\left\langle\left\langle d_i, d_j^\dagger\right\rangle\right\rangle = \left\langle\left\{d_i, d_j^\dagger\right\}\right\rangle + \left\langle\left\langle [d_i, H], d_j^\dagger\right\rangle\right\rangle. \tag{2.19}$$

We see from Eq. (2.19) that the commutators $[d_i, H]$ has to be calculated. The commutators will give rise to other Green functions, that are usually called *higher order Green functions*. It is possible to write additional EOM for those new functions using the general expression (2.19). We end up then with a set of equations that has to be solved. This is a crucial point of the method and we show here an example taking the Hamiltonian (2.4) as a reference. The first step is to remind the commutation relations. For the fermionic operators they are given by:

$$\begin{aligned} \{d_i, d_j^\dagger\} &= \delta_{i,j} \\ \{d_i^\dagger, d_j^\dagger\} &= 0 \\ \{d_i, d_j\} &= 0. \end{aligned} \tag{2.20}$$

For operators A, B and C , an important property of the commutator is the following:

$$[A, BC] = \{A, B\}C - B\{C, A\}. \tag{2.21}$$

The commutator $[d_i, H]$ contains three parts:

$$[d_i, H] = [d_i, H_S] + [d_i, H_{Res}] + [d_i, H_T]\,.$$

The Hamiltonian H_{Res} does not contain d operators, then the corresponding commutator is zero. We are then left with the following equation:

$$[d_i, H] = [d_i, H_S] + [d_i, H_T]\,.$$

In order to illustrate how the *higher order Green functions* appear and how the method works we analyse the commutator $[d_i, H_S]$. The Hamiltonian (2.1) contains four parts. Let us focus on the last term $\sum_{q;jk} \lambda_{jk}^q (a_q^\dagger + a_q) d_j^\dagger d_k$. Using the relations (2.20, 2.21), we can calculate the commutator and obtain:

$$\left[d_i, \sum_{q;jk} \lambda_{jk}^q (a_q^\dagger + a_q) d_j^\dagger d_k \right] = \sum_{q;k} (a_q^\dagger + a_q) d_k.$$

This gives the following new Green function in Eq. (2.19) (we omit the sum) $\left\langle\left\langle (a_q^\dagger + a_q) d_k, d_j^\dagger \right\rangle\right\rangle$. This is a *higher order Green function*. At this point we can for example factorize the function $\left\langle\left\langle (a_q^\dagger + a_q) d_k, d_j^\dagger \right\rangle\right\rangle$ as

$$\left\langle a_q^\dagger + a_q \right\rangle \left\langle\left\langle d_k, d_j^\dagger \right\rangle\right\rangle.$$

With this factorization we obtain a term that is *of the same order* of the initial Green function. This term can then be recollected with the other terms of the left side of Eq. (2.19). Instead of factorizing the new function we can write an EOM for it. Using again the Eq. (2.19) for this new function we obtain:

$$\begin{aligned}
&(\omega + i\eta)\left\langle\left\langle (a_q^\dagger + a_q)d_k, d_j^\dagger \right\rangle\right\rangle \\
= \;& \left\langle a_q^\dagger + a_q \right\rangle \left\langle\left\langle \left\{ d_k, d_j^\dagger \right\} \right\rangle\right\rangle + \left\langle\left\langle \left[(a_q^\dagger + a_q)d_k, H \right], d_j^\dagger \right\rangle\right\rangle . \qquad (2.22)
\end{aligned}$$

We have obtained a new equation that contains other Green functions. We can then factorize them or apply the EOM to them. This procedure has to be applied to every Green function appearing on the right part of the initial equation (2.19). For example the Green functions coming from the other terms of H_S are an energy term (single particle component of H_S) that is already of the same order of the initial Green function $\left\langle\left\langle d_i, d_j^\dagger \right\rangle\right\rangle$, and a term coming from the electron-electron interaction (that can be factorized using the same technique described above for the electron-vibron term). The tunneling Hamiltonian H_T gives rise to the so called lead self-energy in the Green function (awe will see in chapter 3). The idea is to obtain a set of equations like (2.19) and to calculate the initial Green function $\left\langle\left\langle d_i, d_j^\dagger \right\rangle\right\rangle$.

2.3 Density Matrix approach

The other theoretical method we use in our investigations is based on the Density Matrix (DM) formulation. In this context the system is assumed to be almost isolated from the reservoirs. The attention is focused on the evolution of the system *perturbated* by the reservoirs. To this end, the full density matrix of the system coupled to the reservoirs is reduced tracing out the reservoirs degrees of freedom. The tracing procedure produces the so called *Reduced Density Matrix* (RDM). The diagonal entries are called *populations* and the off-diagonal *coherences*. The time-dependence of them describes how the system evolves in time under the influence of the reservoirs. In general all the entries of the *Reduced Density Matrix* have to be taken into account, and this is usually done by the Generalized Master Equation (GME). A simpler description of the system evolution is achieved by taking into account only the populations. This is usually done by using the Master Equation (ME) for the populations, that is the method we use for the thesis. In this chapter we also introduce the GME approach for sake of completeness and in view of possible extensions of the work. We start with the GME and then we introduce the ME.

2.3.1 Generalized Master Equation

The time evolution of the full DM ρ describing the system plus reservoirs is governed by the full Hamiltonian (2.4) and is given by the so-called Liouville-von Neumann equation:

$$i\hbar\frac{\partial\rho}{\partial t} = [H, \rho]\,. \tag{2.23}$$

This equation describes in principle the correct dynamics of the system plus reservoirs but it is in practice impossible to use it directly. This is because the number of degrees of freedom of the reservoirs is in general infinite. Treating the system as almost isolated from the reservoirs, it is possible to introduce the RDM by the following tracing procedure:

$$\sigma = Tr_{Res}\{\rho\} \equiv \sum_{\hat{e}\in Res} <\hat{e}|\rho|\hat{e}>, \tag{2.24}$$

that is a trace of the total density matrix over the degrees of freedom of the reservoirs. The tracing operation reduces the dimension of the problem to the dimension of the system. In this way the problem becomes more simple to handle. Given the RDM (2.24) we need an equation of motion for it. The starting point is the Liouville-von Neumann equation (2.23). The first step is to introduce the interaction picture of the full density matrix in the following way:

$$\tilde{\rho}(t) = \exp\left(\frac{i}{\hbar}(H_S + H_{Res}t\right)\rho(t)\exp\left(-\frac{i}{\hbar}(H_S + H_{Res})t\right). \tag{2.25}$$

The time evolution of $\tilde{\rho}(t)$ is given by:

$$i\hbar\frac{\partial\tilde{\rho}}{\partial t} = \left[\tilde{H}_T, \tilde{\rho}\right], \tag{2.26}$$

where $\tilde{H}_T$ is the interaction picture version of the tunneling Hamiltonian. Using the definition of the RDM (2.24) and the interaction picture version of the full density matrix (2.25) we obtain the following expression for the RDM:

$$\sigma = \exp\left(\frac{i}{\hbar}(H_S)t\right)\tilde{\sigma}\exp\left(-\frac{i}{\hbar}(H_S)t\right), \tag{2.27}$$

where the interaction-picture version for the RDM is $\tilde{\sigma} = Tr_{Res}\{\tilde{\rho}\}$.

The time evolution given by Eq. (2.26) can be integrated from time 0 to time t obtaining the following formal solution:

$$\tilde{\rho}(t) = \tilde{\rho}(0) - \frac{i}{\hbar}\int_0^t dt'\left[\tilde{H}_T(t'), \tilde{\rho}(t')\right]. \tag{2.28}$$

Inserting it back into Eq. (2.26) we obtain the following equation for the evolution of the density matrix:

$$\frac{\partial\tilde{\rho}(t)}{\partial t} = -\frac{i}{\hbar}\left[\tilde{H}_T(t), \tilde{\rho}(0)\right] - \frac{1}{\hbar^2}\int_0^t dt^{'}\left[\tilde{H}_T(t), \left[\tilde{H}_T(t), \tilde{\rho}(t^{'})\right]\right]. \quad (2.29)$$

To proceed further in the derivation, the following standard assumptions are made:

- The external reservoirs are in equilibrium and then the full density matrix can be factorized like $\tilde{\rho}(t) \approx \tilde{\sigma}(t) \otimes \rho_{Res}$
- The system-reservoirs coupling is weak and it is treated as a perturbation at the lowest non-vanishing order
- The dynamics is Markovian, meaning that time-locality is assumed.

Tracing both sides of Eq. (2.29) over the reservoirs degrees of freedom we obtain

$$\frac{\partial\tilde{\sigma}(t)}{\partial t} = -\frac{1}{\hbar^2}\int_0^\infty dt^{'} Tr_{Res}\left\{\left[\tilde{H}_T(t), \left[\tilde{H}_T(t-t^{'}), \tilde{\sigma}(t)\otimes\rho_{Res}\right]\right]\right\}. \quad (2.30)$$

To obtain the Eq. (2.30) we have to assume further that the quantity

$$Tr_{Res}\left[\tilde{H}_T, \tilde{\rho}(0)\right]$$

is zero, that is equivalent to say that $Tr_{Res}\left[\tilde{H}_T, \tilde{\rho}_{Res}\right] = 0$ thanks to the factorization of the total density matrix. This condition means physically that the average of the system-to-reservoirs part of the Hamiltonian over the reservoirs degrees of freedom is zero.

Eq. (2.30) is the starting point for calculating physical quantities. In the following section we introduce ME for the populations.

2.3.2 Master Equation for the populations

The ME is a simpler version of the GME described in the previous section. It does not take into account the off-diagonal entries of the RDM but only the diagonal ones (populations). It has been historically introduced by Pauli. We outline here the essential ingredients. Suppose we are able to diagonalize the Hamiltonian of an isolated system, like for example the one given in (2.1), and to find its eigenstates $|\lambda\rangle$. Introduce the distribution function p_λ, i.e. the probability to find the system in the state $|\lambda\rangle$. Note, that these

states are *many-particle* states, for example for a two-level quantum dot the possible states are $|\lambda\rangle = |00\rangle$, $|10\rangle$, $01|\rangle$, and $|11\rangle$. The first state is empty dot, the second and the third with one electron, and the last one is the double occupied state. The other non-electronic degrees of freedom can be introduce on the same ground in this approach. The only restriction is that some full set of eigenstates should be used

$$\sum_{\lambda} p_{\lambda} = 1. \tag{2.31}$$

The next step is to treat tunneling as a perturbation. Following this idea, the transition rates $\Gamma^{\lambda\lambda'}$ from the state λ' to the state λ are calculated using the Fermi golden rule

$$\Gamma^{fi} = \frac{2\pi}{\hbar} \left| \left\langle f|\hat{H}_T|i \right\rangle \right|^2 \delta(E_f - E_i). \tag{2.32}$$

Then, the master equation can be written as

$$\frac{dp_{\lambda}}{dt} = \sum_{\lambda'} \Gamma^{\lambda\lambda'} p_{\lambda'} - \sum_{\lambda'} \Gamma^{\lambda'\lambda} p_{\lambda}, \tag{2.33}$$

where the first term describes tunneling transition *into the state* $|\lambda\rangle$, and the second term – tunneling transition *out of the state* $|\lambda\rangle$.

In the stationary case the probabilities are determined from

$$\sum_{\lambda'} \Gamma^{\lambda\lambda'} p_{\lambda'} = \sum_{\lambda'} \Gamma^{\lambda'\lambda} p_{\lambda}. \tag{2.34}$$

For noninteracting electrons the transition rates are determined by the single-electron tunneling rates, and are nonzero only for the transitions between the states with the number of electrons different by one. For example, transition from the state $|\lambda'\rangle$ with empty electron level α into the state $|\lambda\rangle$ with filled state α is described by

$$\Gamma^{n_\alpha=1\ n_\alpha=0} = \Gamma_{L\alpha} f_L^0(E_\alpha) + \Gamma_{R\alpha} f_R^0(E_\alpha), \tag{2.35}$$

where $\Gamma_{L\alpha}$ and $\Gamma_{R\alpha}$ are left and right level-width functions

$$\Gamma_{i\alpha} = \frac{2\pi}{\hbar} \sum_{k} |V_{\alpha k}|^2 \delta(E_\alpha - E_k). \tag{2.36}$$

For interacting electrons the calculation is a little bit more complicated. One should establish the relation between *many-particle* eigenstates of the

system and *single-particle* tunneling. To do this, let us note, that the states $|\lambda\rangle$ and $|\lambda'\rangle$ in the golden rule formula (2.32) are actually the states of the whole system, including the leads. We denote the initial and final states as

$$|i\rangle = |\hat{k}_i, \lambda'\rangle = |\hat{k}_i\rangle|\lambda'\rangle, \tag{2.37}$$

$$|f\rangle = |\hat{k}_f, \lambda\rangle = |\hat{k}_f\rangle|\lambda\rangle, \tag{2.38}$$

where $\hat{k}$ is the occupation of the single-particle states in the lead. The parameterization is possible, because we apply the perturbation theory, and isolated lead and nanosystem are independent.

The important point is, that the leads are actually in the equilibrium mixed state, the single electron states are populated with probabilities, given by the Fermi-Dirac distribution function. Taking into account all possible single-electron tunneling processes, we obtain the incoming tunneling rate

$$\Gamma_{in}^{\lambda\lambda'} = \frac{2\pi}{\hbar} \sum_{ik\sigma} f_i^0(E_{ik\sigma}) \left|\left\langle i\bar{k}, \lambda \left| \bar{H}_T \right| ik, \lambda' \right\rangle\right|^2 \delta(E_{\lambda'} + E_{ik\sigma} - E_\lambda), \tag{2.39}$$

where we use the short-hand notations: $|ik, \lambda'\rangle$ is the state with occupied k-state in the $i-$th lead, while $|i\bar{k}, \lambda\rangle$ is the state with unoccupied k-state in the $i-$th lead, and all other states are assumed to be unchanged, E_λ is the energy of the state λ .

To proceed, we introduce the following Hamiltonian, describing single electron tunneling in a more general way with respect to (2.3)

$$\tilde{H}_T = \sum_{k\lambda\lambda'} \left[V_{\lambda\lambda' k} c_k X^{\lambda\lambda'} + V^*_{\lambda\lambda' k} c_k^\dagger X^{\lambda'\lambda} \right], \tag{2.40}$$

the Hubbard operators $X^{\lambda\lambda'} = |\lambda\rangle\langle\lambda'|$ describe transitions between eigenstates of the nanosystem.

Substituting this Hamiltonian one obtains

$$\Gamma_{in}^{\lambda\lambda'} = \frac{2\pi}{\hbar} \sum_{ik\sigma} f_i^0(E_{ik\sigma}) \left|V_{ik\sigma}\right|^2 \left|V_{\lambda\lambda' k}\right|^2 \delta(E_{\lambda'} + E_{ik\sigma} - E_\lambda). \tag{2.41}$$

In the important limiting case, when the matrix element $V_{\lambda\lambda' k}$ is k-independent, the sum over k can be performed, and finally

$$\Gamma_{in}^{\lambda\lambda'} = \sum_{i=L,R} \Gamma_i(E_\lambda - E_{\lambda'}) \left|V_{\lambda\lambda'}\right|^2 f_i^0(E_\lambda - E_{\lambda'}). \tag{2.42}$$

Similarly, the outgoing rate is

$$\Gamma_{out}^{\lambda\lambda'} = \sum_{i=L,R} \Gamma_i(E_{\lambda'} - E_\lambda) \left|V_{\lambda\lambda'}\right|^2 \left(1 - f_i^0(E_{\lambda'} - E_\lambda)\right). \tag{2.43}$$

The current (from the left or right lead to the system) is

$$J_{i=L,R}(t) = e \sum_{\lambda\lambda'} \left(\Gamma^{\lambda\lambda'}_{i\,in} P_{\lambda'} - \Gamma^{\lambda\lambda'}_{i\,out} P_{\lambda'} \right). \tag{2.44}$$

This system of equations solves the transport problem in the sequential tunneling regime. The expression (2.44) takes into account single-electron tunneling processes. Possible higher order processes are neglected in this expression. In the next chapter we address the so called charge-memory effect, using both the EOM and the ME method introduced in the present chapter.

Chapter 3

Single-site junctions: charge memory effects

3.1 Introduction

Within the field of single-molecule electronics [41, 42, 43, 1], beside experimental progress with regard to vibrational properties and their signatures in transport [44, 45, 46, 47, 48], related phenomena such as switching, memory effects and hysteretic behavior in molecular junctions have gained increasing importance and attention. Random and controlled switching of single molecules [9, 28, 35], as well as conformational memory effects [26, 29, 27] have been recently explored. Related to these effects, there is the so-called charge-memory effect, that is basically a hysteretic behavior of the charge-voltage, respectively, current-voltage characteristics arising from the interplay between the polaron shift and Franck-Condon blockade [16] in the presence of electron-vibron interaction. Recent STM experiments [7, 8] show multi-stability of neutral and charged states of single metallic atoms coupled to a metallic substrate through a thin insulating ionic film. The switching was performed by the application of a finite voltage to the STM tip and was explained by the large ionic polarizability of the film [7].

The coupling of a charge to the displacement of ions in the film can be treated as an electron-vibron interaction [31, 32, 33, 34, 21].

We consider a three-terminal device with the central part given by a single level interacting with a vibronic mode (see Fig. 3.1) following essentially our papers [38, 37]. Possible experimental implementations include metal-molecule-metal junctions or STM spectroscopy of a single molecule on a conducting substrate. To describe such a system we use the standard

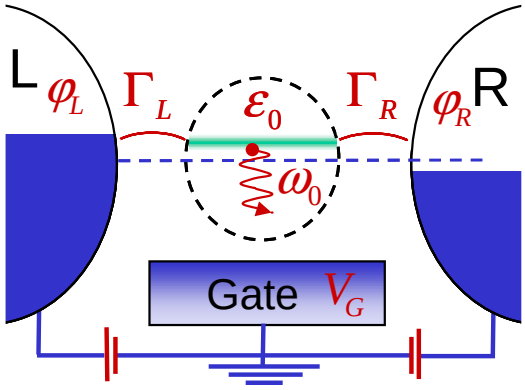

Figure 3.1: Schematic representation of a single-level model system interacting with a vibronic mode and coupled to left and right leads.

electron-vibron Hamiltonian

$$\begin{aligned} H &= (\epsilon_0 + e\varphi_0)d^\dagger d + \omega_0 a^\dagger a + \lambda(a^\dagger + a)d^\dagger d + \\ &\quad + \sum_{i,k}\left[(\epsilon_{i,k} + e\varphi_i)c_{i,k}^\dagger c_{i,k} + (V_{i,k}c_{i,k}^\dagger d + h.c.)\right] . \end{aligned} \tag{3.1}$$

The terms in the first line describe the central system including one electronic state with energy ϵ_0, one vibronic state with frequency ω_0 and their mutual interaction with a coupling strength λ. The second line in Eq. (3.1) contains the Hamiltonian of the two leads with independent-particle states and the tunneling between the leads and the central region via the couplings $V_{i,k}$. The index i denotes the left and right leads, while k labels the electronic states of electrons in the leads. It is convenient to introduce the vibronic "position" and "momentum" operators

$$x = a^\dagger + a \quad ; \quad p = a^\dagger - a\,. \tag{3.2}$$

Starting from the Hamiltonian (3.1), we investigate the charge-memory effect. The energy of the *unoccupied* electron level *without* electron-vibron interaction is ϵ_0 and the *occupied* (charged) state of the *interacting system* will have the energy $\epsilon_1 = \epsilon_0 - \epsilon_p$. The additional term ϵ_p is the so-called polaron shift (or recombination energy). Neutral and charged (polaron) states correspond to local minima of the potential energy surface and they get meta-stable when the electron-vibron interaction is strong enough. Upon applying an external voltage, one can change the state of this bistable system, an effect

that is accompanied by hysteretic charge-voltage and current-voltage curves. In this model we do not include Coulomb interaction.

The energy level ϵ_0 in Eq. (3.1) can be shifted through the gate voltage V_G. We choose $\epsilon_0 = 0$ as reference energy for $V_G = 0$ and assume a linear capacitive coupling, $\epsilon_0 = \alpha e V_G$ setting $\alpha = 1$. The presence of a bias voltage $V_B = \varphi_L - \varphi_R$ can also change the energy of the electronic level via $\varphi_0 = \varphi_R + \eta V_B$. The parameter $0 < \eta < 1$ describes the symmetry of the voltage drop across the junction: $\eta = 0$ corresponds to the completely asymmetric case, while $\eta = 0.5$ stands for the symmetric case. As a result the bias and the gate voltages are taken into account through the potentials of the leads, which can be chosen for example as $\varphi_L = V_B/2$, $\varphi_R = -V_B/2$, and through the effective energy of the level, which is correspondingly $\tilde{\epsilon}_0 = \epsilon_0 + e\varphi_0 = eV_G + e(\eta - 0.5)V_B$. From the expression for $\tilde{\epsilon}_0$ it follows that in the case of asymmetric bias-voltage drop across the junction, $\eta = 0$, the energy of the unoccupied electron level will be centered around the electro-chemical potential of the right lead and moved away from this value through the gate voltage.

This ingredient will be crucial for the effect addressed in this chapter because the additional presence of the polaron shift will then fix the energy of the occupied (charged) state below the electro-chemical potential of the right lead resulting in a blocked charged state under appropriate parameter conditions. In the case of symmetric voltage drop, $\eta = 0.5$, the energy of the unoccupied electron level will be centered around the zero of the energy resulting in a different scenario for what concerns the memory effect. In this chapter we consider the case of an asymmetric junction for which we show that the memory effect occurs for small bias voltage in a wide range of the parameters entering the model Hamiltonian (3.1). The symmetric situation can give rise to a hysteretic behavior as well but only at finite bias voltages, making this case less interesting for the memory effect addressed here.

We show that applying a gate or a bias voltage, it is possible to observe charge-bistability and hysteretic behavior which can be the basis of a charge-memory element. We further perform a systematic analysis of the bistability behavior of the system for different internal parameters such as the electron-vibron and the lead-molecule coupling strength.

3.2 Intermediate coupling to the leads

In this section we consider the polaron problem in the case $\omega_0 \ll \Gamma < \epsilon_p$, corresponding to the regime where the dynamics of internal vibration is slower than the tunneling process. In this situation of intermediate molecule-to-

lead coupling we address the case of time-independent applied voltages, considering then the stationary problem and focusing on the properties of the two charge-states of interest. We consider the parameter ranges for which the fluctuations between the two charge states of interest are negligible. It should be noted that the mean-field solutions we find are meta-stable, but they are physical in the case of very long switching time between them. We call this time τ. The exact equilibrium solution is a superposition of these two states. We assume that all possible relaxation processes are much faster than τ.

3.2.1 Spectral function, average charge and current

We investigate the Hamiltonian (3.1) within the framework of non-equilibrium Green functions [19, 20, 51, 40, 21] in the equation-of-motion (EOM) approach. This allows to study the appearance of the charge-memory effect at different levels of approximation, starting form the self-consistent Hartree level. The analysis is partly built on and further develops ideas introduced in Refs. [49, 50, 32].

This method is an alternative to the Green function techniques earlier applied to the considered problem in Refs. [32, 21, 49, 50]. For a single-level system with Hamiltonian (3.1) the retarded Green function reads

$$G^r(t) = -i\Theta(t)\left\langle\left\{d(t), d^\dagger\right\}\right\rangle . \tag{3.3}$$

From Eq. (3.3) we can obtain the spectral function $A(\epsilon)$ of the system from the expression (2.9). The spectral function is the basic ingredient for obtaining the transport properties of the system such as average current and charge on the molecule. The expression for the current through the molecule is given by [38]

$$I = \frac{e\Gamma_L\Gamma_R}{\Gamma_L+\Gamma_R}\int_{-\infty}^{+\infty} A(\epsilon)[f_L^0(\epsilon - e\varphi_L) - f_R^0(\epsilon - e\varphi_R)]\frac{d\epsilon}{2\pi}, \tag{3.4}$$

where f_i^0 is the equilibrium Fermi function in the i-th lead. The tunneling couplings to the right (Γ_R) and left (Γ_L) leads are

$$\Gamma_i(\epsilon) = 2\pi\sum_k |V_{i,k}|^2\delta(\epsilon - \epsilon_{i,k}), \tag{3.5}$$

where the matrix elements $V_{i,k}$ are assumed to be energy-independent (wide-band limit). The full level broadening is given by the sum $\Gamma = \Gamma_L + \Gamma_R$. Below Γ_R and Γ_L are assumed to be the same.

The average charge (number of electrons), $n = \langle d^\dagger d \rangle$, is obtained from the following equation

$$n = \int_{-\infty}^{+\infty} A(\epsilon) f(\epsilon) \frac{d\epsilon}{2\pi} , \tag{3.6}$$

where $f(\epsilon)$ is the distribution function of electrons inside the molecule and we have used the the Eq.(2.10) expressing the lesser Green function as $G^< = -iA(\epsilon)f(\epsilon)$. For the approximations we will use, we employ the same distribution function as in the non-interacting case,

$$f(\epsilon) = \frac{\Gamma_L f_L^0(\epsilon - e\varphi_L) + \Gamma_R f_R^0(\epsilon - e\varphi_R)}{\Gamma_L + \Gamma_R} , \tag{3.7}$$

because we are focusing on the case of intermediate molecule-lead coupling. Fast tunneling into and out of the molecule makes plausible the assumption that the electrons are in a strong non-equilibrium situation and can then be described via Eq. (3.7) that is obtained assuming only elastic processes. Moreover, within the first approximation we will do , it is possible to obtain the distribution function (3.7) analytically by calculating the lesser Green function of the problem or applying the Hartree approximation directly to the Hamiltonian as in Ref. [32].

3.2.2 Equation of Motion method for the single-level electron-vibron Hamiltonian

Using the EOM method for the Green function introduced in the previous chapter, we perform now two different approximation starting from Hamiltonian (3.1). We apply the Eq. (2.19) Green functions given in Eq.(3.7) obtaining the following set of equations:

$$\begin{aligned} (\epsilon + i\eta) \left\langle\left\langle d, d^\dagger \right\rangle\right\rangle &= 1 + \tilde{\epsilon}_0 \left\langle\left\langle d, d^\dagger \right\rangle\right\rangle + \lambda \left\langle\left\langle xd, d^\dagger \right\rangle\right\rangle \\ &\quad + \sum_{i,k} V_{i,k}^* \left\langle\left\langle c_{i,k}, d^\dagger \right\rangle\right\rangle , \end{aligned} \tag{3.8}$$

$$(\epsilon + i\eta - \epsilon_{i,k}) \left\langle\left\langle c_{i,k}, d^\dagger \right\rangle\right\rangle = V_{i,k} \left\langle\left\langle d, d^\dagger \right\rangle\right\rangle . \tag{3.9}$$

The equation for $\left\langle\left\langle c_{i,k}, d^\dagger \right\rangle\right\rangle$ is closed (including only the function $\left\langle\left\langle d, d^\dagger \right\rangle\right\rangle$). By substituting Eq. (3.9) into Eq. (3.8) and introducing the self-energy Σ of the leads through

$$\Sigma = \sum_{i,k} \frac{|V_{i,k}|^2}{\epsilon + i\eta - \epsilon_{i,k}} , \tag{3.10}$$

we obtain eventually

$$(\epsilon + i\eta - \tilde{\epsilon}_0 - \Sigma) \left\langle\left\langle d, d^\dagger \right\rangle\right\rangle = 1 + \lambda \left\langle\left\langle xd, d^\dagger \right\rangle\right\rangle . \tag{3.11}$$

The last term, describing the interaction between electron and vibron, has to be truncated at this level or found from higher-order equations and then truncated at a higher level of approximation. The lead self-energy will be used below in the wide-band approximation $\Sigma(\epsilon) = -i\Gamma$.

3.2.3 Self-consistent Hartree approximation

The simplest way to close Eq. (3.11) is to perform the truncation by approximating

$$\left\langle\left\langle xd, d^\dagger \right\rangle\right\rangle \approx \langle x \rangle \left\langle\left\langle d, d^\dagger \right\rangle\right\rangle . \tag{3.12}$$

Then we obtain immediately for the Green function

$$G^r_H(\epsilon) = \left\langle\left\langle d, d^\dagger \right\rangle\right\rangle = \frac{1}{\epsilon - \tilde{\epsilon}_0 - \lambda \langle x \rangle + i\Gamma} . \tag{3.13}$$

Here the quantity $\langle x \rangle$ remains to be calculated. To this end we compute, respectively, the time derivatives of the x-operator,

$$i\frac{\partial x}{\partial t} = [x, H] = \omega_0 p , \tag{3.14}$$

and the p-operator,

$$i\frac{\partial p}{\partial t} = \omega_0 x + 2\lambda d^\dagger d . \tag{3.15}$$

Upon combining Eqs. (3.14) and (3.15) we get

$$-\frac{\partial^2 x}{\partial t^2} = \omega_0^2 x + 2\lambda\omega_0 d^\dagger d . \tag{3.16}$$

In the stationary case addressed, Eq. (3.16) yields a direct connection between the "position" of the vibron and the particle number in the dot:

$$\langle x \rangle = -2\frac{\lambda}{\omega_0} \left\langle d^\dagger d \right\rangle = -2\frac{\lambda}{\omega_0} n . \tag{3.17}$$

In view of Eq. (3.13), we finally obtain for the spectral function (2.9) the following self-consistent expression ,

$$A(\epsilon) = \frac{2\Gamma}{\left(\epsilon - \tilde{\epsilon}_0 + 2\frac{\lambda^2}{\omega_0} n\right)^2 + \Gamma^2} . \tag{3.18}$$

This result is equivalent to the one obtained earlier in Refs. [49, 50, 32] using alternative approaches. The same spectral function can be found if one takes the self-energy in Hartree approximation.

3.2.4 Second approximation

In the first approximation above, the self-consistent Hartree treatment, fluctuations of the particle number n and the vibron coordinate x are completely neglected. In order to go one step further and estimate possible corrections, we start from the generated equations for the second-order Green functions, $\langle\langle xd, d^\dagger\rangle\rangle$ and $\langle\langle pd, d^\dagger\rangle\rangle$,

$$\begin{aligned}(\epsilon + i\eta - \tilde{\epsilon}_0)\left\langle\left\langle xd, d^\dagger\right\rangle\right\rangle \\ = \langle x\rangle + \omega_0\left\langle\left\langle pd, d^\dagger\right\rangle\right\rangle + \lambda\left\langle\left\langle x^2 d, d^\dagger\right\rangle\right\rangle + \sum_{i,k} V_{i,k}^*\left\langle\left\langle xc_{i,k}, d^\dagger\right\rangle\right\rangle , \qquad (3.19)\end{aligned}$$

$$\begin{aligned}(\epsilon + i\eta - \tilde{\epsilon}_0)\left\langle\left\langle pd, d^\dagger\right\rangle\right\rangle \\ = \omega_0\left\langle\left\langle xd, d^\dagger\right\rangle\right\rangle + \lambda\left\langle\left\langle pxd, d^\dagger\right\rangle\right\rangle + \sum_{i,k} V_{i,k}^*\left\langle\left\langle pc_{i,k}, d^\dagger\right\rangle\right\rangle . \qquad (3.20)\end{aligned}$$

The second approximation that we consider here is based on the factorization

$$\begin{aligned}\left\langle\left\langle x^2 d, d^\dagger\right\rangle\right\rangle &\approx \langle x\rangle\left\langle\left\langle xd, d^\dagger\right\rangle\right\rangle , \\ \left\langle\left\langle pxd, d^\dagger\right\rangle\right\rangle &\approx \langle x\rangle\left\langle\left\langle pd, d^\dagger\right\rangle\right\rangle + 2\left\langle\left\langle d, d^\dagger\right\rangle\right\rangle , \\ \left\langle\left\langle xc_{i,k}, d^\dagger\right\rangle\right\rangle &\approx \langle x\rangle\left\langle\left\langle c_{i,k}, d^\dagger\right\rangle\right\rangle , \\ \left\langle\left\langle pc_{i,k}, d^\dagger\right\rangle\right\rangle &\approx 0 . \qquad (3.21)\end{aligned}$$

The corresponding set of equations reads

$$\begin{aligned}(\epsilon + i\eta - \tilde{\epsilon}_0 - \Sigma)\left\langle\left\langle d, d^\dagger\right\rangle\right\rangle &= 1 + \lambda\left\langle\left\langle xd, d^\dagger\right\rangle\right\rangle , \\ (\epsilon + i\eta - \tilde{\epsilon}_0 - \lambda\langle x\rangle)\left\langle\left\langle xd, d^\dagger\right\rangle\right\rangle &= \langle x\rangle + \omega_0\left\langle\left\langle pd, d^\dagger\right\rangle\right\rangle + \langle x\rangle\,\Sigma\left\langle\left\langle d, d^\dagger\right\rangle\right\rangle , \\ (\epsilon + i\eta - \tilde{\epsilon}_0 - \lambda\langle x\rangle)\left\langle\left\langle pd, d^\dagger\right\rangle\right\rangle &= \omega_0\left\langle\left\langle xd, d^\dagger\right\rangle\right\rangle + 2\lambda\left\langle\left\langle d, d^\dagger\right\rangle\right\rangle , \qquad (3.22)\end{aligned}$$

from which we obtain the second approximation for the Green function,

$$[G^r(\epsilon)]^{-1} = [G_H^r(\epsilon)]^{-1} - \left(\lambda\langle x\rangle + \frac{\lambda^2}{\omega_0}\right)\frac{\Omega}{\Delta - \Omega} , \qquad (3.23)$$

where we introduced $\Delta = \epsilon + i\eta - \tilde{\epsilon}_0$, $\Omega = \frac{\omega_0^2}{\Delta - \lambda\langle x\rangle}$, and G_H^r is given by the Green function obtained in the Hartree approximation, Eq. (3.13). After inserting the expression (3.17) for the level population $\langle x\rangle$, Eq. (3.23) reads

$$[G^r(\epsilon)]^{-1} = [G_H^r(\epsilon)]^{-1} - (1 - 2n)\,\frac{\lambda^2}{\omega_0}\frac{\Omega}{\Delta - \Omega} . \qquad (3.24)$$

We then calculate the spectral function (2.9) and the average number of electrons, Eq. (3.6). The self-consistent calculation is performed following the chain $G^r(\epsilon) \to A(\epsilon) \to n \to G^r(\epsilon)$.

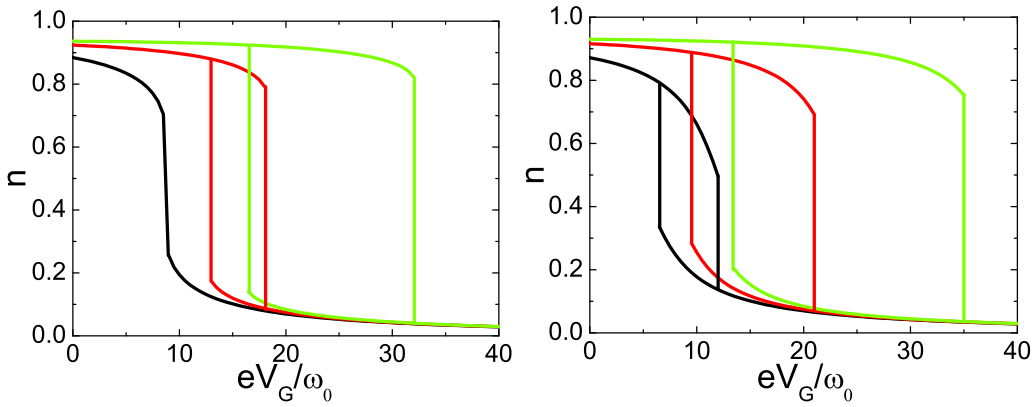

Figure 3.2: Bistable behavior of the level population n in the self-consistent Hartree approximation (left) and second approximation (right) as a function of *gate* voltage for different electron-vibron interaction strength $\lambda = 3\omega_0$ (black), $\lambda = 4\omega_0$ (red), $\lambda = 5\omega_0$ (green), the other parameters are $\Gamma = 5\omega_0$, $T = 0.25\omega_0$, $\eta = 0$ and $V_B = 0$.

Before entering into the discussion of the calculated quantities, we consider the structure of the Green functions obtained in the two different approximations:

- In the limit $\Omega \to 0$ the second approximation reduces to the first one. Although the EOM method is not a systematic expansion, it tells us that the second approximation consistently extends the first one and reproduces it in a limiting case.

- The second term on the right site of Eq. (3.24) represents an additional shift with respect to Eq. (3.13). In the case of very small frequencies ω_0, Eq. (3.24) reduces to $[G_H^r(\epsilon)]^{-1} - (1-2n)\,\lambda^2 \frac{\omega_0}{\Delta(\Delta - \lambda\langle x\rangle)}$, involving the first term of a series expansion in ω_0.

3.2.5 Results and discussion for the intermediate case

Starting from the expressions derived above within the first (self-consistent Hartree) and second approximation we have performed numerical simulations for the average population and current in the molecular junction as a function of gate and bias voltage for the different parameters λ, Γ and T entering the model Hamiltonian. Furthermore we compare the two approximations. The underlying nonlinear equations give rise to bistability in the level population thereby enabling memory effects and affecting the current. Below we analyze

in detail the parameter ranges and conditions for memory effects to occur. We focus here on the case of an asymmetric junction, $\eta = 0$, while keeping the coupling to the leads symmetric, $\Gamma_L = \Gamma_R = \Gamma$, to reduce the parameter space.

First we investigate the gate-voltage dependence of the level population. In Fig. 3.2 it is clearly seen that bistability takes place only at larger values of the electron-vibron coupling λ. The critical values at which bistability occurs and disappears depend on the coupling Γ to the leads and on temperature T; we discuss this parameter dependence below. Note that at large values of λ the level population of the stable states is close to 0 and 1; thus these two memory states are well distinguishable in charge.

Left and right panel of Fig. 3.2, represent the two different levels of approximations in the EOM method. A comparison between them shows that the self-consistent Hartree treatment underestimates the parameter range where bistability occurs: the critical value of λ for the occurrence of bistable behavior is close to $3\omega_0$ (see left panel). At this value a bistable regime has already developed for the second approximation. This can be partially understood taking into account the additional term appearing in the Green function for the second approximation, Eq. (3.24). This term increases the polaron shift thereby enhancing the bistable behavior in the second approximation. Fig. 3.3 shows the bias-voltage dependence of the level population. In this case a qualitative difference arises between electrostatically symmetric ($\eta = 0.5$) and asymmetric ($\eta = 0$) junctions. For asymmetric junctions both states are stable at zero voltage, and both charge states are easily accessible. Asymmetric junctions are thus favorable, since they exhibit memory effects and hysteretic behavior at zero bias, enabling controlled switching upon ramping the bias voltage. For symmetric junctions hysteresis is expected only at finite bias voltage (nonequilibrium bistability [32]), and hence only a single stable state exists at zero bias. Furthermore, at finite voltage the level is only partially occupied by tunneling electrons. These two features render the symmetric system less suited for a memory setup.

We display in Fig. 3.4 the current-voltage characteristics, which reflects the switching behavior of the system. The characteristic feature is a current jump at the bias voltage value where recharging sets in. This behavior can be used to test the state of the system and as readout.

Finally, we depict in Fig. 3.5 "phase diagrams" showing the boundaries between the parameter regions where bistable memory states (below the boundaries in the two panels of Fig. 3.5) and single-valued states exist. The left panel of Fig. 3.5 shows the $\Gamma - T$ parameter plane. The curve separating single-valued and bistable states can be roughly approximated by the condition $\Gamma + T = c(\lambda)$, where $c(\lambda)$ is extracted to be $c(\lambda) \approx \lambda^{1.7}$. This means

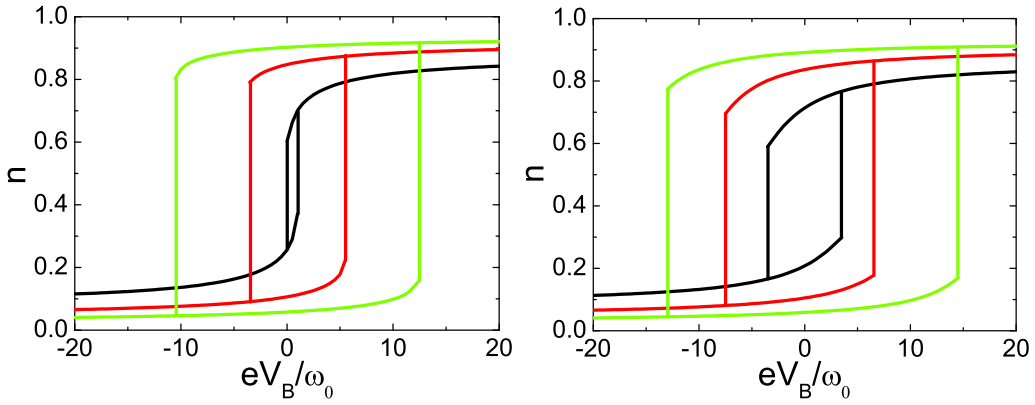

Figure 3.3: Level population n in the self-consistent Hartree approximation (left) and the second approximation (right) as a function of normalized *bias* voltage for different electron-vibron interaction strength $\lambda = 3\omega_0$ (black), $\lambda = 4\omega_0$ (red), $\lambda = 5\omega_0$ (green), the other parameters are $\Gamma = 5\omega_0$, $T = 0.25\omega_0$, $\eta = 0$ and $V_G = \frac{\lambda^2}{\omega_0}$.

that either thermal or quantum tunneling broadening suppresses the hysteresis. The disappearance of the memory effect at high temperature is due to enhanced electron tunneling into the higher-energy state. We note that in the analysis of the temperature dependence the effect of vibronic coordinate fluctuations is neglected that can be relevant close to the threshold between single-valued and bistable regime. The right panel in Fig. 3.5 displays the $\lambda^2 - \Gamma$ parameter plane and shows (on the one hand) that bistable behavior requires increasing electron-vibron coupling λ as long as Γ grows. The boundary between the two regimes is approximately a straight line in the $\lambda^2 - \Gamma$ plane. Hence the condition for finding the memory effect is given by $\Gamma \leq 0.63\lambda^2/\omega_0$. This clearly shows that, for the appearance of the memory effect at low temperature, the level broadening Γ and the polaron shift λ^2/ω_0 are the two energy scales to be compared. A further important conclusion is that the memory effect is suppressed for large coupling to the leads. On the other hand, since larger coupling favors fast information writing and reading and also can additionally suppress effects from quantum tunneling between states, the problem arises to find optimal parameters for utilizing the memory effect. This will be the subject of future work.

To conclude, we considered a *charge-memory effect* and switching phenomena within a single-level polaron model of a molecular junction in the framework of the equation-of-motion approach to the nonequilibrium Green function theory at different levels of approximation. Electrostatically sym-

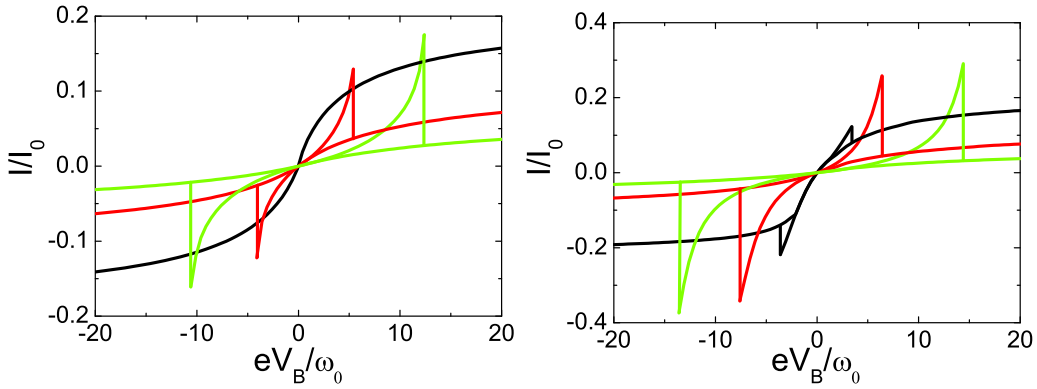

Figure 3.4: Current normalized to $I_0 = \Gamma e/4$ versus bias voltage for the self-consistent Hartree approximation (left) and the second approximation (right) for different electron-vibron interaction strength $\lambda = 3\omega_0$ (black), $\lambda = 4\omega_0$ (red), $\lambda = 5\omega_0$ (green), for the same parameters as in Fig. 3.3.

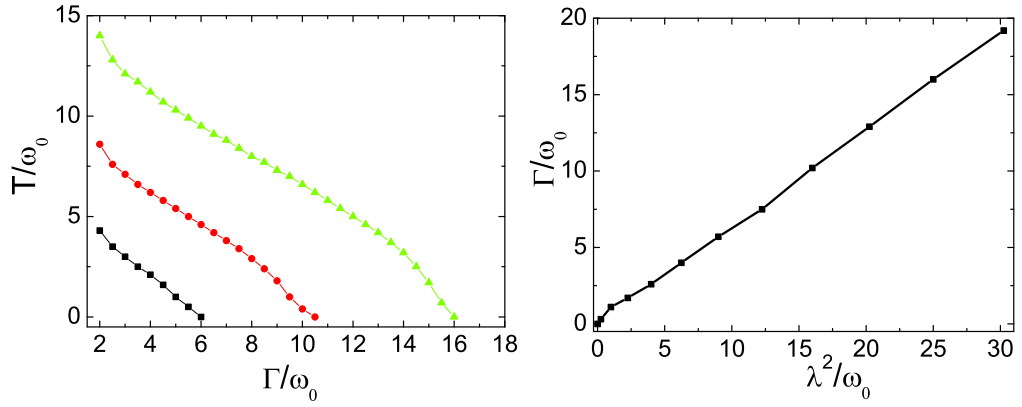

Figure 3.5: "Phase diagram" depicting the boundaries between parameter regimes of bistable memory (below the threshold lines) and single-valued states (above threshold). Left panel: $\Gamma - T$ parameter plane at different electron-vibron interaction strength $\lambda = 3\omega_0$ (black), $\lambda = 4\omega_0$ (red), $\lambda = 5\omega_0$ (green); right panel: $\lambda - \Gamma$ parameter plane for $T = 0.25\omega_0$.

metric and asymmetric junctions show qualitatively different bistability behavior. In the latter case, controlled switching of the molecule is achieved by applying finite voltage pulses. We showed that bistability takes place for sufficiently large electron-vibron coupling for a wide range of further parameters such as molecule-lead coupling and temperature and performed a systematic analysis of this parameter dependence by computing phase diagrams for the

memory effect. In this section we focussed on the investigation of bistability for stationary states. We continue now considering time-dependent phenomena for the charge-memory effect.

3.3 Weak system-to-leads coupling

In the previous section we have investigated the charge-memory effect considering the internal dynamics of the vibration slower than the tunneling events. Now we address time-dependent scenarios. It was shown that quantum switching between the charged and neutral states can limit their lifetime and even result in telegraph noise at finite voltage rather than in a controlled switching [33, 34]. We want to investigate the crossover between these two pictures, depending on the relation between the time-scales of quantum switching and voltage sweep. More precisely, the switching time τ between the two charge states should be compared with the characteristic time of the external voltage sweeping, $\tau_s \sim V(t)/(dV(t)/dt)$. For $\tau \gg \tau_s$, quantum switching can be neglected and hysteresis can be observed, while in the opposite limit, $\tau \ll \tau_s$, the averaging removes the hysteresis. We calculate the charge-voltage curves and describe the crossover between two regimes.

This problem can be solved clearly and transparently in the limit of weak coupling to the leads. For this case the master equation for sequential tunneling can be used.

3.3.1 Eigenstates and Master Equation

The reference model is given in Eq. (3.1). We first introduce explicitly the quantities and the formulas for the master equation, and then we present the results and discuss it. The coupling to the leads is characterized by the level-width function given in Eq. (3.5) In the wide-band limit considered below, the density of states in the leads $\rho(\epsilon)$ is constant and the coupling matrix elements V_{ik} are assumed to be energy-independent, so that Γ_L and Γ_R are constants. The full level broadening is given by the sum $\Gamma = \Gamma_L + \Gamma_R$.

Using the polaron (Lang-Firsov) canonical transformation [56, 49, 65], the eigenstates of the *isolated system* ($\Gamma = 0$) can be calculated exactly

$$|\psi_{nm}\rangle = e^{-\frac{\lambda}{\omega_0}(a^\dagger - a)d^\dagger d}(d^\dagger)^n \frac{(a^\dagger)^m}{\sqrt{m!}}|0\rangle \tag{3.25}$$

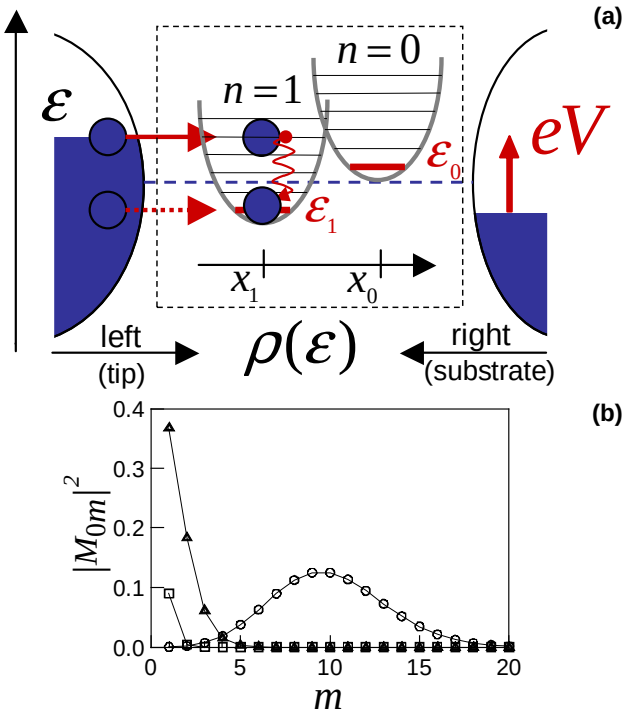

Figure 3.6: (a) The energy diagram of the single-level electron-vibron model, coupled to left and right lead (or tip and substrate in the case of STM). (b) Franck-Condon matrix elements M_{0m} for weak ($g = 0.1$, squares), intermediate ($g = 1$, triangles), and strong ($g = 10$, circles) interaction.

with the eigen-energies

$$E_{nm} = \epsilon_1 n + \omega_0 m, \quad \epsilon_1 = \epsilon_0 - \frac{\lambda^2}{\omega_0}, \quad \epsilon_p = \frac{\lambda^2}{\omega_0}, \tag{3.26}$$

where n denotes the number of electrons, while the quantum number m characterizes vibronic eigenstates, which are superpositions of states with different number of bare vibrons.

When the system is weakly coupled to the leads,

$$\Gamma \ll \omega_0, \epsilon_p, \tag{3.27}$$

the polaron representation, Eqs. (3.25,3.26), is a convenient starting point. The qualitative picture of the sequential tunneling through a polaronic state is given in Fig. 3.6(a). Here the potential energies of the neutral and charged states are sketched as a function of the vibronic coordinate x. When an external voltage is applied, the energy levels are shifted depending on the

asymmetry parameter η. It should be noted that this type of energy diagram is quite general for charge-controlled bistable systems.

In the sequential tunneling regime, the master equation for the probability $p_{nm}(t)$ to find the system in one of the polaron eigenstates (3.25) can be written as [57, 58, 16, 59]

$$\frac{dp_{nm}}{dt} = \sum_{n'm'} \Gamma^{nn'}_{mm'} p_{n'm'} - \sum_{n'm'} \Gamma^{n'n}_{m'm} p_{nm} + I^V[p]. \tag{3.28}$$

Here the first term describes the tunneling transition *into the state* $|n, m\rangle$ and the second term the transition *out of the state* $|n, m\rangle$. $I^V[p]$ is the vibron scattering integral describing the relaxation of vibrons to equilibrium. The transition rates $\Gamma^{nn'}_{mm'}$ are found from the tunneling Hamiltonian (the last term in Eq. (3.1)). Taking into account all possible single-electron tunneling processes, we obtain the incoming and outgoing tunneling rates at zero bias voltage as

$$\Gamma^{10}_{mm'} = \sum_{i=L,R} \Gamma_i(E_{1m} - E_{0m'}) \left|M_{mm'}\right|^2 f_i^0(E_{1m} - E_{0m'}), \tag{3.29}$$

$$\Gamma^{01}_{mm'} = \sum_{i=L,R} \Gamma_i(E_{1m'} - E_{0m}) \left|M_{mm'}\right|^2 \times \left(1 - f_i^0(E_{1m'} - E_{0m})\right). \tag{3.30}$$

Here $f^0(\epsilon)$ is the equilibrium Fermi function, and

$$M_{mm'} = \left\langle 0 \left| \frac{a^m}{\sqrt{m!}} \exp\left[\frac{\lambda}{\omega_0}\left(a^\dagger - a\right)\right] \frac{(a^\dagger)^{m'}}{\sqrt{m'!}} \right| 0 \right\rangle \tag{3.31}$$

is the Franck-Condon matrix element, that is symmetric in $m - m'$ and can be calculated analytically. For $m < m'$ it reads

$$M_{m<m'} = \sum_{l=0}^{m} \frac{(-g)^l \sqrt{m!m'!} e^{-g/2} g^{(m'-m)/2}}{l!(m-l)!(l+m'-m)!}, \tag{3.32}$$

where $g = (\lambda/\omega_0)^2$ is the Huang-Rhys factor [67].

One characteristic feature of these matrix elements in transport is the Franck-Condon blockade [16, 59, 66]: in the case of strong electron-vibron interaction the tunneling with small changes in m is suppressed exponentially, as illustrated in Fig. 3.6(b) for the matrix element $M_{0m} = e^{-g/2}\frac{g^{m/2}}{\sqrt{m!}}$. Hence only tunneling through high-energy states is possible, that is also suppressed at low bias voltage and low temperature.

3.3.2 Charge, current and life-times

The expression for the *average charge* is

$$\langle n \rangle(t) = \sum_m p_{1m}, \tag{3.33}$$

and the *average current* (from the left or right lead) reads

$$I_{i=L,R}(t) = e \sum_{mm'} \left(\Gamma^{10}_{imm'} p_{0m'} - \Gamma^{01}_{imm'} p_{1m'} \right), \tag{3.34}$$

where $\Gamma^{10}_{imm'}$ and $\Gamma^{01}_{imm'}$ are given by the right terms of Eqs. (3.29).

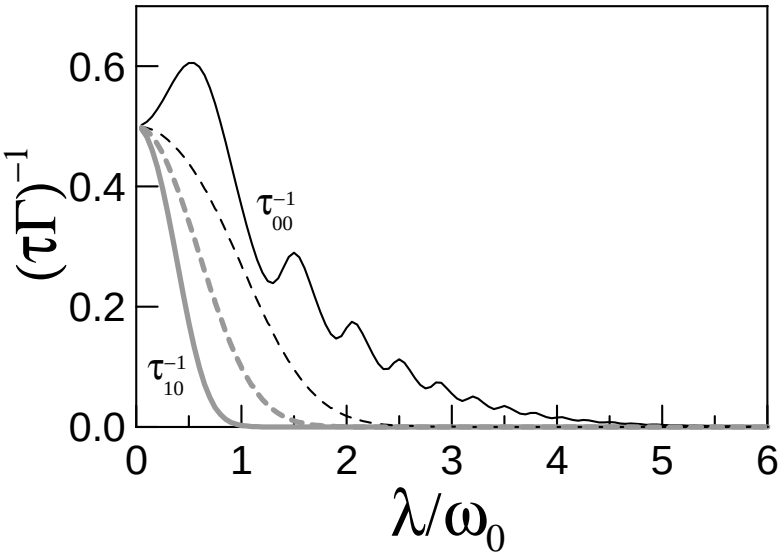

Figure 3.7: Inverse life-time $(\tau\Gamma)^{-1}$ of the neutral state (thin solid line) and the charged state (thick gray solid line) as a function of λ/ω_0 at $\epsilon_0 = \lambda^2/2\omega_0$; and the same at $\epsilon_0 = 0.9\lambda^2/\omega_0$ (dashed lines), $kT = 0.1\omega_0$.

To proceed further, we calculate the characteristic life times of the neutral and charged ground states. The life time τ_{nm} of the generic state $|n, m\rangle$ is given by the sum of the rates of all possible processes which change this state,

$$\tau^{-1}_{nm} = \sum_{n'm'} \Gamma^{n'n}_{m'm}. \tag{3.35}$$

As an example, calculating the life time of the neutral state $|0, 0\rangle$, with an energy higher than the charged ground state $|1, 0\rangle$, we find

$$\tau^{-1}_{00} = \sum_m \sum_{i=L,R} \Gamma_i(E_{1m} - E_{00}) \left| M_{m0} \right|^2 f^0_i(E_{1m} - E_{00}). \tag{3.36}$$

For energy-independent Γ_i (the wide-band limit) we obtain the simple analytical expression

$$\tau_{00}^{-1} = \Gamma \sum_m e^{-g} \frac{g^m}{m!} f^0 \left(\epsilon_0 - \frac{\lambda^2}{\omega_0} + \omega_0 m \right). \tag{3.37}$$

The corresponding expression for the life time of the charged state is (assuming that the equilibrium electro-chemical potential in the leads is zero)

$$\tau_{10}^{-1} = \Gamma \sum_m e^{-g} \frac{g^m}{m!} f^0 \left(-\epsilon_0 + \frac{\lambda^2}{\omega_0} + \omega_0 m \right). \tag{3.38}$$

The dependence of the tunneling rates (3.37,3.38) on the scaled electron-vibron interaction constant λ/ω_0 is shown in Fig. 3.7. It is clearly seen that at large values of λ the tunneling from the neutral state to the charged state and vice versa is exponentially suppressed in comparison with the bare tunneling rate Γ. Hence both states are (meta)stable at low temperatures and zero voltage.

Based on the experimental parameters of Ref. [7], the charged ground state is assumed to be below the equilibrium Fermi energy of the leads, while the neutral ground state is above it. In the experiments [7] the observed relaxation energy $\epsilon_p \approx 2.4$ eV leads to the parameter λ/ω_0 of the order 5 to 10. Thus the system is in the blockade regime at zero voltage, see Fig. 3.7.

Next we consider whether a fast switching between the two states is possible. At finite voltage the switching rates are

$$\begin{aligned} \tau_{00}^{-1} = \sum_m \frac{e^{-g} g^m}{m!} \big[& \Gamma_L f^0 \left(\epsilon_1 + \omega_0 m - (1-\eta) eV \right) \\ & + \Gamma_R f^0 \left(\epsilon_1 + \omega_0 m + \eta eV \right) \big], \end{aligned} \tag{3.39}$$

$$\begin{aligned} \tau_{10}^{-1} = \sum_m \frac{e^{-g} g^m}{m!} \big[& \Gamma_L f^0 \left(-\epsilon_1 + \omega_0 m + (1-\eta) eV \right) \\ & + \Gamma_R f^0 \left(-\epsilon_1 + \omega_0 m - \eta eV \right) \big]. \end{aligned} \tag{3.40}$$

The voltage dependence of the inverse life time $(\tau\Gamma)^{-1}$ is shown in Fig. 3.8 for a junction with the same tunneling coupling, $\Gamma_L = \Gamma_R$, but asymmetric voltage drop ($\eta = 0$), as well as for the completely symmetric junction ($\eta = 0.5$). The results in Fig. 3.8 imply that in both cases one can tune $(\tau\Gamma)^{-1}$ upon sweeping the bias voltage and thereby control the timescales for switching between charged and neutral states. For the symmetric junction both switching rates, τ_{00}^{-1} and τ_{10}^{-1}, (dashed lines) are simultaneously nonzero

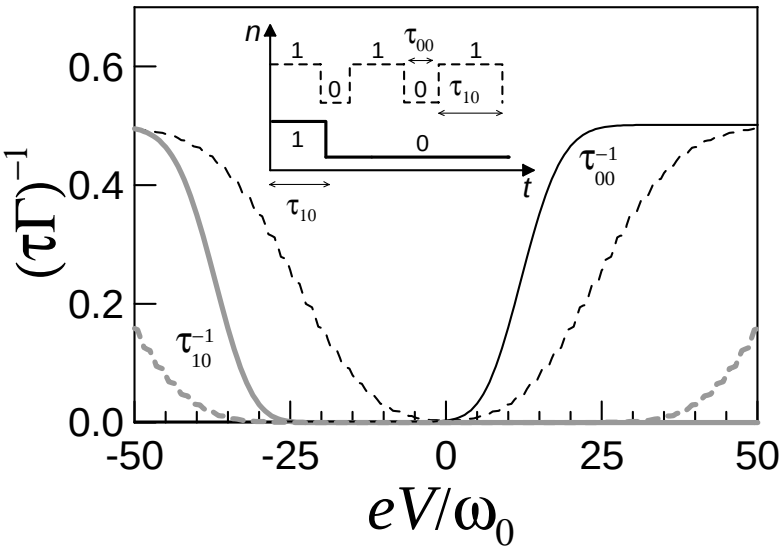

Figure 3.8: Inverse life-time $(\tau\Gamma)^{-1}$ as a function of normalized voltage eV/ω_0 for the asymmetric junction ($\eta = 0$) at $\lambda/\omega_0 = 5$ and $\epsilon_0 = \lambda^2/2\omega_0$ for the neutral state (thin solid line), the charged state (thick gray solid line) and the same for the symmetric junction ($\eta = 0.5$, dashed lines). Inset: random switching between bistable states (dashed line) and single switching into the stable state (full line) after a sudden change of the voltage.

at finite voltage ($eV/\omega_0 \geq 40$ for the parameters of Fig. 3.8) leading to random switching (noise) sketched as dashed line in the inset. On the contrary, for the asymmetric junction controlled switching into the neutral (black solid line) and charged (grey line) state can be achieved at large enough negative and positive voltage, respectively. This qualitatively different behavior is a result of the distinct voltage asymmetry of the two inverse lifetimes which are never both finite. The further peculiar feature of the asymmetric case, namely that the switching rates of the neutral and charged states interchange their role as a function of the bias, i.e., the neutral (charged) state is long-lived at negative (positive) bias, implies hysteretic behavior and a memory effect.

To this end we consider what happens by sweeping the voltage with different velocities. At this point an assumption about the relaxation of vibrons without change of the charge-state should be made. For simplicity we assume that the relaxation of vibrons is fast, $\tau_V \ll \tau, \tau_s$, so that after an electron tunneling event the system relaxes immediately into the vibronic ground state $|1,0\rangle$ or $|0,0\rangle$. In this case the probabilities p_1 of the charged state and p_0 of

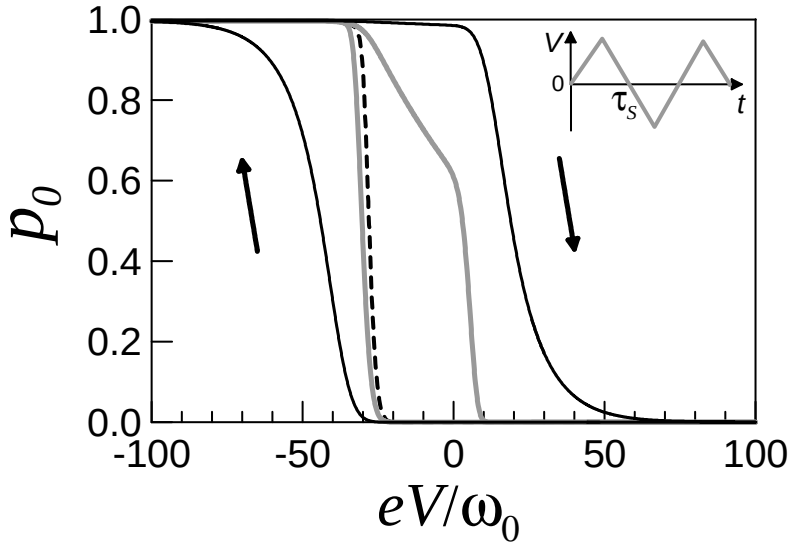

Figure 3.9: Population of the neutral state as a function of normalized voltage eV/ω_0 in the asymmetrical junction ($\eta = 0$) at $\lambda/\omega_0 = 5$ and $\epsilon_0 = \lambda^2/2\omega_0$ for fast voltage sweep (thin solid line), slower sweep (thick gray solid line), and in the adiabatic limit (dashed line). Inset: sketch of voltage time-dependence.

the neutral state are determined by the equations

$$\frac{dp_0}{dt} = \tau_{10}^{-1} p_1 - \tau_{00}^{-1} p_0, \tag{3.41}$$

$$\frac{dp_1}{dt} = \tau_{00}^{-1} p_0 - \tau_{10}^{-1} p_1, \tag{3.42}$$

with the life times τ_{00} and τ_{10} defined in Eqs. (3.39,3.40).

Now let us consider the results for the asymmetric case $\eta = 0$ (Fig. 3.9). If the voltage is changed fast enough, i.e. faster than the life time of charged and neutral states ($\tau \gg \tau_s$ as discussed in the introduction), then both states are stable at zero voltage (hysteresis). In the opposite (adiabatic) limit the voltage change is so slow that the system relaxes into the equilibrium state, and the population-voltage curve is single-valued. Note that this controlled switching is possible only for asymmetric junctions for the reason given above.

3.3.3 Conclusion for weak coupling case

To conclude, we considered a *charge-memory effect* and switching phenomena in taking into account non-stationary effects, in particular the interplay between timescales of voltage sweeping and quantum switching rates from

meta-stable states. We showed that the bistability arises if the quantum switching between neutral and charged states involved are suppressed, e.g. due to Franck-Condon blockade. In the quasi-classical language this means that there are two local minima of the energy and the barrier height between these two states is large enough.

In view of possible experimental realizations and applications of the memory effect, the life time of the memory states should be large compared with the other important time scale of the problem, namely the voltage sweeping time. In this section, employing the time-dependent master equation method, different regimes, characterized by random mutual transitions and by single switching events into a stable configuration are identified. In the latter case, controlled switching of the molecule is achieved by applying finite voltage pulses.

Special attention is paid to the role of the junction asymmetry and its influence on the memory effect. Electrostatically symmetric and asymmetric junctions show qualitatively different bistability behavior. We found that in the case of asymmetric bias-voltage drop across the junction, $\eta = 0$, both neutral and charged states can be unstable at one polarity of bias voltage and stable at the opposite polarity. Under an appropriate choice of parameters, the instability regions for the two memory states do not overlap, thus a definite memory state can be obtained. Moreover both states are (meta)stable at zero bias voltage. Finally, the finite thresholds in bias voltage prevent accidental switching by noise or a weak external signal. These properties enable in principle a memory functionality of the system including writing of two states and readout by a small bias voltage. Note that such an asymmetric case is typically achieved in STM experiments.

In the case of symmetric voltage drop, $\eta = 0.5$, the situation is different. At finite bias voltage the energy level is inside the transport window, between the left and right electro-chemical potential. Consequently, the system is permanently switching between two states, and it is not possible to fix one definite memory state. The symmetric situation can also give rise to a hysteretic behavior but only at finite bias voltages, making this case less interesting for the memory effect addressed here.

Chapter 4

Single-site junctions: spin memory effects

One of the most promising directions in the fields of molecular electronics and spintronics is the experimental and theoretical investigation of spin manipulation in quantum dots and single molecules. In particular, new methods have been recently developed to investigate spin states of single atoms and molecules on substrates using spin-polarized scanning tunneling spectroscopy [53, 52]. Motivated by such achievements the promising question arises whether a single-spin memory effect (namely the controlled switching of the spin state of a single electron using an external voltage applied to a system) is possible. The main challenge is to combine long spin lifetimes and fast switching.

One of the ways for single spin manipulation is based on the interplay of charge, spin, and vibron degrees of freedom in molecular junctions.

In order to investigate those effects, in this chapter we study molecular junctions with ferromagnetic leads essentially following our paper [39]. They give different coupling strength for the two electronic spin species giving the possibility to address spin dependent phenomena. The interplay of spin dependent and switching effects, bring to the idea of spin-memory. This appears as a natural extension of the charge-memory effects addressed in the previous chapter. From a fundamental point of view, such systems are interesting because of the combination of tunneling effects with spin and vibrational effects. From an applied point of view, the effects investigated could bring new possibilities for spin sources based on molecular junctions.

4.1 Model Hamiltonian

In this section we introduce the model we use for our investigation. The system is made of molecule tunnel-coupled to two ferromagnetic leads. The molecule is described with a single spin-degenerate electronic level coupled to a vibronic mode. The leads have have two different magnetization directions, forming an angle θ between each other. The system is sketched in Fig. 4.1

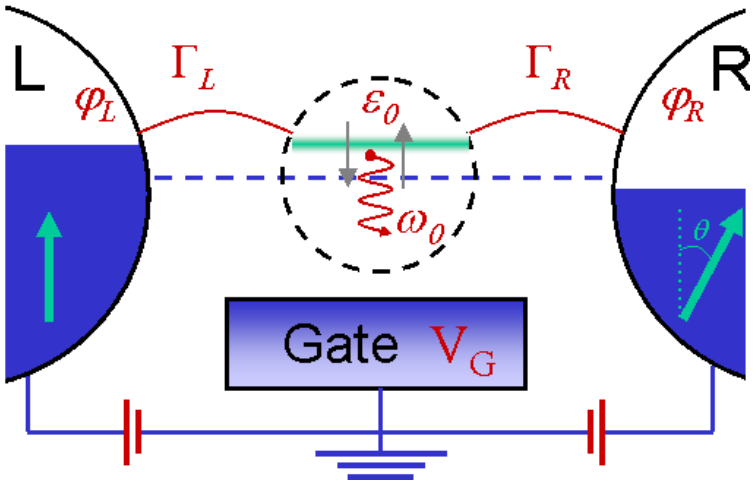

Figure 4.1: Schematization of the Hamiltonian given in Eq. (4.1). The thick dashed (dotted) line represents the on site vibronic (electronic) interaction. The two arrows on top of the leads indicates the magnetization axes in the magnetic leads, with a relative angle θ in the direction of the magnetization

.

and is described by the following Hamiltonian

$$H = \sum_{\sigma} (\epsilon_\sigma + e\varphi_0)\, d_\sigma^\dagger d_\sigma + \omega_0 a^\dagger a + U\hat{n}_\uparrow \hat{n}_\downarrow + \lambda \hat{x} \sum_{\sigma} \hat{n}_\sigma + H_T + H_L, \quad (4.1)$$

where ϵ_σ is the electronic spin-dependent energy, $\varphi_0 = V_R + \eta V_b$ is the shift of the energy levels depending on the asymmetry parameter η, ω_0 is the vibrational frequency and λ and U are the electron-vibron and electron-electron coupling strength respectively. We will consider in the next sections the limit of very large electron-electron interaction. In this which case the double occupancy is negletcted, but the presence of ferromagnetic leads give rise to spin-selective tunneling. This situation is different from the one investigated in the previous chapter. The Hamiltonian (3.1) can be thought as a reduction of a single-degenerate level Hamiltonian in the case of large

electron-electron interaction. Because of the normal metal leads, the tunneling is spin-indipendent in this case and we started directly from the spin-dependent formulation. The leads Hamiltonian in the case of ferromagnetic leadsis

$$H_L = \sum_{ik,\alpha} \epsilon_{ik,\alpha} c^\dagger_{ik,\alpha} c_{ik,\alpha}, \tag{4.2}$$

where i labels the lead, k the energy state in the lead and α indicate the spin according to the relative magnetic field in the considered leads.

We take the orientation of the magnetic field in the left lead as the quantization axes. The magnetic field in the right lead form an angle θ with the left one as showed in Fig. 4.1. We label the electrons in the left lead with $\uparrow$ and $\downarrow$ and the electronic states in the right lead with different indices, $+$ and $-$. The relationship between the spin states of the left and the right lead is given by following rotation matrix

$$R_\theta = \begin{pmatrix} \cos\frac{\theta}{2} & \sin\frac{\theta}{2} \\ -\sin\frac{\theta}{2} & \cos\frac{\theta}{2} \end{pmatrix}. \tag{4.3}$$

Using (4.3) the tunneling Hamiltonians have the following form:

$$H_{T,L} = \sum_{\sigma=\uparrow,\downarrow;k} V_{Lk\sigma} c^\dagger_{Lk\sigma} d_\sigma + h.c, \tag{4.4}$$

for the left lead, and

$$H_{T,R} = \sum_k V_{Rk\uparrow} \left(\cos\frac{\theta}{2} c^\dagger_{Rk\uparrow} + \sin\frac{\theta}{2} c^\dagger_{Rk\downarrow} \right) d_\uparrow + h.c \tag{4.5}$$

$$+ \sum_k V_{Rk\downarrow} \left(\cos\frac{\theta}{2} c^\dagger_{Rk\downarrow} - \sin\frac{\theta}{2} c^\dagger_{Rk\uparrow} \right) d_\downarrow + h.c \tag{4.6}$$

for the right lead. The presence of tunneling processes that mixes the two spin-species imposes the introduction of the off-diagonal terms in the Master Equation and in the Green Function. The description is simplified in the case of collinear magnetic fields: in this case we need only the diagonal terms.

4.2 Weak lead-to-molecule coupling

In this section we investigate a spin memory effect in the case of weak lead-to-molecule coupling. To this end the master equation for sequential tunneling can be used. The controlled switching of the spin state is achieved due

to the interplay between Franck-Condon blockade of electron transport at low voltages and spin-dependent tunneling at high voltages. Spin lifetime, current and spin polarization are calculated as a function of the bias voltage. We also propose to use a third ferromagnetic tunneling contact to probe and readout the spin state.

We study the case of a symmetric junction with anti-parallel magnetizations of left and right leads as in Fig. 4.2; besides the third electrode can be used as a

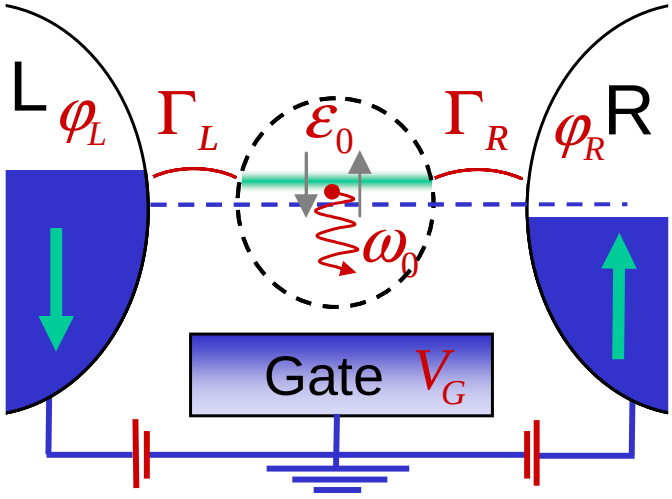

Figure 4.2: Schematic picture of the considered system: a gated single-level quantum dot interacting with a vibron and coupled to ferromagnetic leads.

4.2.1 Model, states and energies

Starting from the general expression of Eq. (4.1), we rewrite it here adapted to the case of anti-parallel magnetizations

$$H = \sum_{\sigma} \tilde{\epsilon}_{\sigma} d_{\sigma}^{\dagger} d_{\sigma} + \omega_0 a^{\dagger} a + \lambda \left(a^{\dagger} + a\right) \hat{n} + U \hat{n}_{\uparrow} \hat{n}_{\downarrow}$$
$$+ \sum_{ik\sigma} \left[(\epsilon_{ik\sigma} + e\varphi_i) c_{ik\sigma}^{\dagger} c_{ik\sigma} + \left(V_{ik\sigma} c_{ik\sigma}^{\dagger} d_{\sigma} + h.c. \right) \right]. \qquad (4.7)$$

Here the first line describes the free electron states with energies $\tilde{\epsilon}_{\sigma}$, the free vibron of frequency ω_0, and the electron-vibron and Coulomb interactions with coupling strength λ and U, respectively; σ is the spin index and $\hat{n}_{\sigma} =$

$d_\sigma^\dagger d_\sigma$, $\hat{n} = \hat{n}_\uparrow + \hat{n}_\downarrow$. The other terms in Eq. (4.7) are the Hamiltonians of the leads and the tunneling coupling ($i = L, R$ is the lead index, k labels the electronic states). The bias voltage V is introduced through the left and right electrical potentials, $V = \varphi_L - \varphi_R$. The energy $\tilde{\epsilon}_\sigma = \epsilon_\sigma + e\varphi_0$ includes the bare level energies ($\epsilon_\uparrow = \epsilon_\downarrow = \epsilon_0$ below) and the electrical potential φ_0 describing the shift of the central level by the gate voltage V_G and by the bias voltage drop between the left and right lead: $\varphi_0 = \varphi_R + \eta(\varphi_L - \varphi_R) + \alpha V_G$, where $0 < \eta < 1$ describes the symmetry of the voltage drop across the junction, $\eta = 0.5$ stands for the symmetric case considered below.

The coupling to the leads is characterized by the level-width function

$$\Gamma_{i\sigma}(\epsilon) = 2\pi \sum_k |V_{ik\sigma}|^2 \delta(\epsilon - \epsilon_{ik\sigma}), \tag{4.8}$$

that is similar to Eq. (3.5) with a spin index σ. In the wide-band limit considered below, the spin-dependent densities of states in the leads and the tunneling matrix elements are assumed to be energy-independent, so that $\Gamma_{L\sigma}$ and $\Gamma_{R\sigma}$ are constants. The full level broadening for a certain spin-species is given by the sum $\Gamma_\sigma = \Gamma_{L\sigma} + \Gamma_{R\sigma}$. Below we consider a symmetric junction with anti-parallel magnetization of the leads and use the notation $\Gamma_{L\downarrow} = \Gamma_{R\uparrow} = \Gamma$ for majority spins and $\Gamma_{L\uparrow} = \Gamma_{R\downarrow} = \kappa\Gamma$ for minority spins, $\kappa \ll 1$.

The spin effects addressed are particularly pronounced in the limit of large U, i.e. we neglect the doubly occupied state, so that only three states in the charge sector should be considered: neutral $|0\rangle$, charged spin-up $|\uparrow\rangle$ and charged spin-down $|\downarrow\rangle$. Employing the polaron canonical transformation [56, 49], the corresponding eigenstates of the isolated system ($\Gamma = 0$) read

$$|\psi_{0q}\rangle = \frac{(a^\dagger)^q}{\sqrt{q!}}|0\rangle, \tag{4.9}$$

$$|\psi_{\sigma q}\rangle = e^{-\frac{\lambda}{\omega_0}(a^\dagger - a)d_\sigma^\dagger d_\sigma} d_\sigma^\dagger \frac{(a^\dagger)^q}{\sqrt{q!}}|0\rangle, \tag{4.10}$$

with the eigenenergies

$$E_{0q} = \omega_0 q, \quad E_{\sigma q} = \tilde{\epsilon}'_\sigma + \omega_0 q, \quad \tilde{\epsilon}'_\sigma = \tilde{\epsilon}_\sigma - \frac{\lambda^2}{\omega_0}, \tag{4.11}$$

where the quantum number q characterizes vibronic eigenstates, which are superpositions of states with different number of bare vibrons.

4.2.2 Rates and Master Equation

Taking into account all possible single-electron tunneling processes for both leads, we obtain the incoming and outgoing tunneling rates

$$\begin{aligned}\Gamma^{\sigma 0}_{qq'} &= \sum_{i=L,R} \Gamma^{\sigma 0}_{iqq'} = \sum_{i=L,R} \Gamma_{i\sigma} \left|M_{qq'}\right|^2 f_i^0(E_{\sigma q} - E_{0q'}) \\ &= \sum_{i=L,R} \Gamma_{i\sigma} \left|M_{qq'}\right|^2 f_i^0(\tilde{\epsilon}'_\sigma + \omega_0(q-q')), \qquad (4.12)\\ \Gamma^{0\sigma}_{qq'} &= \sum_{i=L,R} \Gamma^{0\sigma}_{iqq'} = \sum_{i=L,R} \Gamma_{i\sigma} \left|M_{qq'}\right|^2 \left(1 - f_i^0(E_{\sigma q'} - E_{0q})\right) \\ &= \sum_{i=L,R} \Gamma_{i\sigma} \left|M_{qq'}\right|^2 \left(1 - f_i^0(\tilde{\epsilon}'_\sigma - \omega_0(q-q'))\right). \qquad (4.13)\end{aligned}$$

Here $f_i^0(\epsilon)$ is the equilibrium Fermi function in the lead shifted by the external potential, $f_i^0(\epsilon) = f^0(\epsilon - e\varphi_i)$, and $M_{qq'}$ is the Franck-Condon matrix element that can be calculated analytically (see Refs. [57, 58, 16, 59, 60] for details of the master equation method and calculation of the tunneling rates). The incoming rate $\Gamma^{\sigma 0}_{qq'}$ describes tunneling of one electron with spin σ from the lead to the dot changing the state of the dot from $|0q'\rangle$ to $|\sigma q\rangle$. The outgoing rate $\Gamma^{0\sigma}_{qq'}$ corresponds to the transition from $|\sigma q'\rangle$ to $|0q\rangle$.

In the sequential tunneling regime the master equation for the probability $P_q^n(t)$, $n = 0, \uparrow, \downarrow$ to find the system in one of the polaron eigenstates (4.9), (4.10) can be written as [57, 58, 16, 59, 60]

$$\frac{dP_q^n}{dt} = \sum_{n'q'} \Gamma^{nn'}_{qq'} P^{n'}_{q'} - \sum_{n'q'} \Gamma^{n'n}_{q'q} P^n_q + I^V[P]. \qquad (4.14)$$

Here the first term describes the tunneling transition *into the state* $|nq\rangle$ and the second term the transition *out of the state* $|nq\rangle$. $I^V[P]$ is the vibron scattering integral describing the relaxation of the vibrons to the thermal equilibrium.

4.2.3 Charge, spin polarization and lifetimes

The average charge and the spin polarization are

$$Q = e\sum_q \left(P_q^\uparrow + P_q^\downarrow\right), \quad S = \sum_q \left(P_q^\uparrow - P_q^\downarrow\right), \qquad (4.15)$$

respectively, and the average currents (from the left or right lead) read

$$I_{i=L,R} = e\sum_{\sigma qq'} \left(\Gamma^{\sigma 0}_{iqq'} P^0_{q'} - \Gamma^{0\sigma}_{iqq'} P^\sigma_{q'}\right), \qquad (4.16)$$

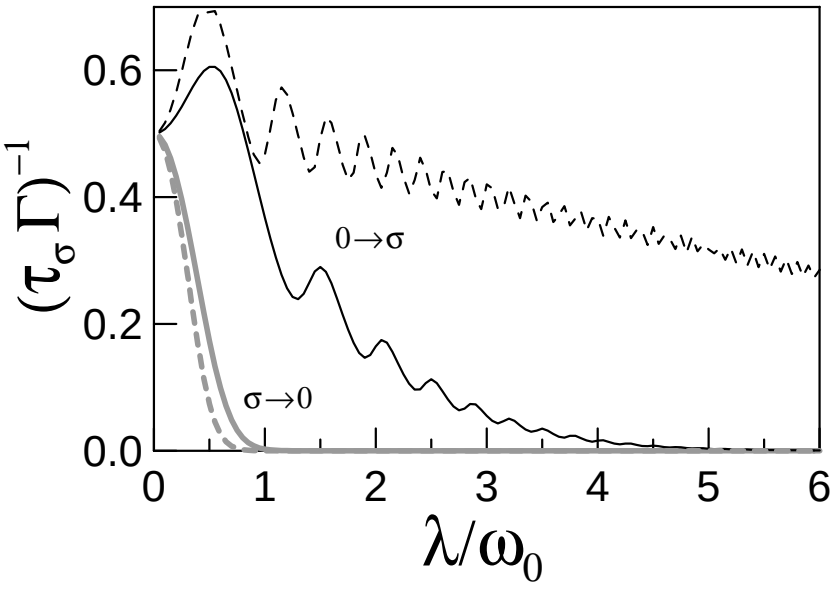

Figure 4.3: Inverse lifetime $\gamma^{\sigma 0}/\Gamma$ of the neutral state (thin solid line) and the inverse spin lifetime $(\tau_\sigma\Gamma)^{-1}$ (thick gray solid line) as a function of the scaled electron-vibron coupling λ/ω_0 at $\epsilon_0 = \lambda^2/2\omega_0$ and at $\epsilon_0 = 0.1\lambda^2/\omega_0$ (corresponding dashed lines), $T = 0.1\omega_0$.

with $\Gamma^{\sigma 0}_{iqq'}$ and $\Gamma^{0\sigma}_{iqq'}$ defined in Eqs. (4.12,4.13).

To proceed further, we calculate the characteristic lifetimes of the neutral, spin-up, and spin-down ground states ($q = 0$). We define the switching rates $\gamma^{\sigma 0}$ from the neutral to the charged state with spin σ and vice-versa as the sum of the rates of all possible processes which change these states:

$$\gamma^{\sigma 0} = \sum_q \Gamma^{\sigma 0}_{q0}, \quad \gamma^{0\sigma} = \sum_q \Gamma^{0\sigma}_{q0}. \tag{4.17}$$

In the sequential tunneling approximation the spin lifetime τ_σ is determined by the switching rate from the charged state $\gamma^{0\sigma}$ through Eqs. (4.13,4.17). It reads (taken zero energy at Fermi level [37], $g = (\lambda/\omega_0)^2$)

$$\tau_\sigma^{-1} = \gamma^{0\sigma} = (1+\kappa)\Gamma \sum_q \frac{e^{-g} g^q}{q!} f^0\left(-\tilde{\epsilon}'_\sigma + \omega_0 q\right). \tag{4.18}$$

At large g the sequential tunneling rates are exponentially suppressed (Franck-Condon blockade) and the cotunneling contribution to τ_σ^{-1} becomes domi-

nant. It can be estimated as [60]

$$\tau_\sigma^{-1(ct)} \approx \frac{\kappa\Gamma^2 T\omega_0^2}{\lambda^4}. \tag{4.19}$$

Although the cotunneling contribution is not suppressed exponentially, it is of second order in the tunneling coupling and suppressed additionally by the small polarization parameter κ and large λ. At typical parameters, considered in this analysis, the cotunneling contribution can be neglected, but it can be essential at larger tunneling couplings and larger temperatures.

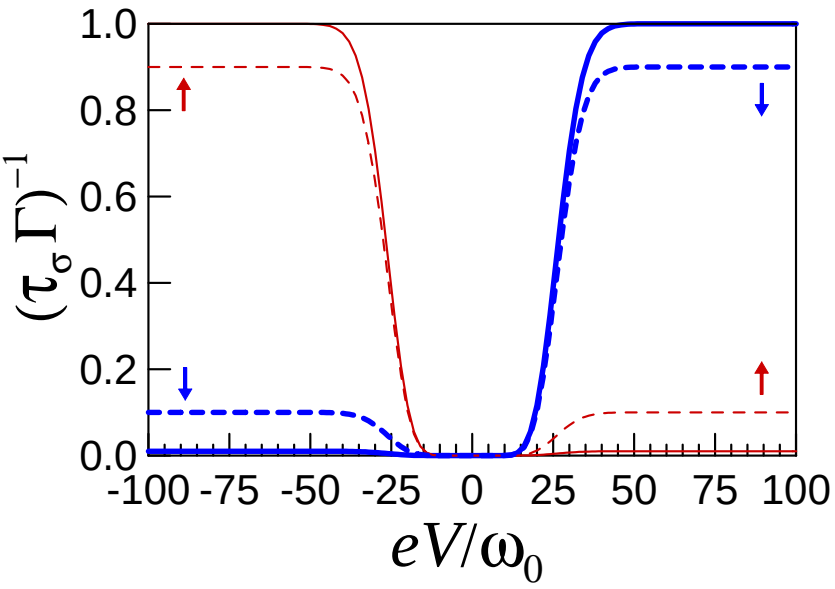

Figure 4.4: Inverse spin lifetime $\tau_\sigma^{-1} = \gamma^{0\sigma}$ as a function of normalized bias voltage eV/ω_0 at $\lambda/\omega_0 = 3$, $\kappa = 0.01$, $\epsilon_0 = \lambda^2/2\omega_0$ for the spin-up state (thin red solid line) and the spin-down state (thick blue solid line) and the same for a less polarized junction ($\kappa = 0.1$, dashed lines).

Fig. (4.3) shows the dependence of τ_σ^{-1} and $\gamma^{\sigma 0}$ on the scaled electron-vibron interaction constant $\sqrt{g} = \lambda/\omega_0$. The transition rates from the neutral state to the charged states and vice versa are suppressed compared to the bare tunneling rate Γ if g is large. Thus all states are meta-stable at low temperatures and zero voltage. Moreover, the lifetime of the charged states can be much larger than that of the neutral state.

In the following we analyze whether fast switching between the two spin states is feasible. To this end we consider voltage sweeps with different

velocities, τ_{exp} being the characteristic time of the voltage change. At this point an assumption about the relaxation time τ_V of the vibrons without change of the charge state is due. We assume that the relaxation is fast, $\tau_V \ll \tau_\sigma, \tau_{exp}$, so that after an electron tunneling event the system relaxes rapidly into the vibronic ground state $|\sigma 0\rangle$ or $|00\rangle$. In this case the probabilities $P^\sigma = \sum_q P^\sigma_q$ of the charged states and $P^0 = \sum_q P^0_q$ of the neutral state are determined from the equations

$$\frac{dP^0}{dt} = \sum_\sigma \left(\gamma^{0\sigma} P^\sigma - \gamma^{\sigma 0} P^0\right), \tag{4.20}$$

$$\frac{dP^\sigma}{dt} = \gamma^{\sigma 0} P^0 - \gamma^{0\sigma} P^\sigma, \tag{4.21}$$

where the switching rates $\gamma^{\sigma 0}$, $\gamma^{0\sigma}$ at finite voltage are calculated from Eqs. (4.12,4.13,4.17):

$$\gamma^{\sigma 0}(V) = \sum_q \frac{e^{-g} g^q}{q!} \left[\Gamma_{L\sigma} f^0\left(\tilde{\epsilon}'_\sigma + \omega_0 q - (1-\eta)eV\right) + \Gamma_{R\sigma} f^0\left(\tilde{\epsilon}'_\sigma + \omega_0 q + \eta eV\right)\right], \tag{4.22}$$

$$\gamma^{0\sigma}(V) = \sum_q \frac{e^{-g} g^q}{q!} \left[\Gamma_{L\sigma} f^0\left(-\tilde{\epsilon}'_\sigma + \omega_0 q + (1-\eta)eV\right) + \Gamma_{R\sigma} f^0\left(-\tilde{\epsilon}'_\sigma + \omega_0 q - \eta eV\right)\right]. \tag{4.23}$$

The voltage dependence of the inverse spin lifetimes is depicted in Fig. 4.4. If the voltage is large enough, the Franck-Condon blockade is overcome and the system is switched into the spin-up (spin-down) state at positive (negative) voltage. If the bias voltage is swept fast enough, i.e. faster than the long spin lifetime at zero voltage, $\tau_{exp} \ll \tau_\sigma(0)$, both spin states can be considered as stable at zero voltage (spin memory effect) and hysteresis can take place. This is shown in Fig. 4.5 where the solid (dashed) lines mark the spin population for increasing (decreasing) bias voltage. In the opposite (adiabatic) limit the voltage change is so slow that the system relaxes into the equilibrium state, and the population-voltage curve is single-valued (Fig. 4.6).

Finally, we study the signatures of the spin polarization in the charge current which is most easily accessible to experiments. In Fig. 4.7 we sketch the bias current and a test current to the additional ferromagnetic electrode, very weakly coupled to the system, so that it does not perturb the state. At large negative voltage applied to the electrode the current is sensitive to the orientation of the magnetization in the test electrode, thus the spin state can

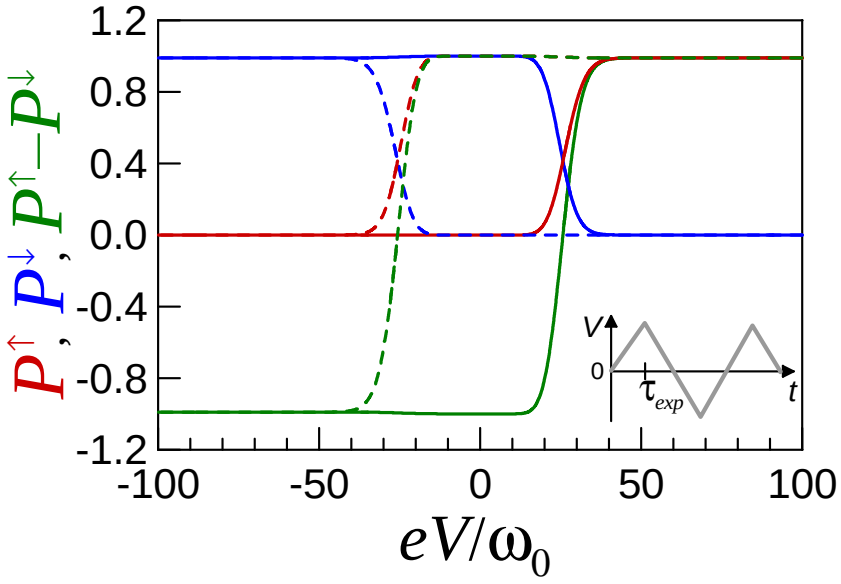

Figure 4.5: Voltage dependence of the populations of the spin-up state (red), spin-down state (blue), and spin polarization (green) for $\lambda/\omega_0 = 3$, $\epsilon_0 = \lambda^2/2\omega_0$, $\kappa = 0.01$, solid (dashed) for increasing (decreasing) voltage.

be monitored during the experiment. Also such a small current can be used to readout the memory element.

We have demonstrated that thanks to the Franck-Condon blockade, the quantum switching between the two spin states of the central system is strongly suppressed at small bias, but applying a finite bias, the population of spin-up and spin-down states can be controlled. By taking into account non-stationary effects, in particular the interplay between the timescales of bias sweeping and spin switching, we show hysteretic behavior and bistability in the spin polarization.

4.3 Intermediate lead-to-molecule coupling

We investigate now the system for non vanishing lead-to-molecule coupling. In this case the Master Equation method is not suitable and we use the EOM technique for the Green functions method. We do not address time-dependent scenarios as before, but we include the electron-electron interaction into account. This is made within the Hartree-Fock approximation, that means we use mean field approximations to treat both electron-vibron and

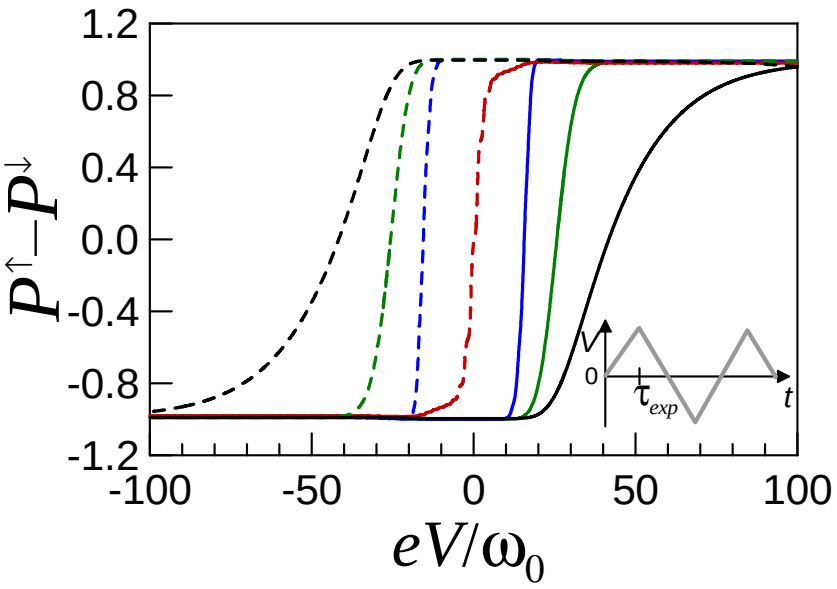

Figure 4.6: Voltage dependence of the spin polarization for $\lambda/\omega_0 = 3$, $\epsilon_0 = \lambda^2/2\omega_0$, $\kappa = 0.01$, for three different sweep velocities $\tau_{exp}\omega_0 = 10^2$ (black), $\tau_{exp}\omega_0 = 10^3$ (green), $\tau_{exp}\omega_0 = 10^5$ (blue) and in the adiabatic limit $\tau_{exp} \to \infty$ (red dashed line).

electron-electron interaction. In order to do that we introduce the following factorizations of the higher order Green functions:

$$\left\langle\left\langle n_{\sigma''} d_\sigma, d^\dagger_{\sigma'} \right\rangle\right\rangle \approx \langle n_{\sigma''} \rangle \left\langle\left\langle d_\sigma, d^\dagger_{\sigma'} \right\rangle\right\rangle \tag{4.24}$$

$$\left\langle\left\langle \hat{x} d_\sigma, d^\dagger_{\sigma'} \right\rangle\right\rangle \approx \langle \hat{x} \rangle \left\langle\left\langle d_\sigma, d^\dagger_{\sigma'} \right\rangle\right\rangle . \tag{4.25}$$

Based on the results obtained for the charge memory effects, we are confident that the mean-field truncations of the Green function gives physical results for the electron-vibron terms. The Coulomb repulsion is then included here in order to see how it modifies the hysteresis given by the vibronic coupling. We are then left with an expression of the Green function that contains both electron-vibron and electron-electron interactions at a mean field level.

As for the weak coupling case, we assume collinear magnetizations in the leads. In this case the Green function of the problem does not contains off diagonal terms because the two spin species are not mixed in the tunnel-

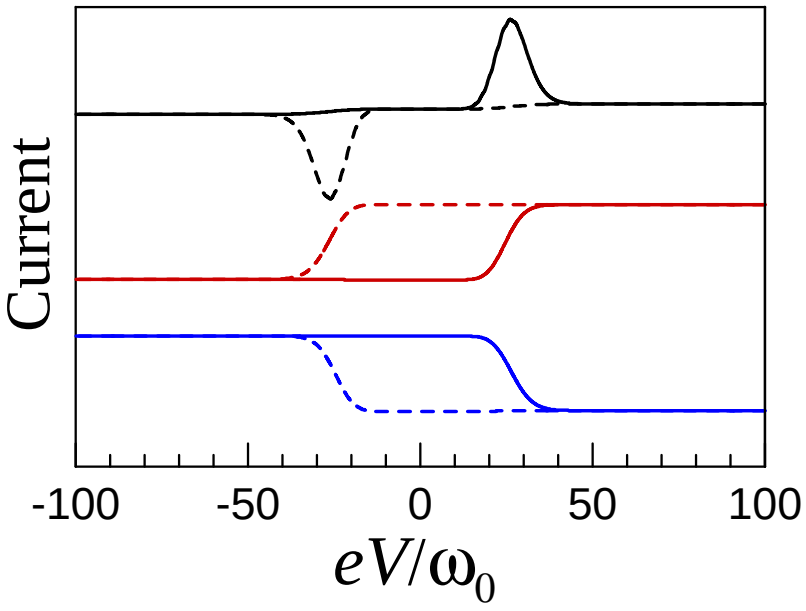

Figure 4.7: Bias current (top black) and test current for spin-up (middle red) and spin-down (bottom blue) test electrode magnetization as a function of normalized voltage eV/ω_0; all other parameters are the same as in Fig. (4.5). The curves are displayed with vertical offset. The magnitude of the test current being much smaller than the bias current, is plotted enhanced.

ing processes. The expression for the spin-dependent Green function is the following one:

$$G^r_\sigma = [\epsilon - \epsilon_0 - \lambda \langle \hat{x} \rangle - U \langle \hat{n}_{\bar{\sigma}} \rangle + i(\Gamma_{L,\sigma} + \Gamma_{R,\pm})]^{-1}\,, \tag{4.26}$$

where $\bar{\sigma}$ represents the other spin with respect to σ and $\pm$ stands for $\uparrow, \downarrow$. This is because an electron with spin σ in the molecule can be coupled with the $\uparrow$ or $\downarrow$ electrons on the right leads depending on the configuration of the magnetizations (parallel or anti-parallel respectively). The mean value of the vibronic position $\langle \hat{x} \rangle$ in the stationary case is

$$\langle \hat{x} \rangle = -2\frac{\lambda}{\omega_0} \langle \hat{n_\uparrow} + \hat{n_\downarrow} \rangle \doteq -2\frac{\lambda}{\omega_0} \langle \hat{n} \rangle\,, \tag{4.27}$$

where $\langle n_\sigma \rangle$ are the mean values of the electronic spin-population in the molecule, and $\langle \hat{n} \rangle$ indicates the total charge in the molecule. The lesser Green function of the electrons inside the molecule in the collinear case is given by following equation

$$G_\sigma^< = -iA_\sigma(f_L + f_R), \tag{4.28}$$

where the leads electrons are taken at thermal equilibrium and distributed according to the Fermi-Dirac distribution. We then calculate the level occupation, the spin-dependent currents and the current-polarization given by the following expression:

$$P = \frac{I_\uparrow - I_\downarrow}{I_\uparrow + I_\downarrow},$$

where

$$I_\sigma = \frac{e\Gamma_L\Gamma_R}{\Gamma_L + \Gamma_R}\int_{-\infty}^{+\infty} A_\sigma(\epsilon)[f_L^0(\epsilon - e\varphi_L) - f_R^0(\epsilon - e\varphi_R)]\frac{d\epsilon}{2\pi}.$$

Results analysis

The plots in Figs. 4.8-4.11 show that the current and the charge inside the molecule assume different values for different spin species. Because of different tunneling couplings for the different spins, we can observe that the bistable behavior is more pronounced for the spin up population. Correspondingly, the spin-polarization of the current oscillates from positive to negative values. The physical mechanism behind the hysteretic behavior is the polaron shift due to the vibronic coupling as in the case of the charge-effects of the previous chapter. The electron-electron interaction shifts the center of the bistable region away from the zero bias voltage, because of the shift introduced in (4.26) by the term $U\langle\hat{n}_{\bar{\sigma}}\rangle$.

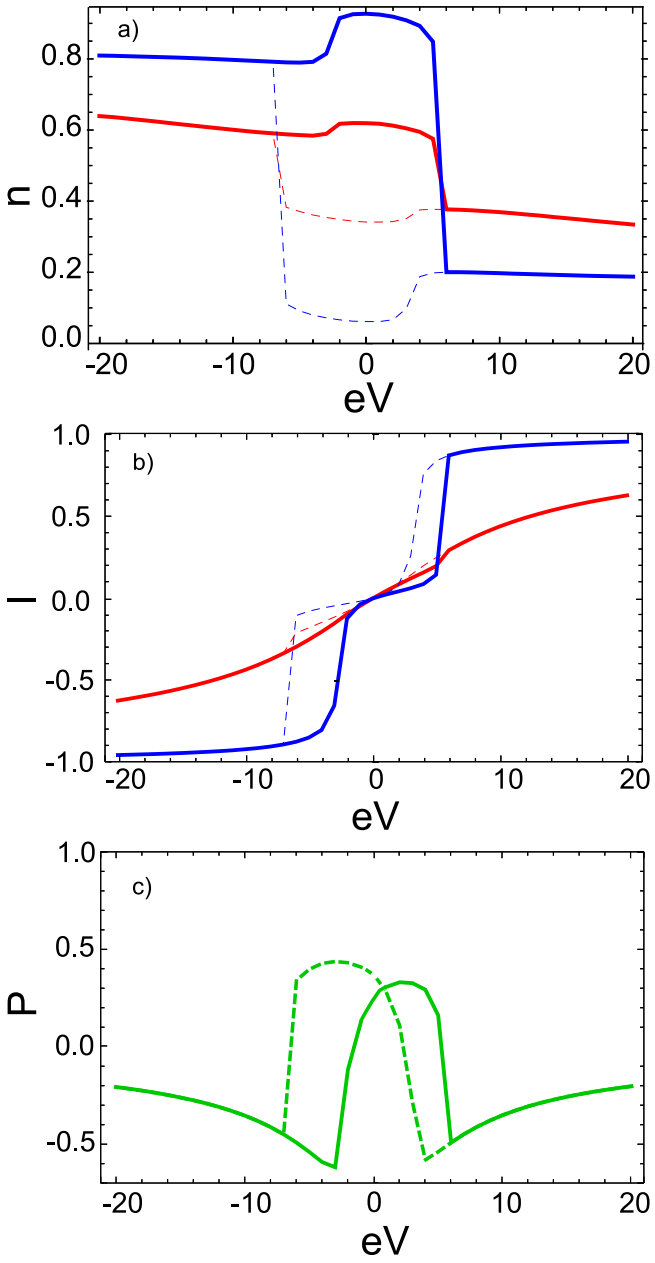

Figure 4.8: a) Spin populations, b) current for the two spin species and c) spin-polarization. In a) and b) the blue curves refer to spin-up and the red curves to spin-up. The full lines refer to increasing values of the voltage and the dashed one to decreasing values. The parameters are $\Gamma_{L,\uparrow} = 1, \Gamma_{L,\downarrow} = 0.1, \Gamma_{R,\uparrow} = 5, \Gamma_{R,\downarrow} = 0.5, \lambda = 0.7, \omega_0 = 0.2, \eta = 0.2, \epsilon_\sigma = 5, U = 0$.

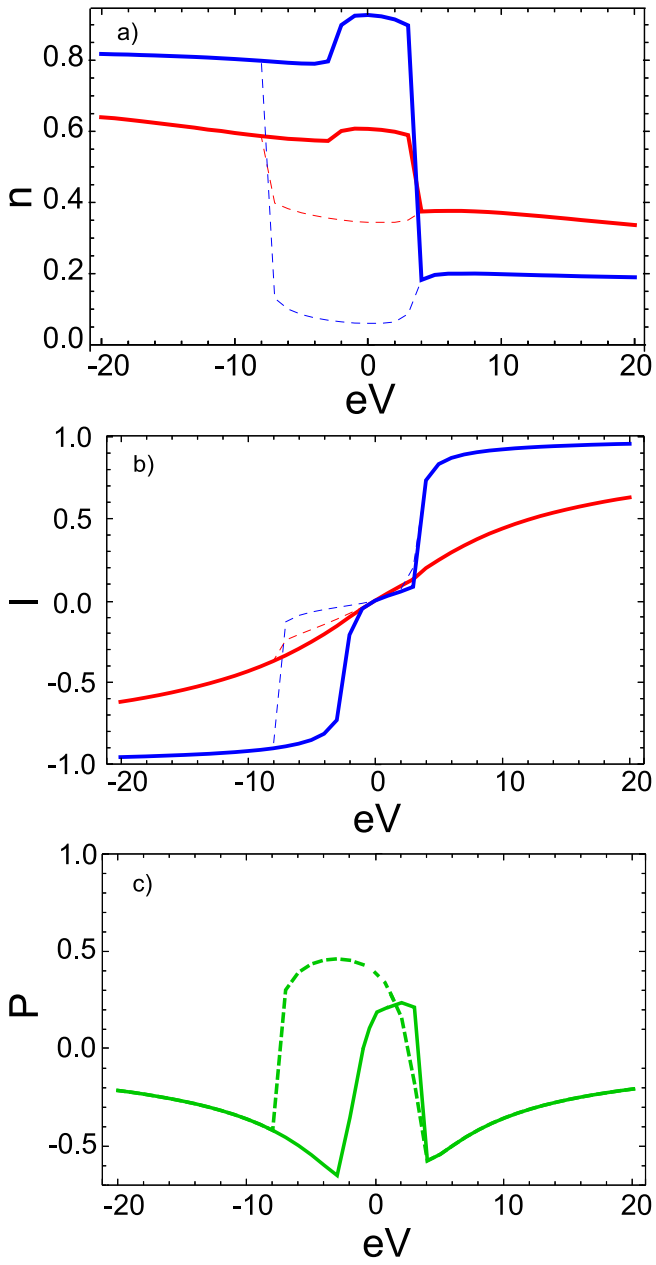

Figure 4.9: a) Spin populations, b) current for the two spin species and c) spin-polarization. In a) and b) the blue curves refer to spin-up and the red curves to spin-up. The full lines refer to increasing values of the voltage and the dashed one to decreasing values. The parameters are $\Gamma_{L,\uparrow} = 1, \Gamma_{L,\downarrow} = 0.1, \Gamma_{R,\uparrow} = 5, \Gamma_{R,\downarrow} = 0.5, \lambda = 0.7, \omega_0 = 0.2, \eta = 0.2, \epsilon_\sigma = 5, U = 0.3$.

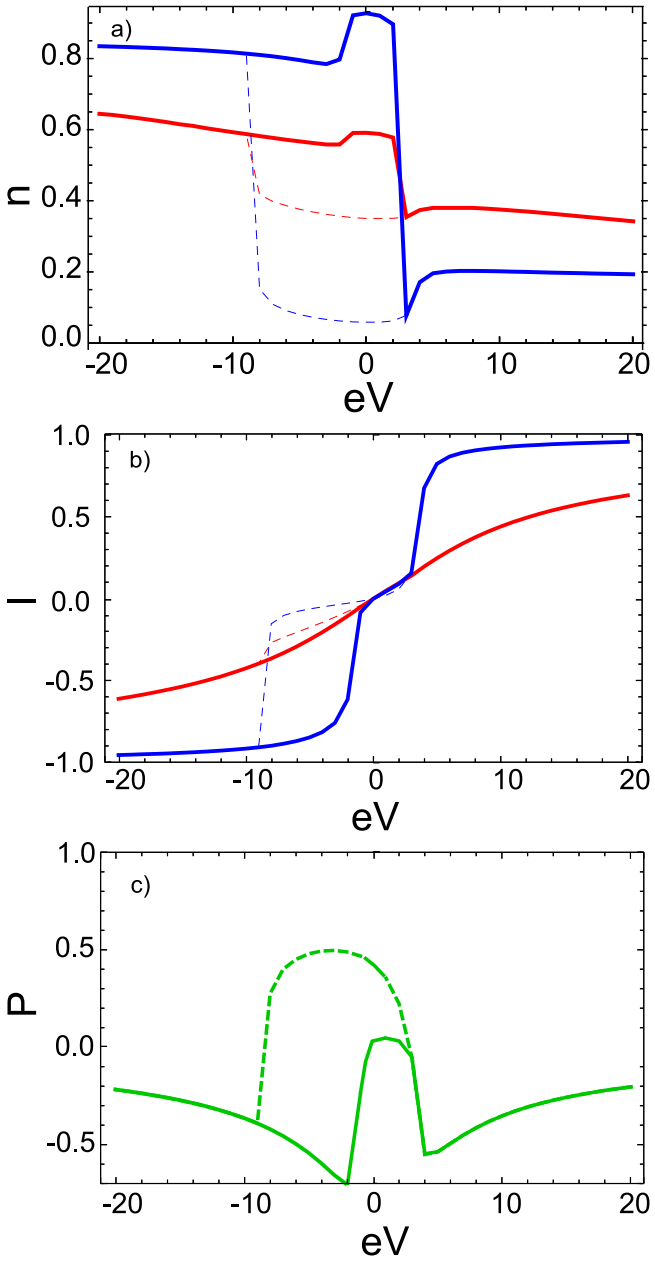

Figure 4.10: a) Spin populations, b) current for the two spin species and c) spin-polarization. In a) and b) the blue curves refer to spin-up and the red curves to spin-up. The full lines refer to increasing values of the voltage and the dashed one to decreasing values. The parameters are $\Gamma_{L,\uparrow} = 1, \Gamma_{L,\downarrow} = 0.1, \Gamma_{R,\uparrow} = 5, \Gamma_{R,\downarrow} = 0.5, \lambda = 0.7, \omega_0 = 0.2, \eta = 0.2, \epsilon_\sigma = 5, U = 0.7$.

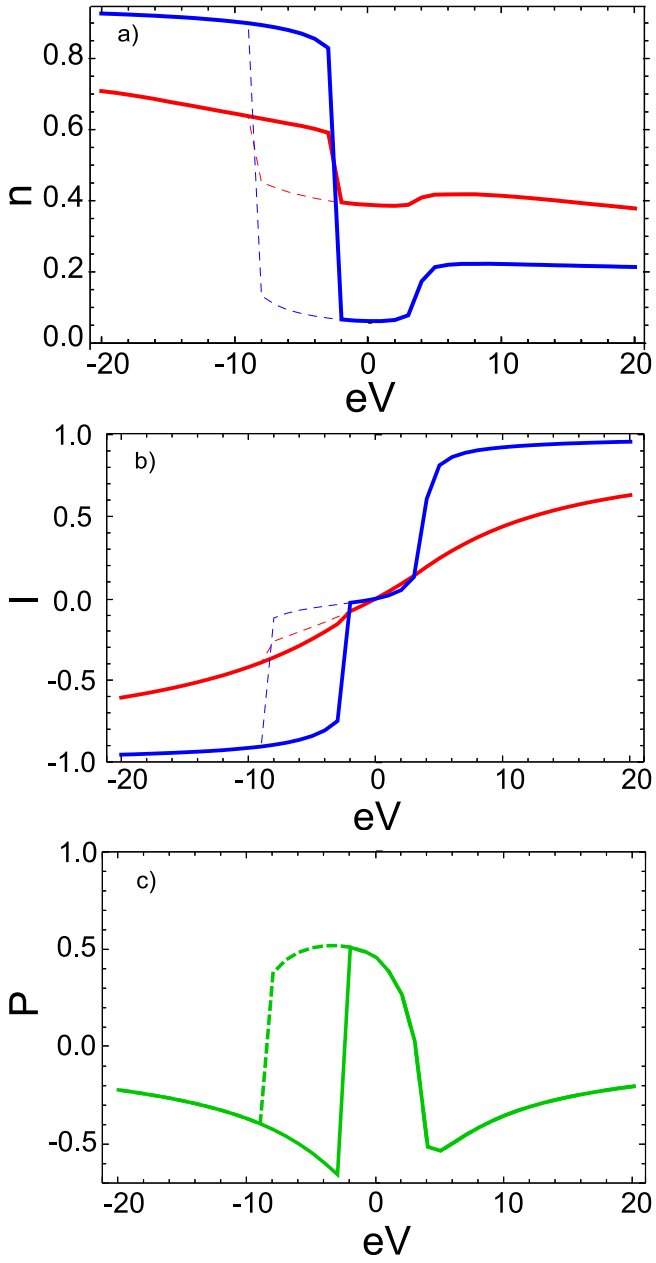

Figure 4.11: a) Spin populations, b) current for the two spin species and c) current-polarization. In a) and b) the blue curves refer to spin-up and the red curves to spin-up. The full lines refer to increasing values of the voltage and the dashed one to decreasing values. The parameters are $\Gamma_{L,\uparrow} = 1, \Gamma_{L,\downarrow} = 0.1, \Gamma_{R,\uparrow} = 5, \Gamma_{R,\downarrow} = 0.5, \lambda = 0.7, \omega_0 = 0.2, \eta = 0.2, \epsilon_\sigma = 5, U = 1$.

Chapter 5

Chains of electron-vibron systems

In this chapter we investigate a natural generalization of the single site junctions discussed in the previous chapters. Instead of having only one electronic level as a bridge between the electrodes, we want now to describe a chain of electronic sites coupled among each other and in presence of electron-vibron interaction. Electron-electron interaction can in principle be present as intra-site and also as inter-site interaction. With a chain of sites it is possible to consider two different kinds of electron-vibron interactions. The general term describing such interaction has the form $\lambda \hat{x} d_i^\dagger d_j + h.c$, where λ is the interaction strength, $\hat{x}$ is the vibron position and the d are electronic operators. If the operators refer to the same electronic level, then we have the same interaction we had in the single site case $\Lambda \hat{y} \hat{n}_i$. We call this term *diagonal* electron-vibron interaction because it has a diagonal structure for what concerns the electronic degrees of freedom of the system. If the operators refer to different electronic sites ($i \neq j$), then we refer to this case as *off-diagonal* electron-vibron interaction. Having in mind this distinction, we write the general Hamiltonian for a chain as follows:

$$\begin{aligned} H &= \sum_{i,\sigma} (\epsilon_{i,\sigma} + \Lambda_i \hat{y}_i) \hat{n}_{i,\sigma} + \sum_{<i,j>,\sigma} (t_{i,j} + \lambda_{i,j} \hat{x}_{i,j}) d_{i,\sigma}^\dagger d_{j,\sigma} \\ &+ \sum_\gamma \omega_\gamma a_\gamma^\dagger a_\gamma + \sum_{<i,j>} \omega_{i,j} a_{i,j}^\dagger a_{i,j} + \sum_i U_i \hat{n}_{i,\uparrow} \hat{n}_{i,\downarrow} + \sum_{<i,j>} V_{i,j} \hat{N}_i \hat{N}_j \\ &+ H_T + H_L. \end{aligned} \tag{5.1}$$

The terms $\hat{y}_i = b_i^\dagger + b_i$ and $\hat{x}_{i,j} = a_{i,j}^\dagger + a_{i,j}$ are the position of the diagonal and off-diagonal vibronic operators. The terms Λ_i and $\lambda_{i,j}$ represent the diagonal and off-diagonal electron-vibron interaction strength. U_i and $V_{i,j}$

are the intra and inter-site Coulomb repulsion. ω_γ are the frequencies of the diagonal vibrons and $\omega_{i,j}$ the off-diagonal ones. The notation $< i, j >$ stands for nearest neighbor and $\hat{N}_i = \hat{n}_{i,\uparrow} + \hat{n}_{i,\downarrow}$. The tunneling between the system and the leads is obtained coupling the first electronic level to the left lead and the last one (N-th level) to the right lead

$$H_T = \sum_k V_{L,k} c^\dagger_{L,k} d_1 + V_{R,k} c^\dagger_{L,k} d_N + h.c.. \tag{5.2}$$

As usual we assume that the leads are Fermi-seas at thermodynamical equilibrium described by the Fermi-Dirac distribution. The model can be used in principle to describe various physical systems. For example one could think of having a chain of small molecules or building blocks being connected in series and having on-site (diagonal) electron-vibron interaction; or oligophenyl-like systems where the different orientation of the rings may oscillate around equilibrium positions, describing the inter-level tunneling through off-diagonal (nearest neighbor) vibronic coupling. In the next sections we will analyze a two sites and a three sites chains. The idea is to generalize the discussion of the memory effects studied in the single site case.

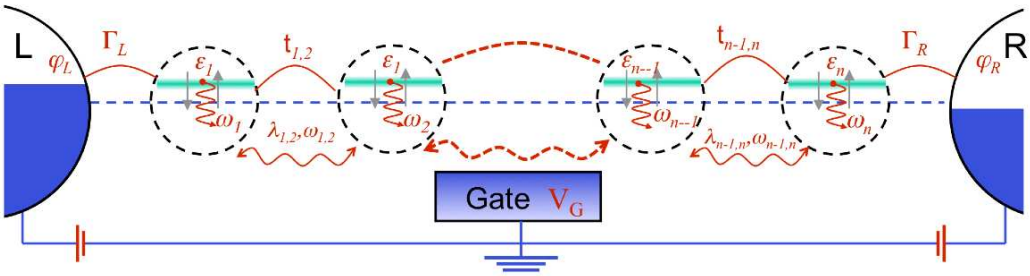

Figure 5.1: The scheme shows a generic chain-like system. The system contains N electronic levels, every level can be occupied by two electrons (the two spin-arrows). The diagonal electron-vibron interaction is represented by the wavy line inside the circle, while the off-diagonal vibrational coupling connects two neighbor circles (also wavy line). The standard inter-dot tunneling is represented by the straight line. The chain is connected to the leads through two tunneling couplings. The electron-electron interaction is not schematically represent because in the following we will focus mainly on the electron-vibron interaction.

5.1 Two-level-systems: intermediate coupling

As already introduced in the previous section, we start the discussion analyzing a two electronic level system, as a natural generalization of the single site junctions. The problem of two levels in presence of vibrational coupling has been studied in different works in the literature addressing aspects like transport in flexible junctions [61], dynamical symmetry breaking [17], nonequilibrium vibrations [81] and rectification [62]. We concentrate on the case of off-diagonal vibrational coupling, where the inter-level electronic tunneling is modulated by the presence of the vibron. The general Hamiltonian for such a system is obtained reducing Eq. (5.1) to two sites:

$$H = \sum_{\sigma=\uparrow,\downarrow} \epsilon_1 \hat{n}_{1,\sigma} + \epsilon_2 \hat{n}_{2,\sigma} + \left[t + \lambda(a^\dagger + a)\right] \sum_{\sigma=\uparrow,\downarrow} (d^\dagger_{1,\sigma} d_{2,\sigma} + h.c) + \sum_{i=1,2} U_i \hat{n}_{i,\uparrow}\hat{n}_{i,\downarrow} + V\hat{N}_1\hat{N}_2 + \omega_0 a^\dagger a + H_T + H_L, \tag{5.3}$$

The Hamiltonian (5.3) can mimic a biphenyl in which each ring has been modeled as a single level dot with spin degeneracy. The torsional vibration between the two rings is modeled via one vibron that couples the two dots. Considering the case of very large Coulomb interaction, we can neglect double occupancy of the electronic levels and reduce the Hamiltonian (5.3) to the following form:

$$H = \sum_{i=1,2} \epsilon_i \hat{n}_i + \left[t + \lambda(a^\dagger + a)\right](d^\dagger_1 d_2 + h.c.) + \omega_0 a^\dagger a + H_T + H_L, \tag{5.4}$$

where H_L describes the leads as Fermi-Dirac reservoirs and the tunneling Hamiltonian is obtained from Eq. (5.2) and is given by

$$H_T = \sum_k V_{L,k} c^\dagger_{L,k} d_1 + V_{R,k} c^\dagger_{L,k} d_2 + h.c.$$

The Hamiltonian describes a system sketched in Fig. 5.2.

In the case of intermediate leads-to-molecule coupling we handle the Hamiltonian (5.4) with the EOM method for the NEGF. We perform truncation for the electron-vibron interaction as already done in the single-level case. The retarded green function matrix-elements $\left\langle\left\langle d_i, d^\dagger_j \right\rangle\right\rangle$ are obtained with the EOM technique discussed in the second chapter (see Eq. (2.19)). We express the result in matrix form:

$$\begin{pmatrix} \epsilon + i\eta - \epsilon_1 - \Sigma_L & -(t + \lambda\langle\hat{x}\rangle) \\ -(t + \lambda\langle\hat{x}\rangle) & \epsilon + i\eta - \epsilon_2 - \Sigma_R \end{pmatrix} \cdot \mathbf{G^r} = \mathbf{1}. \tag{5.5}$$

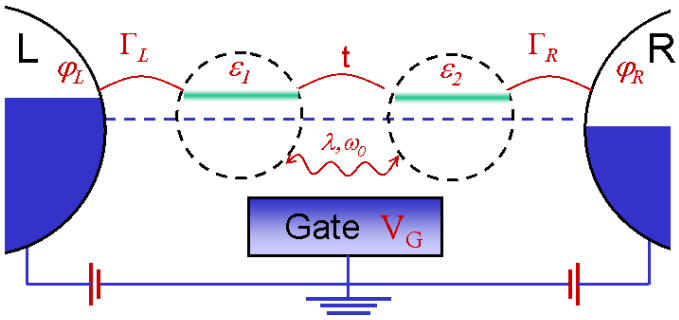

Figure 5.2: Schematic representation of the Hamiltonian given in Eq. (5.4). The lines between the 2 dots represent the tunneling coupling between them (straight line) and the vibronic coupling (wawy line).

The self-energies at this level are considered in the wide-band limit, i.e. they are constant and purely imaginary $\Sigma_i \equiv -i\Gamma_i$. In the Eq. (5.5) it remains to have an expression for the mean value of the vibronic operator $\langle \hat{x} \rangle$. The mean value $\langle \hat{x} \rangle$ can be obtained through the equation of motion for the operator $\hat{x}$ in the Heisenberg representation:

$$i\frac{d\hat{x}}{dt} = [\hat{x}, H] = \omega_0 \hat{p}. \tag{5.6}$$

The $\hat{p}$ operator is given by $a - a^\dagger$ and the EOM for it reads:

$$i\frac{d\hat{p}}{dt} = [\hat{p}, H] = \omega_0 \hat{x} + 2\lambda \left(d_1^\dagger d_2 + d_2^\dagger d_1 \right). \tag{5.7}$$

Assuming to be in the stationary limit where the mean values of the operators are time-independent, from the Eq. (5.7), we obtain the following expression:

$$\langle \hat{x} \rangle = -2\frac{\lambda}{\omega_0} \left(\left\langle d_1^\dagger d_2 \right\rangle + \left\langle d_2^\dagger d_1 \right\rangle \right) = -2\frac{\lambda}{\omega_0} \left(\langle n_{12} \rangle + \langle n_{21} \rangle \right). \tag{5.8}$$

With the equation (5.8) the Eq. (5.5) reads

$$\begin{pmatrix} \epsilon + i\eta - \epsilon_1 - \Sigma_L & -t + 2\frac{\lambda^2}{\omega_0} \left(\langle n_{12} \rangle + \langle n_{21} \rangle \right) \\ -t + 2\frac{\lambda^2}{\omega_0} \left(\langle n_{12} \rangle + \langle n_{21} \rangle \right) & \epsilon + i\eta - \epsilon_2 - \Sigma_R \end{pmatrix} \cdot \mathbf{G^r} = \mathbf{1}. \tag{5.9}$$

The elements $\langle n_{ij} \rangle$ can be expressed in term of the spectral density $n_{ij}(\epsilon) = -2\Im\left[G_{i,j}\right]$ and the distribution function $f(\epsilon) = \frac{\Gamma_L f_L(\epsilon) + \Gamma_R f_R(\epsilon)}{\Gamma_L + \Gamma_R}$ with the following equation (see Eqs. (2.9, 2.10)):

$$n_{ij} = \int A_{ij}(\epsilon) f(\epsilon) \frac{d\epsilon}{2\pi}. \tag{5.10}$$

Considering the expression given in Eq. (5.10), we get a self-consistent problem for the retarded Green function $\mathbf{G^r}$. The equation (5.9) can be written in a more compact way introducing the energy matrix and the self-energy matrix, namely

$$\mathbf{E} = \begin{pmatrix} \epsilon_1 & t \\ t & \epsilon_2 \end{pmatrix}, \tag{5.11}$$

and

$$\mathbf{\Sigma} = \begin{pmatrix} \Sigma_L & -2\frac{\lambda^2}{\omega_0}\left(\langle n_{12}\rangle + \langle n_{21}\rangle\right) \\ -2\frac{\lambda^2}{\omega_0}\left(\langle n_{12}\rangle + \langle n_{21}\rangle\right) & \Sigma_R \end{pmatrix}. \tag{5.12}$$

Using the expressions (5.11, 5.12), the equation for the Green function (5.9) can be written in the following form:

$$\mathbf{G^r} = \left[(\epsilon + i\eta)\mathbf{1} - \mathbf{E} - \mathbf{\Sigma}\right]^{-1}, \tag{5.13}$$

that is the usual way to express it. All the informations concerning interactions and tunneling phenomena, are contained in the self-energy $\mathbf{\Sigma}$. Using the formulas derived above, we can describe the system at intermediate leads-to-molecule coupling, meaning that the tunneling coupling is finite. In the following we show the plots of the relevant physical quantities (electronic populations, currents and oscillator position) as a function of the different parameters. We show normal plots and contour-plots, exploring a large range of parameters in order to have a more complete and systematic understanding of the system. The system is studied in two different regimes, namely the case of bias-independent and bias-dependent energy levels. More precisely, for the bias-dependent case, we use two parameters to describe the shift of the position of the levels $\epsilon_i = \epsilon_0 + \varphi_i V$ where $\varphi_i = \varphi_R + \eta_i(\varphi_L - \varphi_R)$.

5.1.1 Bias-independent and bias-dependent energy levels

In Fig. 5.3 we show the results in the bias-independent case. We observe a characteristic jump of the current at a given value of the bias voltage(twice the value of the energy of the electronic levels) , corresponding to a maximum displacement of the vibronic position. After the jump, the current shows a plateau, that correspond to a return toward the equilibrium position of the oscillator. In addition to that, we can see that the electronic populations of the two levels are switched between each other going from almost zero to almost one and vice-versa. Basically we observe that there is a transfer of the charge from one dot to another in correspondence of the jump of the current (and also the maxima of the vibronic position).

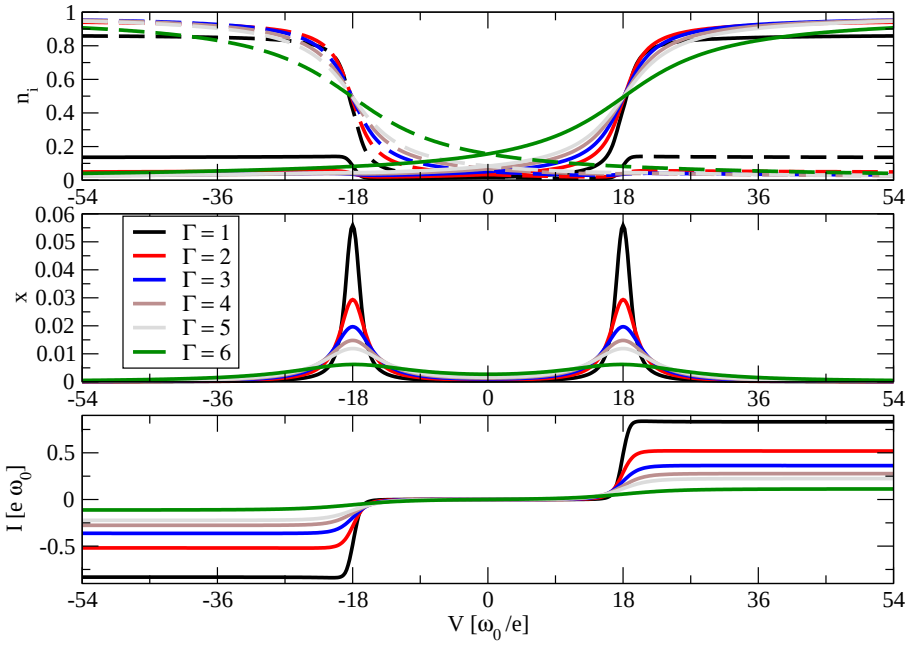

Figure 5.3: Mean number of electrons, mean position and current of a double dot with vibrational coupling as discussed in the model. The parameter here are the following: $t = \lambda = 0.3, T = 0.03, \epsilon_i = 9$. The different curves correspond to differer values of the coupling to the leads Γ. The values are $\Gamma = 1, 2, 3, 4, 5, 6$ from green to black. The system is in the bias-independent case, ie. the bias voltage does not affect the energy levels.

In the bias dependent-case, showed in Fig. 5.4, we obtain a different behavior. The current reach first a maximum and then decays to zero, in contrast with the bias-independent case. Corresponding to the maxima there is a transfer of the charge from one electronic level to the other one, similarly to the previous case. Increasing the bias the two populations reach the same value. In this case the position of the vibron has a maximum at zero bias voltage and then decreases to zero for higher voltages.

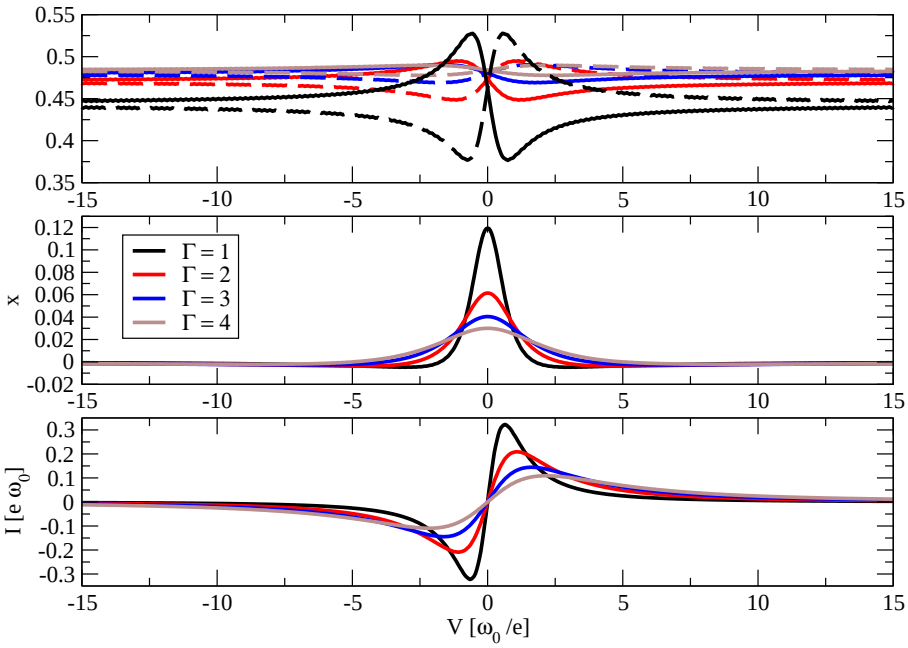

Figure 5.4: Mean number of electrons, mean position and current of a double dot with vibrational coupling as discussed in the model. The parameter here are the following: $t = \lambda = 0.3, T = 0.03, \epsilon_i = 9$. The different curves correspond to different values of the coupling to the leads Γ. The values are $\Gamma = 1, 2, 3, 4$ from brown to black. In this case we consider the bias-dependent case, i.e. the energy levels of the two dots are shifted when a bias voltage is applied as discussed and $\eta_1 = 1$, $\eta_2 = 0$.

5.1.2 Extended analysis for the bias-dependent case

In the previous section we showed and analyzed two sets of plots describing the bias-independent and the bias-dependent situation. In this section we introduce and comment contour-plots obtained for the bias-dependent case. As in the previous section we calculate current, vibronic position and right-left electronic populations. All the sets of plots show on the first row the electronic populations and on the second row the current (left) and the vibronic position (right). Those contour-plots are introduced in order to give a better and wide description of the physics of the system, that contains a rich parameter space.

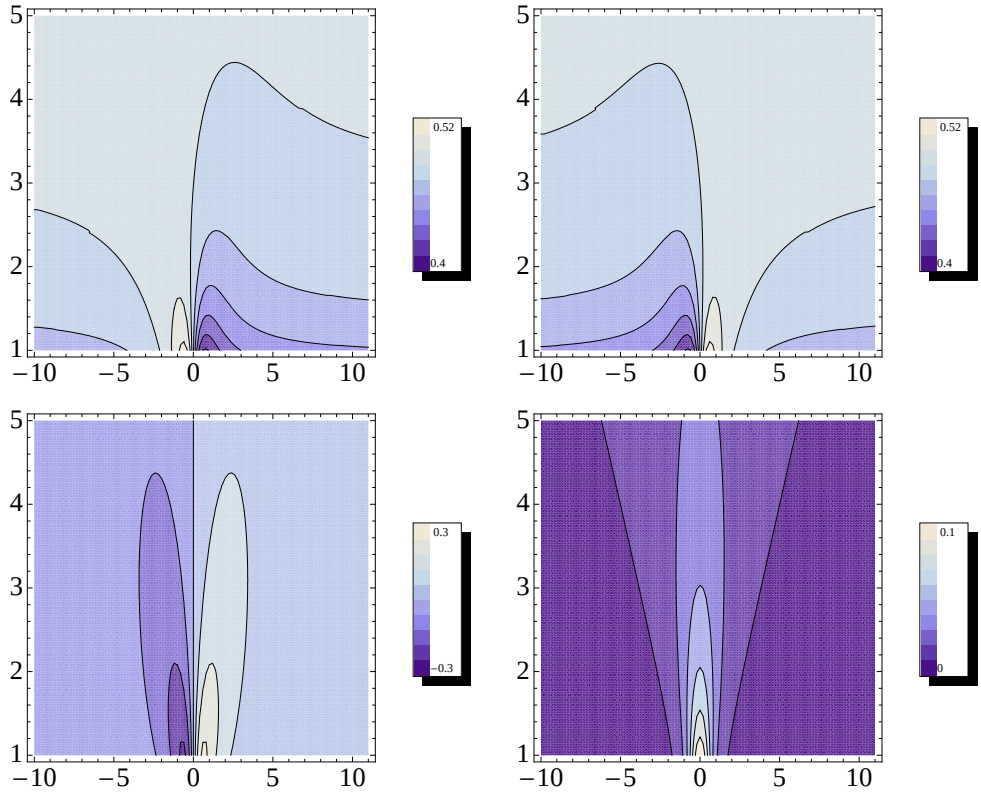

Figure 5.5: Contour plots of the electronic densities (first row), current and vibronic position (second row). The horizontal axes is the voltage V_B and the vertical axes is the lead-to-molecule tunneling coupling Γ. The colors go from blue (low values) to white (high values).

The first set of plots given in Fig. 5.5 extend and generalizes the results given in Fig. 5.4. The current shows the characteristic peaks and then the

return towards zero. We can observe that those peaks disappears when Γ increases, going in a regime where the current changes from negative to positive values when the bias crosses the zero. The vibronic position has a maximum at zero bias and increasing Γ the peak at zero becomes lowest and wider. The two electronic populations are symmetric and for large Γ they reach the same value. The most the system is coupled to the external reservoirs, the most the charge will be distributed through the two levels in the same way.

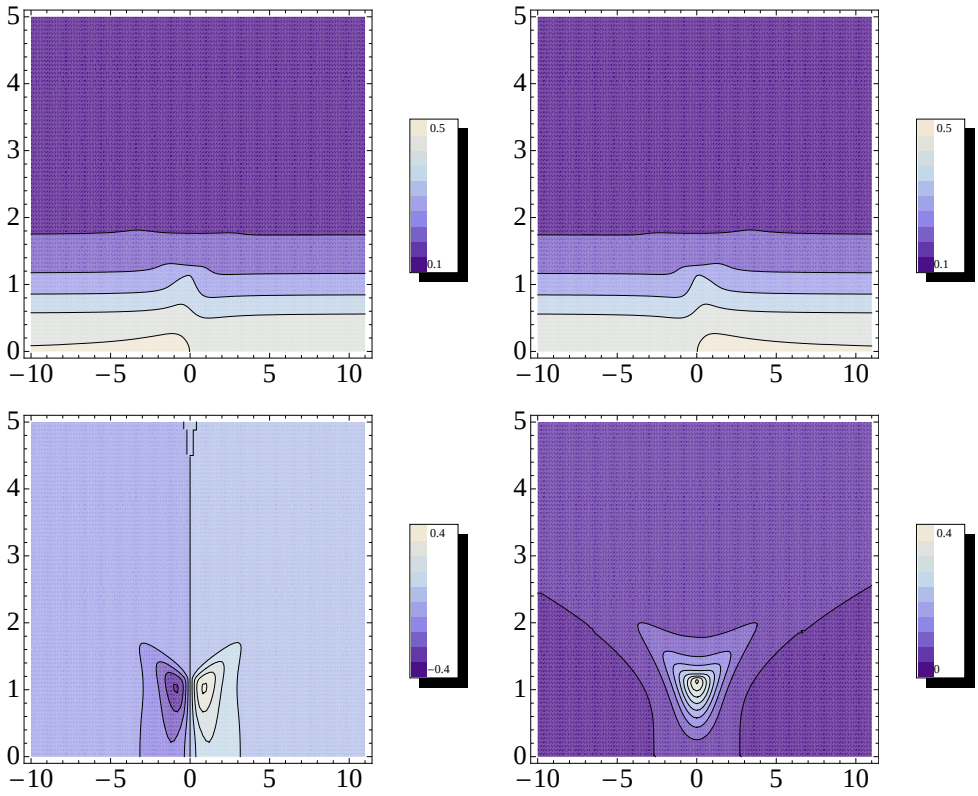

Figure 5.6: Contour plots of the electronic densities (first row), current and vibronic position (second row). The horizontal axes is the voltage V_B and the vertical axes is the electron-vibron interaction strength λ. The colors go from blue (low values) to white (high values).

The set of plots in Fig. 5.6 are on the $V_B - \lambda$ plane. The current and the vibronic position show features similar to the one of Fig. 5.5. There is a region in which the current has two peaks (one negative and one positive) that disappear increasing λ. There is also a region in which the vibronic position has a maximum at zero bias. Of course this similarity is a generic

characteristic and the shapes of the interested regions are different. They occupy a different spot of the parameter-space. For what concerns the electronic population we can observe that they are symmetric and increasing λ they are equilibrated.

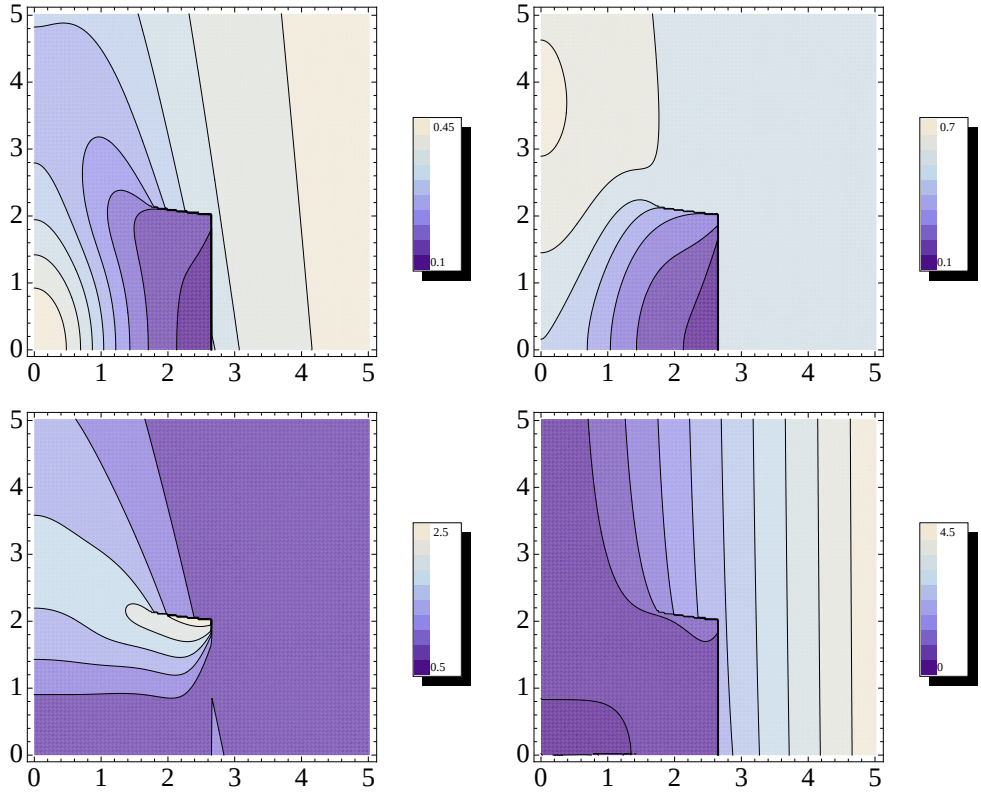

Figure 5.7: Contour plots of the electronic densities (first row), current and vibronic position (second row). The horizontal axes is the inter-dot tunneling coupling t and the vertical axes is the electron-vibron interaction strength λ. The colors go from blue (low values) to white (high values).

The last set of color plots in Fig. 5.7 are given on the λ-t plane. Those plots are showed with the idea of making a comparison on the two inter-dot tunneling coupling, namely the standard one and the vibron-mediated tunneling. As we can observe, there is a value on the t axes over which the quantities are not λ-dependent any more. It should be noticed that those plots are bias-independent, because in this case the bias-voltage is fixed at zero and it is not changed.

5.1.3 Memory effects

Although they are interesting for the understanding of the double-site system, the results of the previous sections do not show hysteretic behavior. This arises at different values of the parameters in the case of bias-independent position of the energy levels. Here we show two representative current-plots for this case. The plot in Fig. 5.8 shows the current for different values of the tunneling parameter t. As we can observe the hysteresis shows up for all the curves. This suggests that the responsible for the hysteresis is the electron-vibron coupling. In fact in Fig. 5.9 we show that increasing the value of λ the hysteresis take place.

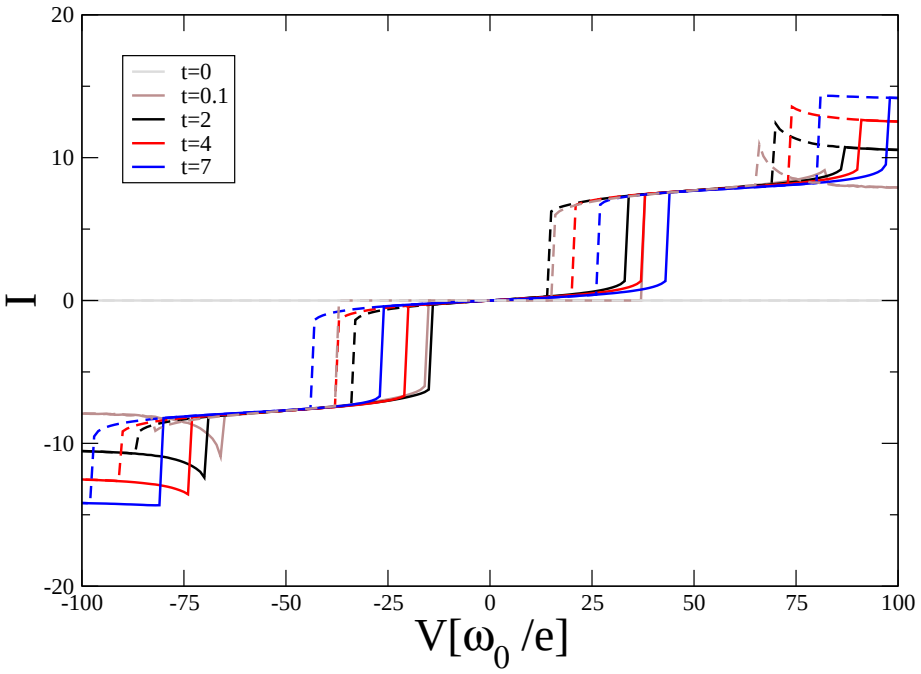

Figure 5.8: Current-voltage curves for different values of the tunneling t calculated with $\Gamma = 5$, $\lambda = 5$, $\epsilon_i = 0$, $T = 0.03$.

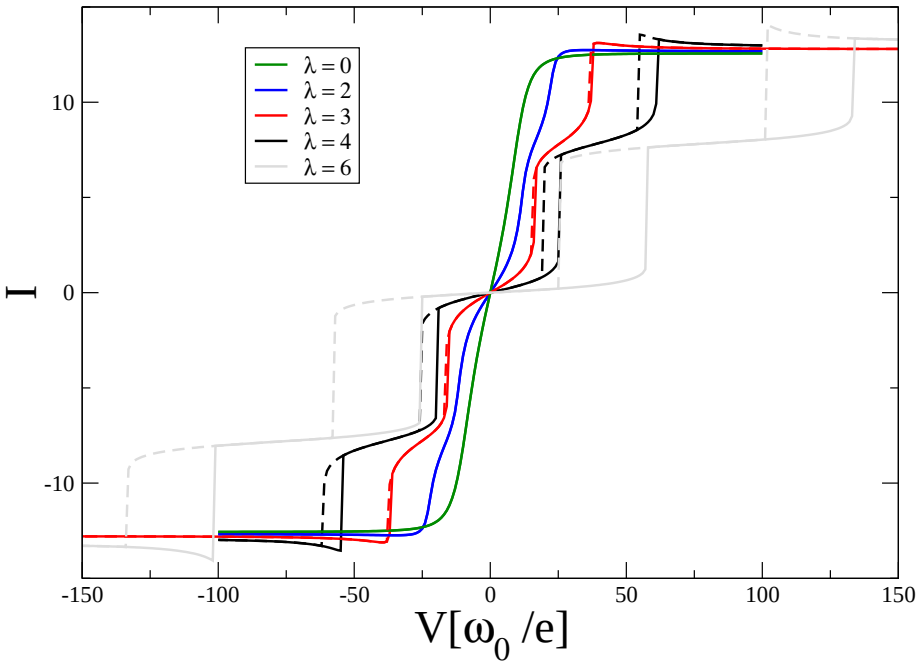

Figure 5.9: Current-voltage curves for different values of the electron-vibron coupling λ, calculated with $\Gamma = t = 5$, $\epsilon_i = 0$, $T = 0.03$..

5.2 Two-level-system: analytical considerations for weak coupling

In this section we derive analytical expressions for the two-level-system in the case of weak coupling to the leads. The starting point is Eq. (5.4) that we rewrite here for convenience:

$$\begin{aligned} H &= \sum_{i=1,2} \epsilon_i \hat{n}_i + \left[t + \lambda(a^\dagger + a)\right](d_1^\dagger d_2 + h.c.) + \omega_0 a^\dagger a + H_T + H_L \\ &\equiv H_S + H_T + H_L \end{aligned} \tag{5.14}$$

In the weak coupling regime ($\Gamma \ll \omega_0$) the two level system can be treated as almost isolated from the leads. If we are able to diagonalize the part that represents the isolated system $\sum_{i=1,2} \epsilon_i \hat{n}_i + \left[t + \lambda(a^\dagger + a)\right](d_1^\dagger d_2 + h.c.) + \omega_0 a^\dagger a$, then we can treat the coupling to the leads with a master equation approach considering single-electron transitions processes. To this end we consider, along the line of Lang and Firsov[56], a canonical transformation

$$\begin{aligned} O' &= e^S O e^{-S} \\ &= O + [S, O] + \frac{1}{2!}[S, [S, O]] + ..., \end{aligned} \tag{5.15}$$

where the transformation operator is given by $S = \frac{\lambda}{\omega_0}(a^\dagger - a)(d_1^\dagger d_2 + h.c.)$. In order to apply this transformation to the original Hamiltonian we need to express the transformed operators. To this end we have to calculate the commutators of the original operators with S. The electronic creation operators commutes with S as follows

$$\left[S, d_i^\dagger\right] = -\frac{\lambda}{\omega_0}(a^\dagger - a)d_j \tag{5.16}$$

while for the annihilation ones we obtain

$$[S, d_i] = \frac{\lambda}{\omega_0}(a^\dagger - a)d_j. \tag{5.17}$$

With those commutators at hand we use Eq. (5.15) to obtain the transformed operators:

$$\begin{aligned} d_i^{'} &= d_i - \frac{\lambda}{\omega_0}(a^\dagger - a)d_j + \frac{1}{2!}(\frac{\lambda}{\omega_0})^2(a^\dagger - a)^2 d_i - ... \\ &= \sum_n \frac{1}{2n!}\left(\frac{\lambda}{\omega_0}\right)^{2n} p^{2n} d_i - \sum_n \frac{1}{(2n+1)!}\left(\frac{\lambda}{\omega_0}\right)^{2n+1} p^{2n+1} d_j \\ &= \cosh(X)d_i - \sinh(X)d_j \\ d_i^{\dagger'} &= d_i^\dagger + \frac{\lambda}{\omega_0}(a^\dagger - a)d_j^\dagger + \frac{1}{2!}(\frac{\lambda}{\omega_0})^2(a^\dagger - a)^2 d_i^\dagger + ... \\ &= \sum_n \frac{1}{2n!}\left(\frac{\lambda}{\omega_0}\right)^{2n} p^{2n} d_i^\dagger + \sum_n \frac{1}{(2n+1)!}\left(\frac{\lambda}{\omega_0}\right)^{2n+1} p^{2n+1} d_j^\dagger \\ &= \cosh(X)d_i^\dagger + \sinh(X)d_j^\dagger, \end{aligned} \tag{5.18}$$

where we have introduced $X = \frac{\lambda}{\omega_0}(a^\dagger - a)$. The vibronic operators transform in a more simple way:

$$\begin{aligned} a^{'} &= a - \frac{\lambda}{\omega_0}(d_1^\dagger d_2 + h.c.) \\ a^{\dagger'} &= a^\dagger - \frac{\lambda}{\omega_0}(d_1^\dagger d_2 + h.c.). \end{aligned} \tag{5.19}$$

Using the transformed operators, the initial Hamiltonian for the isolated system reads (in the case of degenerate levels: $\epsilon_1 = \epsilon_2 = \epsilon$)

$$H_S = \epsilon \sum_{i=1,2} \hat{n}_i + \left[t - \frac{\lambda^2}{\omega_0}\right](d_1^\dagger d_2 + d_2^\dagger d_1) + \omega_0 a^\dagger a. \tag{5.20}$$

Going in the even-odd basis, i.e. applying the following further transformation

$$d_{e(o)} = \frac{d_1 \pm d_2}{\sqrt{2}} \tag{5.21}$$

and the equivalent one for the creation operators, the Hamiltonian for the isolated system has the final form:

$$H_S = \epsilon \sum_{i=e,o} \hat{n}_i + \omega_0 a^\dagger a. \tag{5.22}$$

where

$$\epsilon_{e(o)} = \epsilon \pm \left(t - \frac{\lambda^2}{\omega_0}\right). \tag{5.23}$$

The spectrum of the isolated system has then the following structure:

$$E_{nmq} = n\epsilon_e + m\epsilon_o + q\omega_0, \tag{5.24}$$

where the corresponding states are given by:

$$|\psi_{nmq}\rangle = e^{-X(d_e^\dagger d_e + d_o^\dagger d_o)} \left(d_e^\dagger\right)^n \left(d_o^\dagger\right)^m \frac{\left(a^\dagger\right)^q}{\sqrt{q!}} |vacuum\rangle. \tag{5.25}$$

The modified tunneling after the two transformations are given by:

$$H_{T,L(R)} = \sum_k V_{kL(R)} c_{kL(R)}^\dagger \left[\frac{d_e e^{-X} \pm d_o e^X}{2} + h.c.\right]. \tag{5.26}$$

Thanks to the transformation (5.15) we are basically able to rewrite the interacting problem in a non-interacting one exactly. Starting from this result we discuss in the following two possible directions of investigation: switching (memory) investigation where only the vibrational ground state is taken into account and a more general approach where the numbers of possible vibrational excitations is in principle a free parameter.

Assuming that every time a tunneling process occurs the system relaxes very fast (compared to the other time-scales) to the vibrational ground states, then we only have to consider the following four states

$$|0,0,0\rangle, |0,1,0\rangle, |1,0,0\rangle, |1,1,0\rangle.$$

The life times of those states are given by the following formula

$$\begin{aligned}
\tau_{000}^{-1} &= \Gamma \sum_{m,i} |M_{m,0}|^2 \left(f_i(E_{10m} - E_{000}) + f_i(E_{01m} - E_{000})\right) \\
\tau_{100}^{-1} &= \Gamma \sum_{m,i} |M_{m,0}|^2 \left(f_i(E_{11m} - E_{100}) + f_i(E_{00m} - E_{100})\right) \\
\tau_{010}^{-1} &= \Gamma \sum_{m,i} |M_{m,0}|^2 \left(f_i(E_{11m} - E_{010}) + f_i(E_{00m} - E_{010})\right) \\
\tau_{110}^{-1} &= \Gamma \sum_{m,i} |M_{m,0}|^2 \left(f_i(E_{10m} - E_{110}) + f_i(E_{01m} - E_{110})\right),
\end{aligned} \tag{5.27}$$

where the $M_{m,0}$ are the so called Franck-Condon matrix elements as in Eq.(3.31). With the lifetimes of Eqs. (5.27) for the vibrational ground states, we can set a master equation for the occupation probabilities in the single electron tunneling regime. Introducing a time-dependent bias voltage, we can then look at the evolution of the occupations (as for the single-level

cases analyzed in the third and fourth chapters). This discussion is made in order to generalize the ideas introduced in the single level case to memory effects also in the case of double dot with inter-dot vibrational coupling.

Considering the problem from a more general point of view, i.e. looking at the evolution of all the states of the system, one can use the Generalized Master Equation approach for the reduced density matrix in order to describe the properties of our system in the stationary limit. This approach, as discussed in the introductory chapter, takes into account also the evolution of the coherences among different energy-degenerate states. Coherences among states with different number of electrons are not taken into account. In our case this means that we can look at the subspaces of $0, 1$ and 2 electrons inside the system in a block-diagonal form. The coherences are only present among states with 1 electron and different number of vibrational excitations. From the spectrum in Eq. (5.24), we see that degeneracies are present among states with a difference in the number of vibrational excitations given by:

$$\Delta q = \frac{|\epsilon_e - \epsilon_o|}{\omega_0} = \frac{2|t - \frac{\lambda^2}{\omega_0}|}{\omega_0}. \tag{5.28}$$

In the case of strong electron-vibron interaction, for example $\lambda = 5\omega_0$, and with inter-dot tunneling coupling of the same order $t = 5$, we can calculate that the condition to obtain 2 single electron states degenerate is $\Delta q = 40$. This means that one should consider states with 40 vibrational excitations in order to get coherences in the problem. One could then think to start describing the system taking into account only the evolution of the diagonal part of the density matrix, i.e. only the populations. Nevertheless it has to be noticed that possible corrections could arise when coherences of the density matrix are included. Labeling the states as $|n, m, q\rangle$, the rate equation for the population of a given state read:

$$\frac{\partial p_{n,m,q}}{\partial t} = \sum_{i,j,p} \Gamma^{n,m,q}_{i,j,p} p_{i,j,p} - p_{n,m,q} \sum_{i,j,p} \Gamma^{i,j,p}_{n,m,q}. \tag{5.29}$$

The condition of stationary limit is obtained requiring that $\frac{\partial p_{n,m,q}}{\partial t} = 0$. The Eq. (5.29) can be written in the following compact form:

$$\frac{\partial \vec{p}}{\partial t} = \mathbf{L} \cdot \vec{p}, \tag{5.30}$$

and then the stationary limit condition become $\mathbf{L} \cdot \vec{p} = 0$. The introduction of a relaxation mechanism toward equilibrium vibrational states, gives rise to

a new term in the rate equation that modifies the stationary limit condition in the following way:

$$\mathbf{L}\cdot\vec{p}-\frac{\vec{p}_{eq}}{\tau_{rel}}=0, \tag{5.31}$$

where $\vec{p}_{eq}$ is the equilibrium occupation probability vector and τ_{rel} is the relaxation time, i.e. the time that the system needs to reach the equilibrium state. Combining Eq. (5.30) and (5.29) we obtain the relation between the tunneling matrix elements $\Gamma^{n,m,q}_{i,j,p}$ and the matrix elements $L^{n,m,q}_{i,j,p}$:

$$\begin{aligned}
L^{0,0,q}_{0,0,q} &= -\sum_p \Gamma^{1,0,p}_{1,0,p}+\Gamma^{0,1,p}_{0,1,p} \\
L^{1,0,q}_{1,0,q} &= -\sum_p \Gamma^{0,0,p}_{0,0,p}+\Gamma^{1,1,p}_{1,1,p} \\
L^{0,1,q}_{0,1,q} &= -\sum_p \Gamma^{0,0,p}_{0,0,p}+\Gamma^{1,1,p}_{1,1,p} \\
L^{1,1,q}_{1,1,q} &= -\sum_p \Gamma^{0,0,p}_{1,0,p}+\Gamma^{1,1,p}_{0,1,p} \\
L^{i,j,p}_{n,m,q} &= \Gamma^{i,j,p}_{n,m,q}.
\end{aligned} \tag{5.32}$$

The tunneling matrix elements are given by the following relations:

$$\begin{aligned}
\Gamma^{b,p}_{a,q} &= \frac{\Gamma}{2}\sum_{i=L,R}|M_{q,p}|^2 f_i^0(E_{b,p}-E_{a,q}) \\
\Gamma^{b,p}_{a,q} &= \frac{\Gamma}{2}\sum_{i=L,R}|M_{q,p}|^2 (2-f_i^0(E_{b,p}-E_{a,q})),
\end{aligned} \tag{5.33}$$

where we have use the following notation,

$$\begin{aligned}
|0,0,q\rangle &= |0,q\rangle \\
|0,1,q\rangle &= |1,q\rangle \\
|1,0,q\rangle &= |2,q\rangle \\
|1,1,q\rangle &= |3,q\rangle.
\end{aligned} \tag{5.34}$$

In Eq. (5.33) the first row refers to tunneling into the system, and the second one to tunneling outside the system. With those formulas the current across the system can be expressed in the following way:

$$\begin{aligned}
I = \sum_{q,p} & p_{0,q}\left(\Gamma^{1,p}_{0,q}+\Gamma^{2,p}_{0,q}\right)+p_{1,q}\left(\Gamma^{3,p}_{1,q}-\Gamma^{o,p}_{1,q}\right) \\
& +p_{2,q}\left(\Gamma^{3,p}_{2,q}+\Gamma^{3,p}_{2,q}\right)-p_{3,q}\left(\Gamma^{1,p}_{3,q}+\Gamma^{2,p}_{3,q}\right).
\end{aligned} \tag{5.35}$$

5.3 Three-level system in the intermediate lead-to-molecule coupling

The next step we do is the analysis of a 3-dots system, going in the direction of a chain of electron-vibron system. Starting with the double-site system analyzed in the previous chapter, another level is inserted into the system with an additional off-diagonal vibronic term. The Hamiltonian describing the system is given by:

$$H = \sum_i \epsilon_i \hat{n}_i + \left[t_1 + \lambda_1(a_1^\dagger + a_1)\right](d_1^\dagger d_2 + h.c.) + \omega_{0,1} a_1^\dagger a_1 \qquad (5.36)$$
$$+ \left[t_2 + \lambda_2(a_2^\dagger + a_2)\right](d_2^\dagger d_3 + h.c.) + \omega_{0,2} a_2^\dagger a_2 + H_T + H_L,$$

where the lead-Hamiltonian H_L describes the usual equilibrium electronic system, and the tunneling Hamiltonian H_T couples the first level to the left lead and the third level to the right lead in the following way:

$$H_T = \sum_k \left(V_{k,L} c_{k,L}^\dagger d_1 + V_{k,R} c_{k,R}^\dagger d_3 + h.c.\right) \qquad (5.37)$$

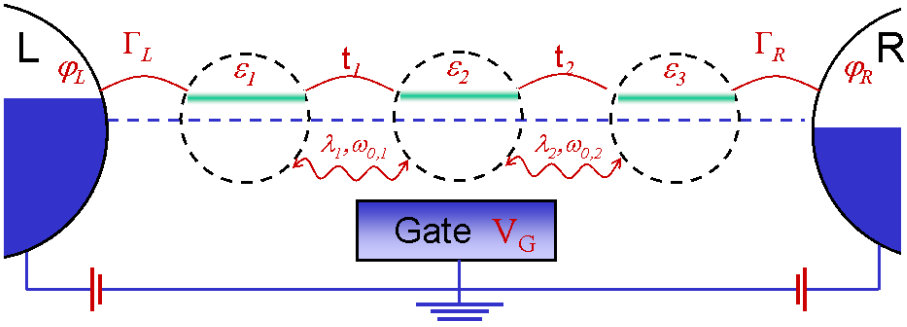

Figure 5.10: The scheme represents a system made of three sites represented by energy levels ϵ_1, ϵ_2 and ϵ_3 tunnel coupled in a tight binding fashion with coupling strength t_1 and t_2 and in presence of off-diagonal vibronic coupling λ_1 and λ_2. The junction is then coupled to two external leads attaching the first energy level to the left lead and the third energy level to the right lead. A bias voltage and a gate voltage are also sketched in the scheme.

The system is schematically represented in Fig. 5.10. We consider the situation of non-vanishing lead-to-molecule coupling, employing the EOM formalism for the Green functions. We perform the same kind of truncation

we have used for the previous systems in the EOM approach, called usually Hartree approximation for the electron-vibron interaction. For the system of Fig. 5.10 the inverse of the retarded Green function matrix has the following structure:

$$\begin{pmatrix} \epsilon + i\eta - \epsilon_1 - \Sigma_L & \alpha & 0 \\ \alpha & \epsilon + i\eta - \epsilon_2 & \beta \\ 0 & \beta & \epsilon + i\eta - \epsilon_3 - \Sigma_R \end{pmatrix} \cdot \mathbf{G^r} = \mathbf{1}, \qquad (5.38)$$

where

$$\begin{aligned} \alpha &= -t_1 + 2\frac{\lambda_1^2}{\omega_{0,1}} \left(\langle n_{12} \rangle + \langle n_{21} \rangle \right) \\ \beta &= -t_2 + 2\frac{\lambda_2^2}{\omega_{0,2}} \left(\langle n_{23} \rangle + \langle n_{32} \rangle \right). \end{aligned}$$

With a similar procedure used for the two-level system, we obtain a self-consistent problem $n_{i,j} \to G^r_{i,j} \to A_{i,j} \to n_{i,j} \cdots$. The following results are obtained in the case of bias-independent energy levels. The results refer to different values of the electronic energy levels, as indicated in the captions. For simplicity we have reduced the parameter space assuming equal the two inter-dot tunneling and the electron-vibron interaction parameters: $\lambda_1 = \lambda_2 \equiv \lambda$, $t_1 = t_2 \equiv t$, and $\omega_{0,1} = \omega_{0,2} \equiv \omega_0$. We also fix the energy levels at the same value: $\epsilon_1 = \epsilon_2 = \epsilon_3 \equiv \epsilon$.

As we can see in Fig. 5.11 different bistable regions develop, depending on the energy of the levels. We can observe a transition from a single hysteretic loop to two hysteretic loops. In Figs. 5.12, 5.13 the positions of the two oscillators and the electronic densities are showed in order to investigate the mechanism behind the hysteresis in the current. As one can see, in correspondence to the current loops the positions and the densities shows similar behaviors. In this case the hysteretic loops in the current are not directly related to a switching between an almost-well-defined charge state of the molecule as it was for the single-level junction. The electron-vibron interaction is the only one present in the system, so the hysteresis has to be related to that (as in the single level case). It remain to understand why the two loops appears only when the energy of the levels diminishes. We give the following physical interpretation: the maximum value of the energy of the levels (red curve) is also higher than (or comparable to) the energy required for the double transition associated to the two vibrons. Because of that we see only one loop. If the energy diminishes, then when the bias increases the polaron mechanism associated to the first vibron (between dots 1 and 2) and the one associated to the second vibron (between dot 2 and 3) becomes separated in energy so that they appear distinctly in the current curve. Intuitively we can say that the two loops are "merged" into one when the energy of the levels is higher than the typical energy associated to the

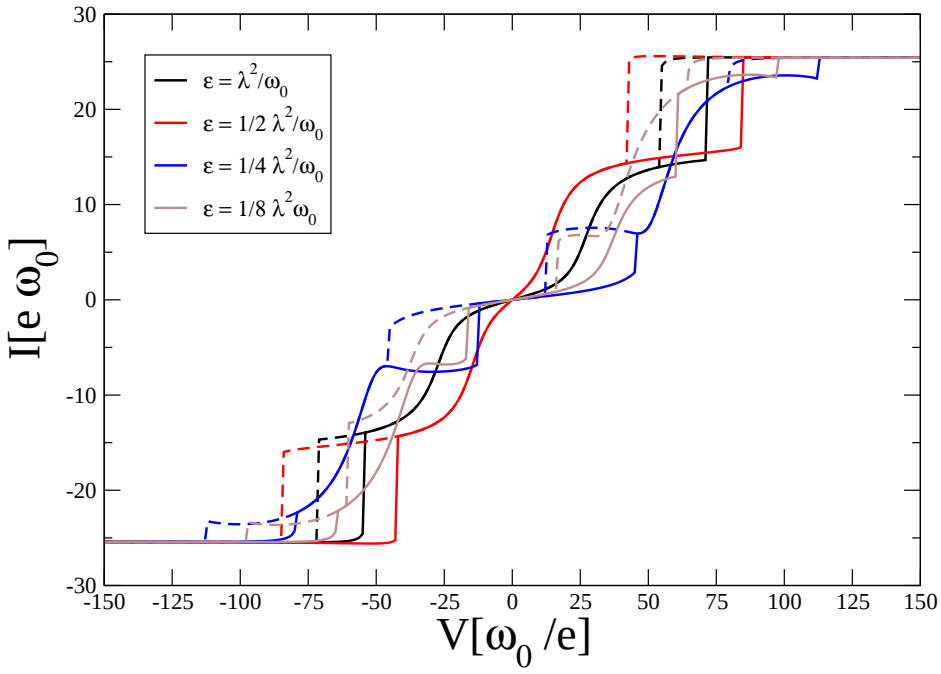

Figure 5.11: Current calculated for different values of the energy of the levels. The full (dashed) line describes the path going from negative (positive) to positive (negative) values of the bias voltage. The values of the energy ϵ are the following: (red , black, violet and blue) $= (1, 1/2, 1/4, 1/8)\frac{\lambda^2}{\omega}$. The other parameters are: $\Gamma = 5, \lambda = 5, t = 5$ and $T = 0.25$.

polaron shift (as in the single dot case) and they appear separated when the energy difference between the transitions is bigger than the energy of the levels itself.

5.4 Conclusions

In this chapter we have investigated two and three sites junctions. We have considered the systems for non-vanishing coupling to the leads, using the EOM technique for Green functions. For the two sites junctions we have first performed calculations in a parameter-region where the hysteresis does

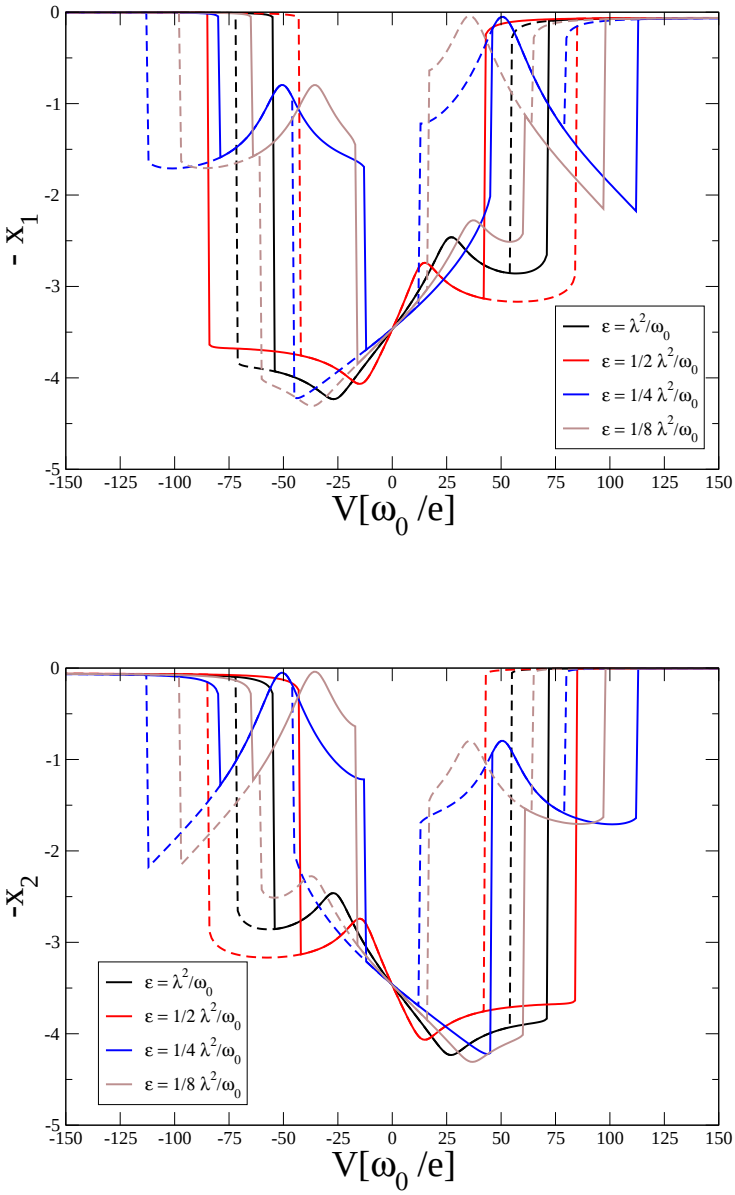

Figure 5.12: Positions of the two vibrons calculated for different values of the energy levels. The full (dashed) line describes the path going from negative (positive) to positive (negative) values of the bias voltage. The values of the energy ϵ are the following: (red , black, violet and blue) $= (1, 1/2, 1/4, 1/8)\frac{\lambda^2}{\omega}$. The other parameters are: $\Gamma = 5, \lambda = 5, t = 5$ and $T = 0.25$.

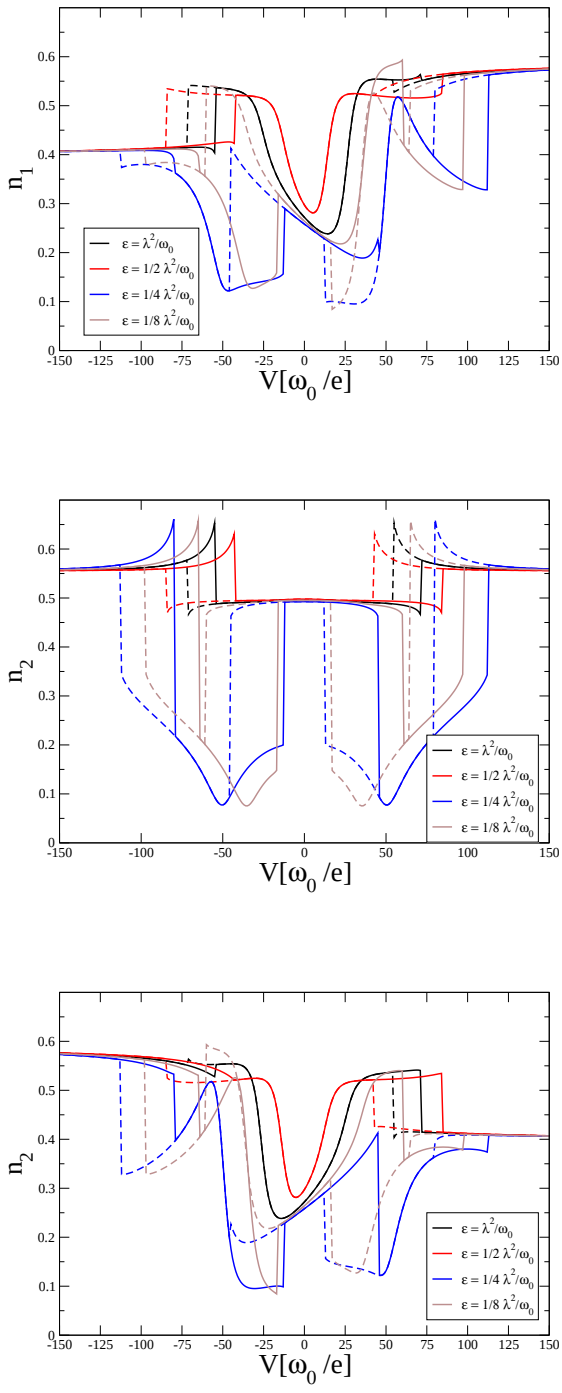

Figure 5.13: Populations of the three electronic levels calculated for different values of the energy levels. The full (dashed) line describes the path going from negative (positive) to positive (negative) values of the bias voltage. The values of the energy ϵ are the following: (red , black, violet and blue) $= (1, 1/2, 1/4, 1/8)\frac{\lambda^2}{\omega}$. The other parameters are: $\Gamma = 5, \lambda = 5, t = 5$ and $T = 0.25$.

not take place. Then we have shown that for both two and three sites junctions it is possible to obtain hysteretic behavior of the currents (and of the populations). We can then conclude that also linear electron-vibron chains are potentially switching elements. For two sites junctions we additionally performed analytical calculations for the weak coupling case, showing that it is possible to diagonalize exactly the system Hamiltonian.

Chapter 6

Networks of electron-vibron elements

6.1 Introduction

We want now to extend the models introduced in the previous chapters in order to describe arrays of electron-vibron elements. The idea is to connect electron-vibron elements through nearest neighbor tunneling coupling. The networks we want to investigate are square lattices, where every point of the lattice is made by an electron-vibron system. The lattice is thought to be placed on top of an STM-like setup and it is probed through the tip of the STM. The geometry we have in mind is sketched in Fig. 6.1. Every point in the lattice can act as a memory-element. Suppose there is a given configuration of the charges on the sites of the lattice. By placing the tip of the STM on one of those elements, a current will flow through the system. We want to investigate how the charge configuration rearranges, and what are the hysteretic behaviors of the system. Every element is coupled to the substrate and only one element can be coupled to the tip of the STM. This is substantially different from the case of a chain, where only two electronic levels are coupled to the leads. Because of that there are different possible configurations available. For example one could think of placing the tip right in the middle of the array or at the border and see how the system behaves in the different cases when a voltage is applied. In the following we introduce the model Hamiltonian of the system and show results for given examples.

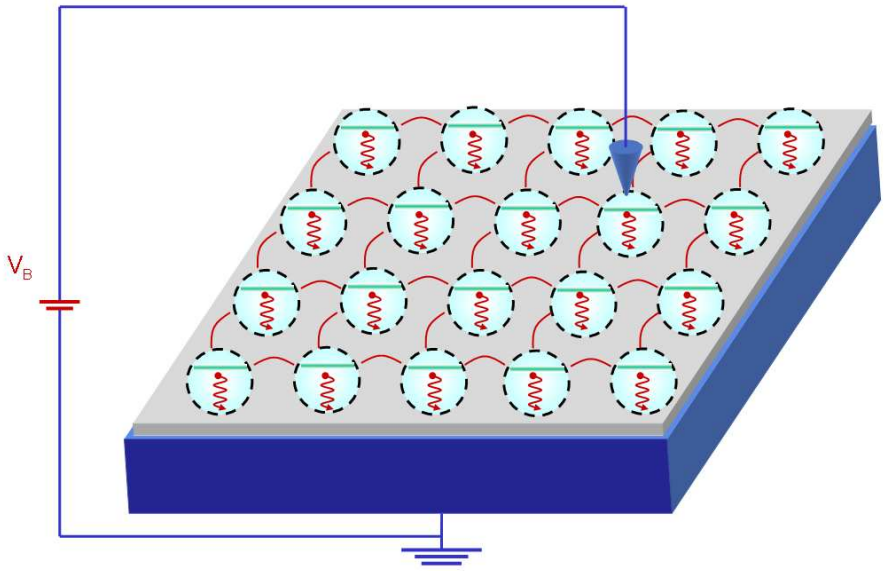

Figure 6.1: The figure represents schematically the STM-like-system we want to investigate. The gray layer represent a ultra-thin insulating layer, deposited on top of a metallic (blue) substrate. On top of the insulator there is a lattice of electron-vibron elements represented by small circles with a straight-blue line (electronic level) and a wavy-red line (vibron), connected in a nearest-neighbor fashion (red lines). A bias V_B between the metallic layer and the tip (placed on top of one of the lattice elements) is also shown. The *substrate* and the *tip* tunneling rate are not shown, but they can be thought as Γ_{sub} and Γ_{tip} as we will use in the text. The complete structure is at a given temperature T.

6.2 Model Hamiltonian

Considering the system sketched in Fig. 6.1, we write the Hamiltonian in the following way:

$$\begin{aligned} H &= \sum_i (\epsilon_i + \lambda_i \hat{x}_i)\hat{n}_i + \omega_i a_i^\dagger a_i + \sum_{<i,j>} (t_{i,j} d_i^\dagger d_j + U_{i,j}\hat{n}_i\hat{n}_j) \\ &+ H_T + H_L. \end{aligned} \tag{6.1}$$

The model in Eq. (6.1) is a sum of electron-vibron elements characterized by energies ϵ_i, frequencies ω_i and electron-vibron interaction strength λ_i. The electronic levels are tunnel coupled in a nearest neighbor way among each

other with tunneling strength $t_{i,j}$. The $U_{i,j}$ represent the electron-electron interaction strength among the nearest neighbor assuming non degenerate electronic sites. The lead Hamiltonians H_L represent the usual equilibrium Fermi-Dirac reservoirs and the tunneling Hamiltonian in this case is the following:

$$H_T = \sum_{i,k} V_{i,sk} c^\dagger_{s,k} d_i + V_{tip,tk} c^\dagger_{t,k} d_{tip} + h.c. \tag{6.2}$$

In Eq. (6.2) the operators $c^\dagger_{s,k}$ and $c^\dagger_{t,k}$ refer to the *substrate* and to the *tip* of the STM. Only one electron-vibron element is coupled to the tip and his operators are indicated with the subscript *tip*. We first investigate a two by two square lattice and then a three by three array. All the results are obtained with the EOM for the Green functions. For sake of simplicity the parameters describing the different lattice sites are set to the same value. This means that the inter-elements tunneling $t_{i,j}$, the vibrational frequencies and the electron-vibron coupling strength are site-independent. To furher reduce the parameter space we set the tunneling couplings to the same value:

$$\Gamma_{tip} = \Gamma_{s(ubstrate)}.$$

The currents that pass through the system is related only to the element that is in contact with the tip. We want to investigate how the presence of the other elements of the lattice modifies the behavior of the current, depending on the parameters we choose. The solid and dashed lines correspond in every of the following plot to different direction of the changes of the bias voltage, namely going from negative to positive and vice-versa.

6.3 2 by 2 square lattice

The most simple lattice is naturally a 2 by 2 square lattice. We have described the general structure of the system and introduced the general Hamiltonian in the previous section. The Hamiltonian (6.1) for this case has indices that go from 1 to 4 (we start labeling from the upper row, first element on the left). We calculate the current-voltage characteristic and the populations of the electronic levels for different values of the energy of the electronic levels, the inter-element tunneling and the electron-electron interaction. Every site of the 2 by 2 lattice is equivalent by symmetry and we can then fix the tip position on one of those. We choose the first. It should be noticed that by symmetry reasons, two of the four populations should be the same. In some plots among the ones shown in Fig. 6.3, 6.5, 6.7, we observe a small discrepancy between those populations, that we mainly attribute to

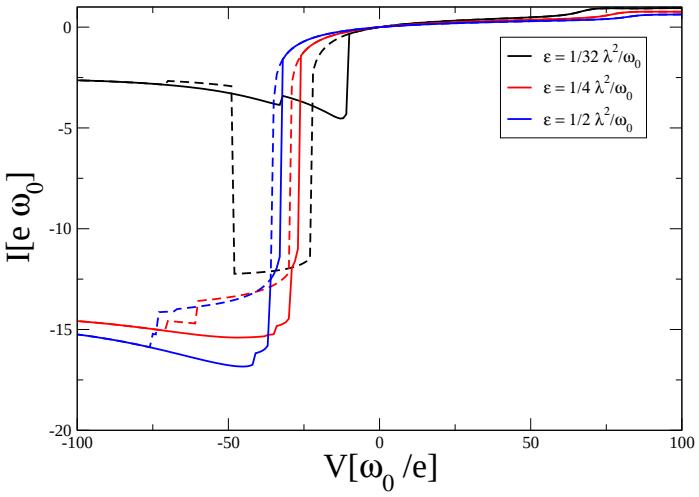

Figure 6.2: Current-voltage curves calculated for $\epsilon_1 = \lambda^2/2, \lambda^2/4, \lambda^2/32$. The other parameters are $\Gamma_{sub} = \Gamma_{tip} = 5$, $t = 5$, $U = 0$, $\lambda = 5$ and $T = 0.3$.

numerics. In the results we present, the hysteretic behavior shows up in different ways. In Fig. 6.2 we show the current profiles for different values of the energies of the electronic levels and in Fig. 6.3 the corresponding populations of the four levels. The current profile is asymmetric and upon increasing the energy of the electronic level, the overall profile shifts up in current. For $\epsilon_i = \frac{\lambda^2}{2}$ the hysteresis is more pronounced. In Fig. 6.4 we show the current profiles for different values of the inter-levels tunneling and in Fig. 6.5 the corresponding populations of the four levels. Also in this case the current profile is asymmetric and increasing the tunneling parameter the current increases for large values of the bias. In the populations there are two hysteresis taking place, one around zero bias voltage and the other two at higher biases. Interestingly, the population of the first site (the one under the tip) and the third level shows hysteresis around zero, and the other two show hysteresis around non zero bias. This is reflected in the current profile, and the value of the tunneling parameter modifies slightly the populations and governs the behavior of the current at high biases.

In Fig. 6.6 we show the current profiles for different values of the electron-electron interaction and in Fig. 6.7 the corresponding populations of the four levels. We use a mean field truncation for the electron-electron interaction terms. This is reflected in the Green function where terms like $\left\langle\left\langle \hat{n}_i d_j, d_k^\dagger \right\rangle\right\rangle$

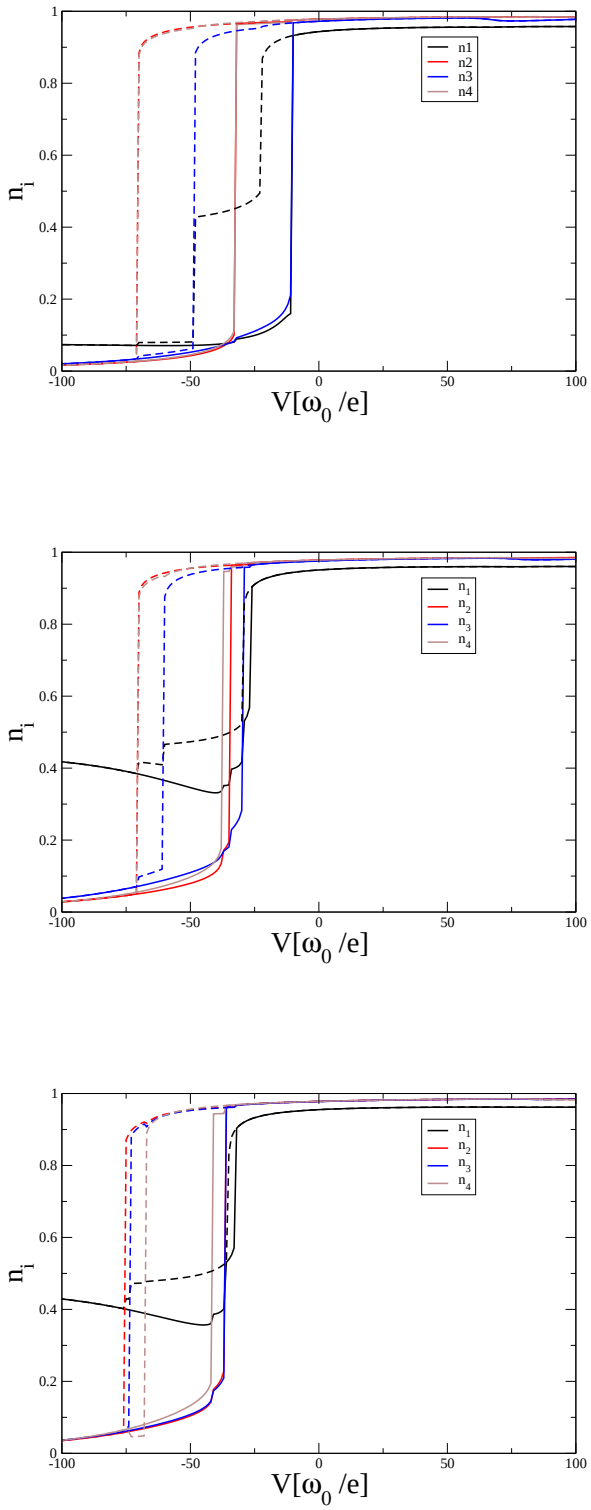

Figure 6.3: Electronic populations as a function of the bias voltage calculated for $\epsilon_1 = \lambda^2/2, \lambda^2/4, \lambda^2/32$ (first, second and third plot respectively). The other parameters are $\Gamma_{sub} = \Gamma_{tip} = 5$, $t = 5$, $U = 0$, $\lambda = 5$ and $T = 0.3$.

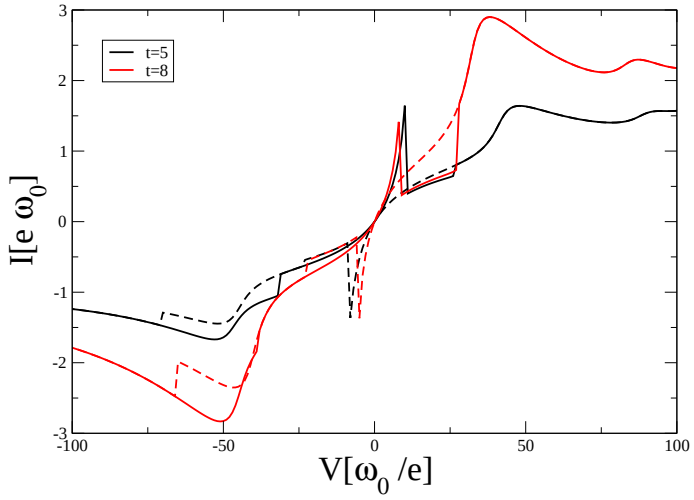

Figure 6.4: Current-voltage curves calculated for $t = 3, 5, 8$. The other parameter are $\Gamma_{sub} = \Gamma_{tip} = 5$, $\epsilon_1 = 0$, $U = 0$, $\lambda = 5$ and $T = 0.3$.

are factorized like $\langle \hat{n}_i \rangle \left\langle \left\langle d_j, d_k^\dagger \right\rangle \right\rangle$. For this case we can argue that the hysteresis of the current is present at any value of the electron-electron interaction strength, already for $U = 0$. This means that the hysteresis is due to the electron-vibron interaction and the Coulomb interaction acts modifying the structure of the current (at least in this approximation). What we see is that increasing the electron-electron interaction the hysteresis for positive bias values become more pronounced. This can be interpreted as follows: when the interaction increases, the escape of the electrons through the level connected to the tip get more pronounced because the electrons repel each other, and they are more likely to escape through the tip of the STM.

6.4 3 by 3 square lattice

In this section we investigate a 3 by 3 square lattice. The system in this case does not have the same symmetry as the previous one. In fact we can identify three different groups of elements that are equivalent by symmetry. The tip position will be then chosen in only one element of every group. Labeling the elements of the array from 1 to 9 (starting from the left element of the first row), then we can identify the following three groups: $(1, 3, 7, 9)$,

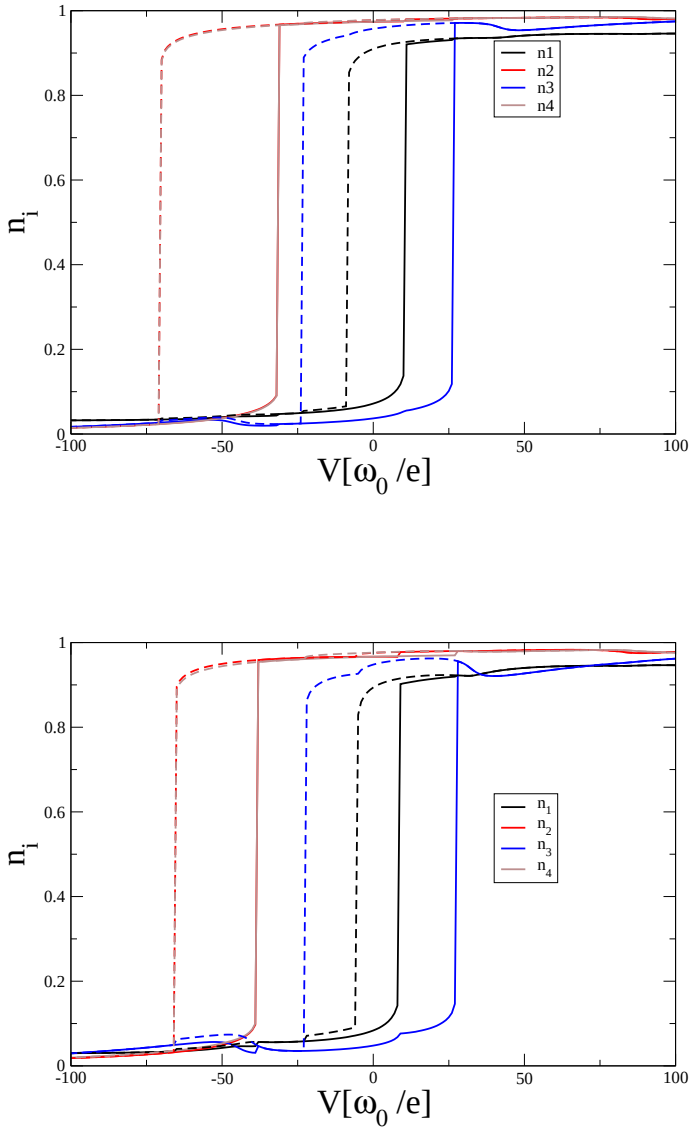

Figure 6.5: Electronic populations as a function of the bias voltage calculated for $t = 5, 8$ (first and second plot respectively). The other parameters are $\Gamma_{sub} = \Gamma_{tip} = 5$, $\epsilon_1 = 0$, $U = 0$, $\lambda = 5$ and $T = 0.3$.

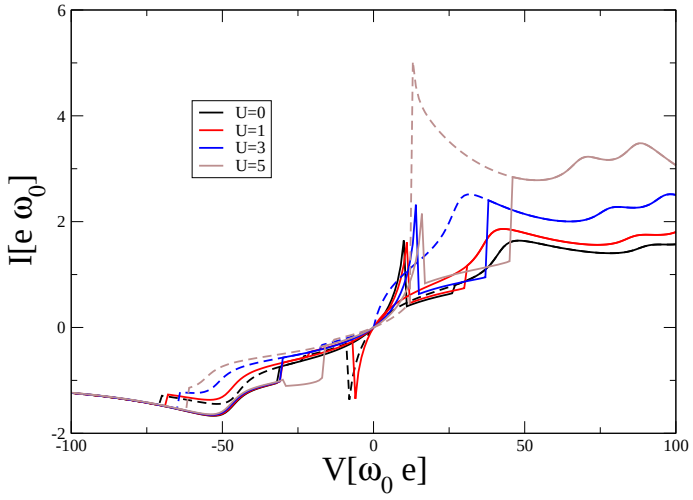

Figure 6.6: Current-voltage curves calculated for $U = 0, 1, 3, 5$. The other parameter are $\Gamma_{sub} = \Gamma_{tip} = 5$, $\epsilon_1 = 0$, $t = 5$, $\lambda = 5$ and $T = 0.3$.

$(2, 4, 6, 8)$ and 5. What we show in the following are three current-voltage plots corresponding to different values of the electron-electron interaction. Each of those plot contains currents calculated at different points of the lattice, namely at points $3, 5$ and 6 that represent the vertex, the center and the middle of the border. Again the current profiles are not symmetric, reflecting the structure of the problem: the levels are all coupled to the substrate but only one is probed through the tip. Changing the interaction parameter from $U = 1$ to $U = 3$ (Fig. 6.8 and 6.9) we see that the change in the current gets more pronounced if we go from the site 3(vertex) to the site 6(middle border) and to the site 5 (the middle of the lattice). This can be explained with the consideration we made in the previous section: going from the vertex to the border and then to the middle of the lattice the number of nearest neighborhood increases from 2 to 4. An electron placed in the corresponding lattice-site *feels* more and more electronic repulsion. Looking at the curve with $U = 5$ Fig. 6.8 we see that the current changes by order of magnitude. For this last case it is not clear at the moment how good is the mean-field approximation we have used $\left\langle\left\langle \hat{n}_i d_j, d_k^\dagger \right\rangle\right\rangle \approx \langle \hat{n}_i \rangle \left\langle\left\langle d_j, d_k^\dagger \right\rangle\right\rangle$.

In this last chapter we have investigated two by two and three by three arrays of electron-vibron elements in STM-like setups. In the calculations we have seen that the array potentially act also as a switching source. Depending

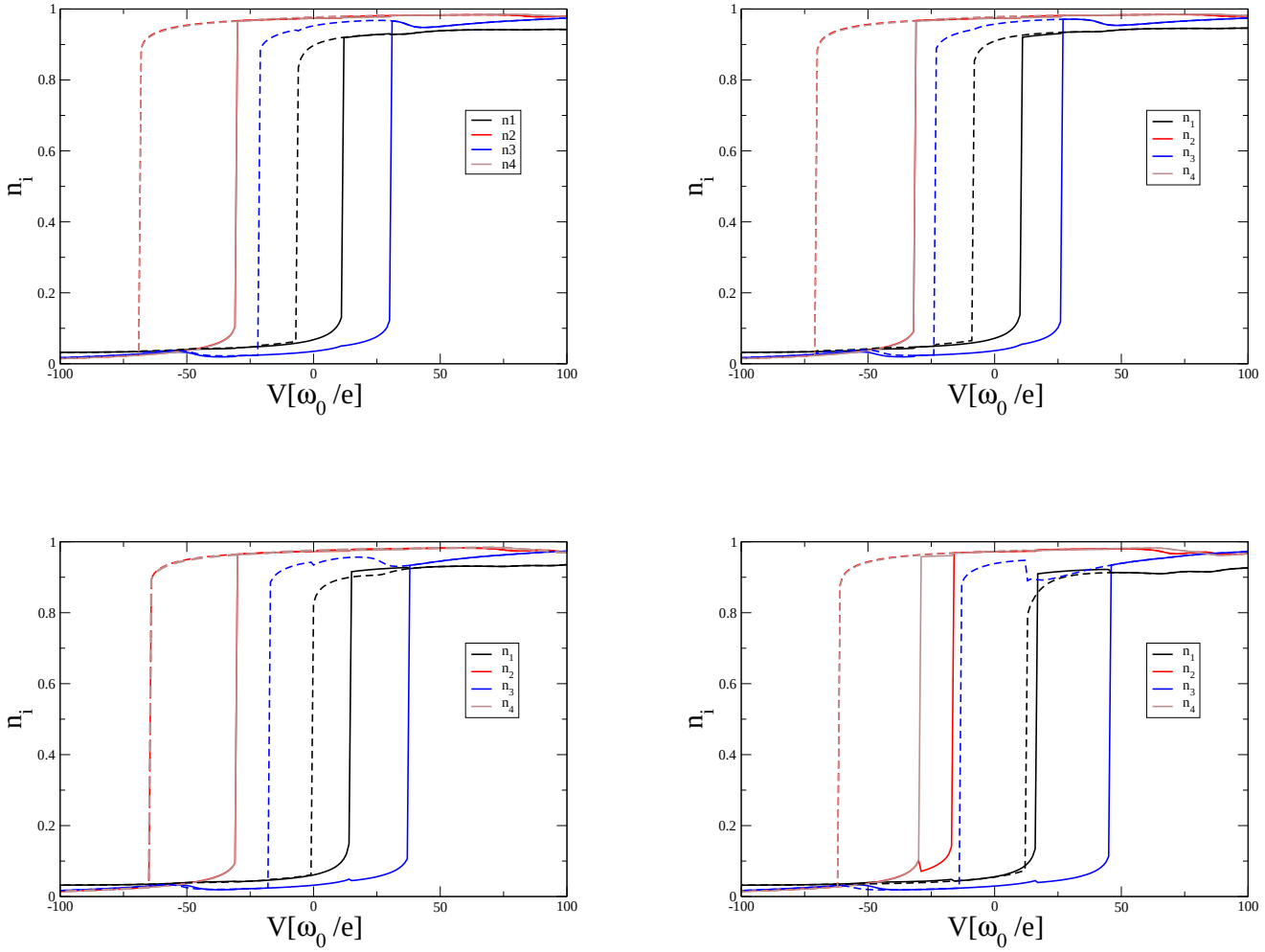

Figure 6.7: Electronic populations as a function of the bias voltage calculated for $U = 0, 1$ (up left and right) and $U = 3, 5$ (down left and right). The other parameters are $\Gamma_{sub} = \Gamma_{tip} = 5$, $\epsilon_1 = 0$, $t = 5$, $\lambda = 5$ and $T = 0.3$.

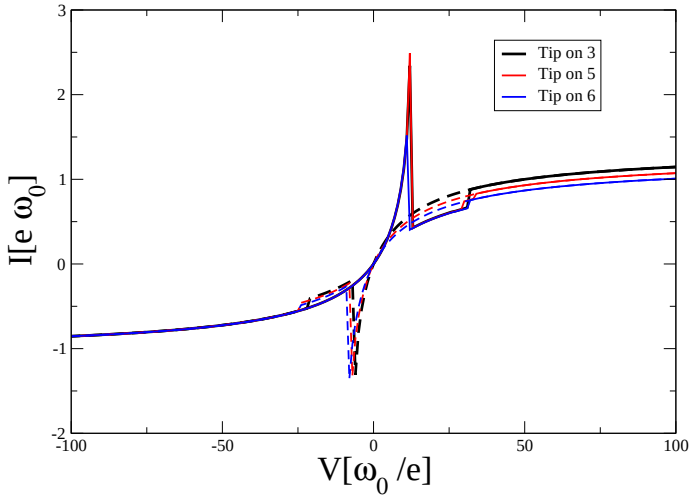

Figure 6.8: Current-voltage curves calculated at tip positions 3,5 and 6. The parameters used are the following: $\Gamma_{sub} = \Gamma_{tip} = 5$, $\epsilon_1 = 0$, $U = 1$, $t = 5$, $\lambda = 5$ and $T = 0.3$.

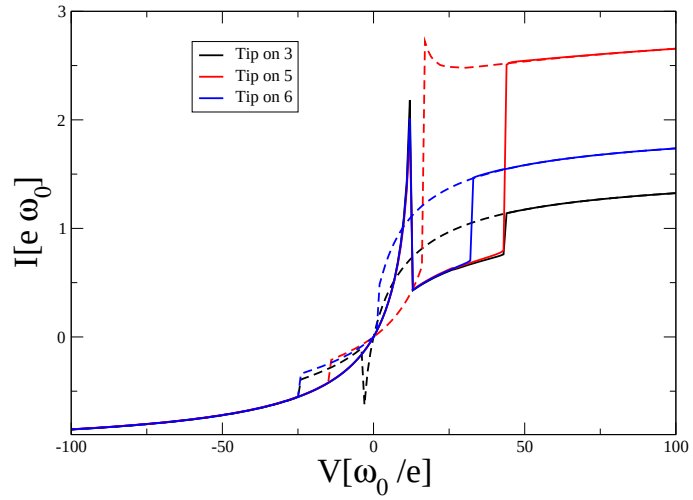

Figure 6.9: Current-voltage curves calculated at tip positions 3,5 and 6. The parameters used are the following: $\Gamma_{sub} = \Gamma_{tip} = 5$, $\epsilon_1 = 0$, $U = 3$, $t = 5$, $\lambda = 5$ and $T = 0.3$.

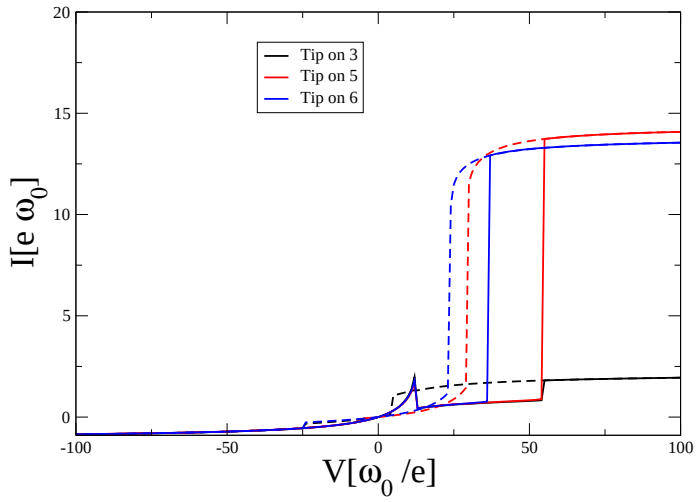

Figure 6.10: Current-voltage curves calculated at tip positions 3,5 and 6. The parameters used are the following: $\Gamma_{sub} = \Gamma_{tip} = 5$, $\epsilon_1 = 0$, $U = 5$, $t = 5$, $\lambda = 5$ and $T = 0.3$.

on the value of parameters like tunneling coupling t and Coulomb interaction strength U the current can increase significantly, making the switching effect more accessible.

Chapter 7

Conclusions and perspectives

In the following we conclude resuming the essential part of the work. This thesis deals with switching and memory effects in systems made by electron-vibron systems in contact with external leads. The electron-vibron system is the *active* part and plays the role of the molecule in the field of *molecular electronics*. We started our investigation from the single electronic and vibronic level case, investigating the *charge-memory* effect.

The model in this case is well known, and certain aspects of switching effects have been already proposed and investigated in the work [32]. Starting from those works we have introduced new ideas in the case of normal-metal leads: the role of the asymmetry in the bias-voltage drop across the molecule and the time-dependent evolution of the occupation-probabilities under external potentials. We have shown that the asymmetry plays a crucial role in order to obtain a hysteretic behavior around the zero of the bias voltage. In the weak leads-to-molecule coupling regime we have shown that using time-dependent bias voltages it is possible to obtain charge-memory effects.

After those two initial results, we have enriched the model inserting ferromagnetic leads instead of normal leads. With the spin as a new degree of freedom, we have introduced the natural extension of the charge-memory effect: the single-spin memory effect. Thanks to the combination of electron-vibron interaction and spin-selective tunneling, we find that a single charge with a well defined spin can be stored into the molecule in the case of weak lead-to-molecule coupling. We also found hysteresis of the current-polarization in the intermediate coupling regime.

We have then extended the model to chain and array-like systems. In the case of two and three site chains, we have introduced off-diagonal (inter-site) vibronic coupling, having in mind oligophenyl-like molecules. For the two site system in the regime of intermediate coupling to the leads, we have found hysteresis-like behavior as in the single dot junction. We have shown that

the electron-vibron coupling is responsible for the hysteretic features also in this case. In the weak coupling regime we have analytically diagonalized the molecular Hamiltonian, applying a Lang-Firsov-like transformation in a off-diagonal fashion. In the case of three-site junctions we have found again hysteretic behavior of the current-voltage characteristic in specific parameter ranges. We can conclude that chain-like electron-vibron systems with off-diagonal coupling are potentially switching-sources too.

The last extension is to electron-vibron arrays in STM-like setups. The idea is to use the studied single electron-vibron memory elements as a basic unit for operations in array structures. The system in this case has a different structure compared to the chain, because every site is connected to the *substrate* and only a chosen one to the *tip*. In all our calculations we have found hysteretic behavior, and we have investigated how the different parameters modify the current profile. Increasing the energy of the sites, the current hysteresis occour at higher values of the bias and for large positive bias it is independent on the energy. Increasing the inter-site tunneling or the electron-electron interaction, the current reaches higher values. The current increases if the the tip is moved from the vertex to the side and the center of the array. From an experimental point of view, the STM setup is a very natural candidate for arrays-like logical operations. The accurate control of atomic and molecular deposition and the ultra-thin insulating-film technologies make the STM very interesting for this kind of investigations.

From a theoretical point of view, the present work can be extended in different directions.

- A first extension could be done computing with *ab-initio* methods the parameters of the model-based approaches we have used. Through geometry optimization and structural relaxation calculations, electron-vibron interaction strenght, vibrational eigenmodes and molecule to lead coupling strenght can be extracted. In this way it should be possible to consider specific molecules, obtain more quantitative results and possibly make comparison with specific experiments.

- Another extension can start from the result of the exact diagonalization of the two-site system in the weak molecule to lead coupling. A Rate Equation and more generally a Generalized Master Equation approach could be applied to this case. Stationary limit properties and time-dependent effects can be investigated as we have done in the single-site case.

- Longer chains and larger lattices of electron-vibron sites could be studied in order to investigate the properties of the system as a function of

the number of sites. To this end, an attempt to analytically diagonalize general Hamiltonians for electron-vibron sites can bring new insight in the field.

- The introduction of ferromagnetic electrodes could be considered also for chains and lattices, in order to investigate a possible generalization of the spin-memory effect we have proposed.

- Thermal properties (such as thermopower) in presence of memory effects can be studied starting from the single site case and generalizing to more site systems.

- A interesting scenario can be considered introducing superconducting electrodes instead of normal or ferromagnetic ones.

Bibliography

[1] G. Cuniberti, G. Fagas, and K. Richter, eds., *Introducing Molecular Electronics*, (Springer, Berlin, 2005).

[2] A. Aviram, and M. A. Ratner, *Molecular Rectifiers*, Chem. Phys. Lett. **29,** 277 (1974).

[3] M. Elbing, R. Ochs, M. Koentopp, M. Fischer, C. von Hänisch, F. Weigend, F. Evers, H. B. Weber, and M. Mayor, *A single-molecule diode*, PNAS **102**, 8815 (2005).

[4] M. A. Reed, C. Zhou, C. J. Muller, T. P. Burgin, and J. M. Tour, *Conductance of a Molecular Junction*, Science **278,** 252 (1997).

[5] H. Park, A. K. L. Lim, and A. P. Alivisatos, *Fabrication of metallic electrodes with nanometer separation by electromigration*, Appl. Phys. Lett. **75,** 301 (1999).

[6] J. Repp, G. Meyer, S. Paavilainen, F. E. Olsson, and M. Persson, *Scanning Tunneling Spectroscopy of Cl Vacancies in NaCl Films: Strong Electron-Phonon Coupling in Double-Barrier Tunneling Junctions*, Phys. Rev. Lett. **95,** 225503 (2005).

[7] J. Repp, G. Meyer, F. E. Olsson, and M. Persson, *Controlling the Charge State of Individual Gold Adatoms*, Science **305,** 493 (2004).

[8] F. E. Olsson, S. Paavilainen, M. Persson, J. Repp, and G. Meyer, *Multiple Charge States of Ag Atoms on Ultrathin NaCl Films*, Phys. Rev. Lett. **98,** 176803 (2007).

[9] E. Lörtscher, H. B. Weber, and H. Riel, *Statistical Approach to Investigating Transport through Single Molecules*, Phys. Rev. Lett. **98,** 176807 (2007).

[10] M. Buongiorno Nardelli, J. L. Fattebertand, and J. Bernholc, *O(N) real-space method for ab initio quantum transport calculations: Application to carbon nanotube metal contacts*, Phys. Rev. B **64**, 245423 (2001).

[11] J. Taylor, H. Guo, and G. Wang, *Ab initio modeling of quantum transport properties of molecular electronic devices*, Phys. Rev. B **63**, 245407 (2001).

[12] M. Brandbyge, J. L.Mozos, P. Ordejn, J. Taylor, and K. Stokbro, *Density-functional method for nonequilibrium electron transport,* , Phys. Rev. B **65**, 165401 (2002).

[13] Y. Xue and M. A. Ratner, *Theoretical principles of Single-Molecule electronics: A Chemical and Mesoscopic view*, Int. J. Quantum Chem. **102**, 911 (2005).

[14] J. Heurich, J. C. Cuevas, W. Wenzel, and G. Schön, *Electrical Transport through single-Molecule Junctions: From Molecular Orbitals to Conduction Channels*, Phys. Rev. Lett. **88**, 256803 (2002).

[15] A. Calzolari, N. Marzari, I. Souza, and M. Buongiorno Nardelli, *Ab initio transport properties of nanostructures from maximally localized Wannier functions*, Phys. Rev. B **69**, 035108 (2004).

[16] J.Koch and F.von Oppen, *Franck-Condon Blockade and Giant Fano Factors in Transport through Single Molecules*, Phys. Rev. Lett. **94,** 206804 (2005).

[17] A. Donarini, M. Grifoni, and K. Richter, *Dynamical symmetry breaking in transport through molecules*, Phys. Rev. Lett. **97**, 166801 (2006).

[18] Georg Begemann, Dana Darau, Andrea Donarini, and Milena Grifoni, *Symmetry fingerprints of a benzene single-electron transistor: Interplay between Coulomb interaction and orbital symmetry*, Phys. Rev. B (R) **77**, 201406 (2008).

[19] Y. Meir and N. S. Wingreen, *Landauer Formula for the Current through an Interacting Electron Region*, Phys. Rev. Lett. **68**, 2512 (1992).

[20] A.-P. Jauho, N. S. Wingreen, and Y. Meir, *Time-dependent transport in interacting and noninteracting resonant-tunneling systems*, Phys. Rev. B **50**, 5528 (1994).

[21] D. A. Ryndyk, R. Gutiérrez, B. Song, and G. Cuniberti, *Green function techniques in the treatment of quantum transport at the molecular scale*, in Vol. 93 of *Springer Series in Chemical Physics* (Springer, Berlin, 2009).

[22] J. A. Smith, and L. Martin, *Do Cells Cycle?*, PNAS **70**, 1263 (1973).

[23] S. Ben, T. de-Leon, and E. H. Davidson, *Gene Regulation: Gene Control Network in Development*, Annu. Rev. Biophys. Biomol. Struct. **36**, 191 (2007).

[24] J. F. R. Kerr, A. H. Wyllie, and A. R. Curriet, *Apoptosis: A basic biological phenomenon with wideranging implications in tissue kinetics*, Br. J. Cancer **26**, 239 (1972).

[25] T. Wilhelm, *The smallest chemical reaction system with bistability*, BMC Systems Biology **3**, 90 2009.

[26] B.-Y. Choi, S.-J. Kahng, S. Kim, H. Kim, H. W. Kim, Y. J. Song, J. Ihm, and Y. Kuk, *Conformational Molecular Switch of the Azobenzene Molecule: A Scanning Tunneling Microscopy Study*, Phys. Rev. Lett. **96,** 156106 (2006).

[27] P. Liljeroth, J. Repp, and G. Meyer, *Current-Induced Hydrogen Tautomerization and Conductance Switching of Naphthalocyanine Molecules*, Science **317,** 1203(2007).

[28] E. Lörtscher, J. W. Ciszek, J. Tour, and H. Riel, *Reversible and Controllable Switching of a Single-molecule Junction*, Small **2**, 973 (2006).

[29] M. Martin, M. Lastapis, D. Riedel, G. Dujardin, M. Mamatkulov, L. Stauffer, and P. Sonnet, *Mastering the Molecular Dynamics of a Bistable Molecule by Single Atom Manipulation*, Phys. Rev. Lett. **97,** 216103 (2006).

[30] V. Meded, A. Bagrets 1, A. Arnold, F. Evers, *Molecular Switch Controlled by Pulsed Bias Voltages*, Small **5**, 2218 (2009).

[31] A. S. Alexandrov and A. M. Bratkovsky, *Memory effect in a molecular quantum dot with strong electron-vibron interaction*, Phys. Rev. B **67,** 235312 (2003).

[32] M. Galperin, M. A. Ratner, and A. Nitzan, *Hysteresis, Switching, and Negative Differential Resistance in Molecular Junctions: A Polaron Model*, Nano Lett. **5,** 125 (2005).

[33] A. Mitra, I. Aleiner, and A. J. Millis, *Semiclassical analysis of the nonequilibrium local polaron*, Phys. Rev. Lett. **94,** 076404 (2005).

[34] D. Mozyrsky, M. B. Hastings, and I. Martin, *Intermittent polaron dynamics: Born-Oppenheimer approximation out of equilibrium*, Phys. Rev. B **73,** 035104 (2006).

[35] M. del Valle, R. Gutiérrez, C. Tejedor, and G. Cuniberti, *Tuning the conductance of a molecular switch*, Nature Nanotechnology **2,** 176 (2007).

[36] F. Pistolesi, Ya. M. Blanter, and Ivar Martin, *Self-consistent theory of molecular switching* , Phys. Rev. B **78**, 085127 (2008).

[37] D. A. Ryndyk, P. D'Amico, G. Cuniberti, and K. Richter, *Charge-memory polaron effect in molecular junctions* Phys. Rev. B **78,** 085409 (2008).

[38] P. D'Amico, D. A. Ryndyk, G. Cuniberti, and K. Richter, *Charge-memory effect in a polaron model: equation-of-motion method for Green functions*, New J. Phys. **10,** 085002 (2008).

[39] D. A. Ryndyk, P. D'Amico, and K. Richter, *Single-spin polaron memory effect* Phys. Rev. B. **81,** 115333 (2010).

[40] H. Bruus and K. Flensberg, *Many-Body Quantum Theory in Condensed Matter Physics*, (Oxford University Press, Oxford, 2004).

[41] M. A. Reed and J. M. Tour, *Computing with Molecules* , Sci. Am. **282,** 86 (2000).

[42] A. Nitzan and M. A. Ratner, *Electron Transport in Molecular Wire Junctions*, Science **300,** 1384 (2003).

[43] C. Joachim and M. A. Ratner, *Molecular electronics: Some views on transport junctions and beyond*, PNAS **102,** 8801 (2005).

[44] H. Park, J. Park, A. K. L. Lim, E. H. Anderson, A. P. Alivisatos, and P. L. McEuen, *Nanomechanical oscillations in a single-C_{60} transistor*, Nature **407,** 57 (2000).

[45] R. H. M. Smit, Y. Noat, C. Untiedt, N. D. Lang, M. C. van Hemert, and J. M. van Ruitenbeek, *Measurement of the conductance of a hydrogen molecule*, Nature **419,** 906 (2002).

[46] L. H. Yu, Z. K. Keane, J. W. Ciszek, L. Cheng, M. P. Stewart, J. M. Tour, and D. Natelson, *Inelastic Electron Tunneling via Molecular Vibrations in Single-Molecule Transistors*, Phys. Rev. Lett. **93,** 266802 (2004).

[47] X. H. Qiu, G. V. Nazin, and W. Ho, *Vibronic states in single molecule electron transport*, Phys. Rev. Lett. **92,** 206102 (2004).

[48] E. A. Osorio, K. O'Neill, N. Stuhr-Hansen, O. F. Nielsen, T. Bjornholm, and H. S. J. van der Zant, *Addition Energies and Vibrational Fine Structure Measured in Electromigrated Single-Molecule Junctions Based on an Oligophenylenevinylene Derivative*, Adv. Mater. **19,** 281 (2007).

[49] A. C. Hewson and D. M. Newns, *Effect of the image force in chemisorption*, Japan. J. Appl. Phys. Suppl. **2, Pt. 2,** 121 (1974).

[50] A. C. Hewson and D. M. Newns, *Polaronic effect in mixed- and intermediate-valence compounds*, J. Phys. C: Solid State Phys. **12,** 1665 (1979).

[51] H. Haug and A.-P. Jauho, *Quantum Kinetics and Optics of Semiconductors*, Vol. 123 of *Springer Series in Solid-State Sciences* (Springer, Berlin, 1996).

[52] C. Iacovita, M. V. Rastei, B. W. Heinrich, T.Brumme, J.Kortus, L.Limot, and J. P. Bucher, *Visualizing the Spin of Individual Cobalt-Phthalocyanine Molecules* Phys. Rev. Lett., **101,** 116602 (2008).

[53] F. Meier, L. Zhou, J. Wiebe, and R. Wiesendanger, *Revealing Magnetic Interactions from Single-Atom Magnetization Curves*, Science **320,** 82 (2008).

[54] S. W. Wu, G. V. Nazin, X.Chen, X. H. Qiu, and W.Ho, *Control of Relative Tunneling Rates in Single Molecule Bipolar Electron Transport*, Phys. Rev. Lett. **93,** 236802 (2004).

[55] J. Repp, G. Meyer, S. M. Stojković, A. Gourdon, and C. Joachim, *Control of Relative Tunneling Rates in Single Molecule Bipolar Electron Transport*, Phys. Rev. Lett.**94**, 026803 (2005).

[56] I. G. Lang and Y. A. Firsov, Sov. Phys. JETP **16,** 1301 (1963).

[57] S. Braig and K. Flensberg, *Vibrational sidebands and dissipative tunneling in molecular transistors*, Phys. Rev. B **68,** 205324 (2003).

[58] A. Mitra, I. Aleiner, and A. J. Millis, *Phonon effects in molecular transistors: Quantal and classical treatment*, Phys. Rev. B **69,** 245302 (2004).

[59] J. Koch, M. Semmelhack, F.von Oppen, and A. Nitzan, *Current-induced nonequilibrium vibrations in single-molecule devices*, Phys. Rev. B **73,** 155306 (2006).

[60] J. Koch, F.von Oppen, and A. V. Andreev, *Theory of the Franck-Condon blockade regime*, Phys. Rev. B **74**, 205438 (2006).

[61] M. Cizek, M. Thoss, and W. Domcke, *Charge transport through a flexible molecular junction*, Czech. J. of Phys. **55**, 189 (2005)

[62] G. A. Kaat, and K. Flensberg, *Rectification in single molecular dimers with strong polaron effect*, Phys. Rev. B **71,** 155408 (2005).

[63] S. Datta, W. Tian, S. Hong, R. Reifenberger, J. I. Henderson, and C. P. Kubiak, *Current-Voltage Characteristics of Self-Assembled Monolayers by Scanning Tunneling Microscopy*, Phys. Rev. Lett. **79**, 2530 (1997);

[64] T. Rakshit, G.-C. Liang, A. W. Gosh, M. C. Hersam, and S.Datta, *Molecules on silicon: Self-consistent first-principles theory and calibration to experiments*, Phys. Rev. B **72,** 125305 (2005).

[65] G. Mahan, *Many-Particle Physics* (Plenum, N. Y., 1990).

[66] K. C. Nowack and M. R. Wegewijs, *Vibration-assisted tunneling through competing molecular states*, cond-mat/0506552.

[67] K. Huang and A. Rhys, *Theory of Light Absorption and Non-Radiative Transitions in F-Centres*, Proc. R. Soc. London Ser. A **204**, 406 (1950).

[68] L. Kadanoff and G. Baym, *Quantum Statistical Mechanics* (Benjamin, New York, 1962).

[69] L. V. Keldysh, Zh. Eksp. Teor. Fiz. **47,** 1515 (1964), [Sov. Phys. JETP **20**, 1018 (1965)].

[70] J. Rammer and H. Smith, *Quantum field-theoretical methods in transport theory of metals*, Rev. Mod. Phys. **58**, 323 (1986).

[71] A.-P. Jauho, *Modelling of inelastic effects in molecular electronics*, Journal of Physics: Conference Series **35,** 313 (2006).

[72] P. Král, *Nonequilibrium linked cluster expansion for steady-state quantum transport*, Phys. Rev. B **56**, 7293 (1997).

[73] K. Flensberg, *Tunneling broadening of vibrational sidebands in molecular transistors*, Phys. Rev. B **68**, 205323 (2003).

[74] M. Galperin, M. A. Ratner, and A. Nitzan, *On the Line Widths of Vibrational Features in Inelastic Electron Tunneling Spectroscopy*, Nano Lett. **4**, 1605 (2004).

[75] M. Galperin, M. A. Ratner, and A. Nitzan, *Inelastic electron tunneling spectroscopy in molecular junctions: Peaks and dips*, J. Phys. Chem. **121**, 11965 (2004).

[76] T. Frederiksen, *Master's thesis*, Technical University of Denmark (2004).

[77] M. Hartung, *Master's thesis*, University of Regensburg) (2004.

[78] T. Frederiksen, M. Brandbyge, N. Lorente, and A.-P. Jauho, *Inelastic Scattering and Local Heating in Atomic Gold Wires*, Phys. Rev. Lett. **93**, 256601 (2004).

[79] D. A. Ryndyk and J. Keller, *Inelastic resonant tunneling through single molecules and quantum dots: Spectrum modification due to nonequilibrium effects* , Phys. Rev. B **71**, 073305 (2005).

[80] M. Galperin, M. A. Ratner, and A. Nitzan, *Resonant inelastic tunneling in molecular junctions* , Phys. Rev. B **73**, 045314 (2006).

[81] D. A. Ryndyk, M. Hartung, and G. Cuniberti, *Nonequilibrium molecular vibrons: An approach based on the nonequilibrium Green function technique and the self-consistent Born approximation*, Phys. Rev. B **73**, 045420 (2006).

[82] M. Galperin, M. A. Ratner, and A. Nitzan, *Molecular transport junctions: vibrational effects*, J. Phys.: Condens. Matter **19**, 103201 (2007).

[83] D. A. Ryndyk and G. Cuniberti, *Nonequilibrium resonant spectroscopy of molecular vibrons*, Phys. Rev. B **76**, 155430 (2007).

Aknowledgements

At the end of this experience, I would like to thank people that made it possible. I want to thank Klaus for his infinite patience. He gave me essential hints to go on with the work. He is really a mentor for me. Special thanks also to Dima, that has been a point of reference for me during the PhD. Thanks to Giovanni that also gave me the possibility to enter in the group. Thanks to my office-mates Martin, Alex and Christian ... it was really nice to share the office with you. Thanks also to Angie and Ulla. Their support has been very important for me. And finally I want to thank all the Italian crowd, Fabio, Giuseppe, Andrea C., Andrea N. Andrea D. (Italians like the name Andrea :)), Francesco, Pasquale, Paolo. Thanks to both *Richters* and *Grifoni* groups. The scientific environment has been great. Thank to the UniOrchester ... with you guys I discovered a bit more the german culture and lifestyle. Finally I want to thank my mother Marta, my father Ottavio and my brother Luca. They have always supported me. You are really wonderfull. Last thought to my lovely wife Sara. She has been wonderfull in helping me during difficult periods, expecially the final-writing one. Thanks to everybody I forgot to mention here.